A THEORETICAL AND EXPERIMENTAL STUDY

OF CONTRACTION CONES

by

GEORGE FRIESEN

This thesis is submitted as partial fulfillment for the degree of Master of Science in Mechanical Engineering.

The Faculty of Graduate Studies,
Department of Mechanical Engineering,
University of Manitoba,
Winnipeg, Manitoba

May, 1970.

ACKNOWLEDGEMENTS

The author would like to express his appreciation to Dr. R. S. Azad for the guidance received during the experimental investigation and writing of this thesis and to H. Krueger, who assisted with the tests. The author would also like to express his gratitude to the National Research Council of Canada for supplying the experimental equipment and for partial financial assistance during the experimental testing.

ABSTRACT

Different methods of design of three-dimensional axi-symmetric contraction cones using potential flow theory have been developed and several methods were discussed. The design method by Bossel (1969) was adopted and was tested in the experimental apparatus, which consisted of a contraction cone, a pipe section, and diffuser.

Velocity profiles were measured in the test section and turbulence measurements, using hot wire anemometry, were also made.

It was found that this flow in the test section was symmetric and that the design method by Bossel was supported by experimental evidence.

The turbulence parameters, such as turbulence intensities, correlation coefficients, turbulent shear stresses, and turbulent kinetic energy were found to show the same general trend as those of published data.

TABLE OF CONTENTS

LIST OF TABLES

LIST OF FIGURES

I. INTRODUCTION

For the past several years the fluid mechanics section of the Mechanical Engineering Department of the University of Manitoba has been conducting research on air flow in a straight conical diffuser with an 8^{o} included angle and an outlet to inlet area ratio of 4:1. This diffuser was chosen since work by H. Sprenger (1959), Cockrell and Markland (1963), and Mcdonald and Fox (1965) showed that diffusers of this configuration had the best pressure recovery characteristics.

It was found by previous investigators, Van der Spiegel (1969),and Sluser (1969), that the flow entering the diffuser was unsymmetrical and that the static pressure on the diffuser wall was fluctuating considerably. Several modifications were therefore made on the experimental apparatus before further tests were conducted.

It is the purpose of the present work to test the method of designing a contraction cone by Bossel (1969), and to study the flow in a straight pipe. A contraction cone, as in a wind tunnel, must fulfill two basic requirements. Firstly, the exit velocity at the narrow end must be uniform and parallel. Secondly, there must be no regions of separation caused by adverse pressure gradients at the wall which may appear at the start of the contraction and at the neck. The analysis of the flow was based on velocity measurements using the pitot tube and the turbulence measurements using hot-wire anemometry.

Measurements were made at the contraction inlet and outlet and at the diffuser inlet, which was done in order to determine the nature of the flow entering the diffuser, where turbulence and velocity measurements were taken by Krueger (1970).

II. THEORY

Several different methods for the design of axisymmetric contractions have been developed over the years. Bossel (1969), has grouped the methods for computation of axisymmetric potential flow into four categories: 1) adaptation of two-dimensional results, 2) distributed singularities, 3) relaxation, and 4) separation of variables. Various methods using separation of variables have been used and some of these methods will now be discussed.

From potential flow theory, the condition of continuity for axisymmetric flow of an ideal fluid is

$$u = \frac{1}{r}\frac{\partial \Psi}{\partial r} \quad \text{.....(2.1)}$$

$$\text{and} \quad v = \frac{-1}{r}\frac{\partial \Psi}{\partial x}$$

Where r and x are the radial and axial distances non-dimensionalized with respect to the contraction inlet radius and u and v are the velocity components made non-dimensional with respect to the exit velocity.

Also, for irrotational flow

$$\frac{\partial u}{\partial r} - \frac{\partial v}{\partial x} = 0. \quad \text{.....(2.2)}$$

Substituting (2.1) into (2.2), we obtain

$$\frac{\partial^2 \Psi}{\partial x^2} + \frac{\partial^2 \Psi}{\partial r^2} - \frac{1}{r}\frac{\partial \Psi}{\partial r} = 0, \quad \text{.....(2.3)}$$

which is the equation for Stokes' stream function in inviscid axi-

symmetric flow.

If it is assumed that $\Psi(r,x) = F(r)G(x)$, then equation (2.3) separates into two ordinary differential equations for $F(r)$ and $G(x)$. Lamb (1879) obtained three different series solutions to equation (2.3) which are:

$$\Psi_a(r,x) = \frac{r^2}{2} + \sum_{n=2}^{\infty} r^{2n} G_n(x) = \frac{1}{2} \sum_{n=1}^{\infty} \frac{(-1)^{n-1} U_{ax}^{(2n-1)}(x) r^{2n}}{2^{2n-2} n\{(n-1)!\}^2}$$

$$\Psi_b(r,x) = \frac{r^2}{2} + r \sum_{n=1}^{\infty} J_1(\mu_n r)\{a_n \exp(\mu_n x) + b_n \exp(-\mu_n x)\},$$

and

$$\Psi_c(r,x) = \frac{r^2}{2} + r \sum_{n=1}^{\infty} I_1(\mu_n r)\{c_n \sin(\mu_n x) + d_n \cos(\mu_n x)\},$$

where: Ψ_a, Ψ_b, Ψ_c are the stream functions,

J_n is the ordinary Bessel function,

I_n is modified Bessel function,

$U_{ax}(x)$ is the velocity distribution on the axis.

Tsien (1943), Szczeniowski (1943) and Cohen and Ritchie (1962) used the same basic approach to solving (2.3) by using solution Ψ_a of (2.4). This solution requires that the derivatives of the velocity distribution $U_{ax}(x)$ can be expressed analytically. Tsien solved for Ψ_a using

$$U_{ax}(x) = 0.55 + \frac{0.90}{2\pi} \int_0^x e^{-x^2/2} dx. \quad \text{.....(2.5)}$$

Szczenkowski used $U_{ax}(x) = a+b \tanh(cx)$, ...(2.6)

a, b, and c being constants.

The above solutions require a considerable amount of calculation and the length of the contraction cannot be determined before hand. In an attempt to gain more control over the design of the contraction cone, Cohen and Ritchie (1962) used

$$U_{ax}(x) = a+b,\ \tanh\ (k,x) + \ e^{-k_2x^2} \qquad \text{.....(2.7)}$$

a and b are constants, which are obtained from the desired velocities at inlet and outlet. The slenderness of the contraction was found by the designers to be largely determined by k, and the introduction of the term $b_2\ e^{-k_2x^2}$, according to Cohen and Ritchie, advanced the point of inflection of the wall. The designer may choose these parameters to suit his particular conditions, however, some experience with the method is required before a proper choice can be made. Cohen and Ritchie had some difficulty in obtaining the proper contraction ratio. The solution they obtained gave too small a contraction ratio to fit their test section. In order to alleviate this problem they shifted the axis of the contraction up relative to the wall contour to obtain the proper contraction ratio.

The velocity components u and v may also be derived from a velocity potential ϕ, such that

$$u = \frac{\partial \phi}{\partial x}$$

and

$$v = \frac{\partial \phi}{\partial r} \qquad \text{.....(2.8)}$$

Substituting (2.8) into the general equation of continuity which is

$$\frac{\partial v}{\partial r} + \frac{1}{r} v + \frac{\partial u}{\partial x} = 0, \ldots\ldots\ldots (2.9)$$

one obtains

$$\frac{\partial^2 \phi}{\partial r^2} + \frac{\partial^2 \phi}{\partial x^2} + \frac{1}{r} \frac{\partial \phi}{\partial r} = 0. \quad \ldots\ldots (2.10)$$

Thwaites (1946) solved this equation by expressing the velocity on the axis as a Fourier series, which is the Ψ_c solution of (2.4). The assumption was made by Thwaites that the velocity potential was constant on the plane $x = 0$, and $x = \pi$, and that $a_o \pi$ was the potential difference between the two planes.

The function $\phi = a_o x$ satisfies (2.10) and the conditions that $\phi(0) = 0$, and $\phi(\pi) = a_o \pi$. If we choose $\phi_o(0) = \phi_o(\pi)$, and if (2.10) is satisfied by ϕ_o then $\phi = a_o x + \phi_o \ldots\ldots\ldots (2.11)$ satisfies the required conditions. Putting

$$\phi_o = f_o(r) \sin px, \ldots\ldots\ldots\ldots\ldots (2.12)$$

where $f_o(r)$ is a function of r alone and p a position integer, then the condition $\phi_o(0) = \phi_o(\pi) = 0$ is satisfied. Substituting (2.12) into (2.11) and then substituting this equation into (2.10), the following is obtained :

$$p \sin px\, f_o(r) + \sin px \frac{\partial^2 f_o(r)}{\partial r^2} + \sin px \frac{1}{r} \frac{\partial f_o(r)}{\partial r} = 0$$

or

$$\frac{\partial^2 f_o(r)}{\partial r^2} + \frac{1}{r} \frac{\partial f_o(r)}{\partial r} - p^2 f_o(r) = 0 \ldots\ldots\ldots (2.13)$$

After using the transformation R = ipr, (2.13) becomes

$$\frac{\partial^2 f_o(R)}{\partial R^2} + \frac{1}{R}\frac{\partial f_o(R)}{\partial R} + f_o(R) = 0 \quad \ldots\ldots\ldots\ldots (2.14)$$

This is Bessel's equation of zero order, with the solution

$$f_o(r) = AJ_o(R), \quad \ldots\ldots\ldots\ldots\ldots\ldots (2.15)$$

A being a constant. The velocity potential can then be expressed as

$$\phi_o = a_p \sin px J_o(ipr)$$

or

$$\phi_o = a_p \sin px I_o(pr) \quad \ldots\ldots\ldots\ldots\ldots\ldots (2.16)$$

where $I_n(z) = i^{-n} J_n(iz)$.

The velocity potential

$$\phi(x,r) = a_o x + \sum_{p=1}^{N} \frac{a_p}{p} \sin px I_o(pr) \quad \ldots\ldots\ldots\ldots (2.17)$$

satisfies the above conditions in that

$$\phi(o,r) = 0, \quad \phi(\pi,r) = a_o \pi \text{ , for all r.}$$

Substituting (2.17) into (2.8) the components of velocity may be derived

$$v = \sum_{p=1}^{N} a_p \sin px I_1(pr), \quad \ldots\ldots\ldots\ldots\ldots\ldots (2.18)$$

and

$$u = a_o + \sum_{n=1}^{N} a_p \sin px I_o(pr).$$

Integration of (2.1) gives

$$\Psi = \int_o^r ur\,dr. \quad \ldots\ldots\ldots\ldots\ldots\ldots (2.19)$$

Then, substituting (2.18) into (2.19), the equation for the stream func-

tion may be obtained as

$$\Psi = \frac{1}{2} a_o r^2 + r \sum_{p=1}^{N} \frac{a_p}{p} \cos(px) I_1(pr). \quad \ldots\ldots(2.20)$$

If the coefficients can be determined, the entire flow field in the contraction can then be calculated. For the design of a contraction cone, Thwaites defined the length of the contraction cone to be $\pi/2r(\pi)$, where $r(\pi)$ is the value of a function $r(x)$ at $x = \pi$ at the boundary. The high velocity end of the contraction corresponded to $x = 0$; the low velocity end corresponded to $x = \pi$.

In order to achieve a monotonic velocity on the boundary, $(\partial u/\partial x)r = R$ was chosen to be

$$(\partial u/\partial x)_{r=R} = -B(1+\cos x)^{N-1} \sin x, \quad B>0. \quad \ldots\ldots(2.21)$$

From (2.18)

$$(\partial u/\partial x)_{r=R} = \sum_{p=1}^{N} p a_p \sin(px) I_o(pr) \quad \ldots\ldots\ldots\ldots(2.22)$$

The number of coefficients a_o, a_1, $\ldots a_N$ to be calculated may be artibrarily set by the designer. However, if $N>6$ the work in determining a solution is considerable.

Several contraction cones were designed by Thwaites and an example using his method will now be worked out. For a contraction ratio of 8.163 = 1, $r(0) = .35$ and $r(\pi) = 1$. The length of contraction, made non-dimensional by dividing by the inlet diameter, is set equal to $\pi/2$, and the surface velocity is specified to be monotonic requiring

$$\left(\frac{\partial u}{\partial x}\right)_{r=R}$$

to be as in (2.21).

If the first four terms are to be determined then $a_p = v$ for $p>4$, and $N=3$. From (2.22),

$$\left(\frac{\partial u}{\partial x}\right)_{r=1} = -\{(a_1 \sin x I_o(1) + 2a_2 \sin 2x I_o(2) + 3a_3 \sin 3x I_o(3)\}$$

$$= -\{a_1 I_o(1) + 4a_2 \cos x I_o(2) + 3I_o(3) a_3 \{3+4(\cos^2 x - 1)\}$$

$$(\sin x) \quad \ldots\ldots\ldots\ldots\ldots\ldots\ldots\ldots\ldots\ldots (2.23)$$

$$= -B(1+2\cos x + \cos^2 x) \sin x. \text{ (from 2.21)}$$

Taking B = 1 and then equating the coefficients of cosx and $\cos^2 x$, one obtains the following relationships:

$$I_o(1) a_1 - 3a_3 I_o(3) = 1,$$

$$\frac{4a_2 I_o(2)}{2} = 1, \quad \ldots\ldots\ldots\ldots\ldots\ldots\ldots\ldots (2.24)$$

and $$12a_3 I_o(3) = 1.$$

Therefore,

$$a_1 I_o(1) - 3a_3 I_o(3) = \frac{4a_2 I_o(2)}{2} = 12a_3 I_o(3). \quad \ldots\ldots\ldots\ldots (2.25)$$

If a_1 is arbitrarily taken as equal to 1, then

$$a_2 = \frac{2I_o(1)}{5I_o(2)} = .22216,$$

$$a_3 = \frac{1}{15} \frac{I_o(1)}{I_o(3)} = 0.01729.$$

The term a_o still remains to be determined. The wall stream line has a constant value and for a contraction ratio of 8.163:1 it must pass through the points x=0, r=0.35 and $x=\pi$,r=1. By substituting the above values into (2.20) and equating the stream function at the inlet to the stream function at the outlet, a_o may be determined. In this case a_o was found to be 1.11481. The wall streamline may now be calculated by substituting the values of a_p back into (2.20),in which case $\Psi_{wall} = 0.14614$. Substituting for the values of Ψ_{wall}, $a_o,\ldots,a_4$ into equation (2.20),the ordinates of the bounding streamline may be found as the solution of the equation

$$0.14614 = \frac{1}{2} a_o r + \sum_{p=1}^{3} r \frac{a_p}{p} \cos px I_o(pr) \quad \ldots\ldots\ldots\ldots (2.26)$$

The value of x may be found for a given value of r by expressing the right hand side of (2.26) as a cubic in cosx. Equation (2.18) may then be used to determine the velocity at any point in the contraction.

Bossel also used equation (2.20) to determine the flow fluid in the contraction cone. Instead of prescribing the velocity distribution, he prescribed the wall contour. Truncating the series after N terms and prescribing the wall contour r_i at N+1 points x_i ,then a system of N+1 equations for the unknown Fourier coefficients a_p is obtained.

$$\Psi = a_o \frac{r_i^2}{2} + \sum_{p=1}^{N} \frac{a_p}{p} r_i I_1(pr_i) \cos px_i, \quad i=1,2,\ldots,N+1. \qquad \ldots\ldots\ldots\ldots(2.27)$$

The condition Ψ=constant must be satisfied by the wall streamline. The approximate value of Ψ at the wall may be determined from (2.19). If the velocity profile is assumed to be uniform and normalized to 1 at the exit, then

$$\Psi = \int_o^{r_{exit}} r\,dr = \frac{r^2_{exit}}{2} . \qquad \ldots\ldots\ldots\ldots(2.28)$$

Therefore, as in the method by Thwaites, the stream and velocities can be calculated in the entire flow field, once the a_p have been determined. If it is desired to normalize the velocity with respect to the exit velocity on the contraction center line, the coefficient may be multiplied by a constant to obtain $u_{exit\ \ell} = 1$. The corresponding value of Ψ_{wall} may then also be obtained.

The solution to (2.27) was obtained in the following manner for the contraction cone in the experimental test apparatus. A large scale drawing was made of the profile of the contraction cone and the coordinates were read off at 20 points. The number of points used may be varied by the designer. The coordinates were then read into a computer program as described in the appendix. Once the coefficients had been determined, the stream function and velocities were computed at 20 stations along the contraction and at 10 points on the radius at each station.

Bossel solved the flow fields in contraction cones having contraction ratios of 16:1 and 36:1. The solution for the 16:1 contraction ratio designed by Bossel was repeated in order to check the computer program. The results obtained for the 89:1 contraction ratio in the test apparatus will be discussed in Chapter V.

In this method, if the prescribed wall contour produces an adverse pressure gradient, the original contour may be changed. Therefore, by using a trial and error procedure prescribing of wall contour a contraction free of adverse pressure gradients and with an acceptable exit velocity profile may be obtained. Also, the wall contour may be adjusted to give the required type of pressure distribution.

III. EXPERIMENTAL APPARATUS

3.1 INTRODUCTION

A description of the test apparatus and the modifications that were made are given in this chapter. The experimental set-up consisted mainly of:

1. Air moving device
2. Flow straighteners and windtunnel
3. Contraction nozzle
4. Straight pipes for boundary layer growth
5. Diffuser
6. Traversing mechanisms
7. Platform
8. Test equipment

A schematic diagram of the main components is given in Figure 3.1(a) and a description of the components is given below.

3.2 Air Moving Device

The air moving device consisted of a centrifugal fan with backward curved blades, driven by a 25 Horsepower variable speed DC motor. Some difficulty was experienced by Van der Spiegel and Slusar with the experimental apparatus during the series of tests they conducted. A considerable amount of fluctuation was observed in the instrument readings and it was thought that the cause might have been due to vibration of the probe and wind tunnel, and the fluctuating flow.

An attempt was made to determine the cause of the vibration

and then the necessary changes were made to eliminate them. A Reeds vibrometer was used to determine the frequency of vibration at the motor, fan, and test section. It was found that the frequencies of vibration at these three points were identical and coincided with the fan and motor rotational speed. It was concluded that the fan was the cause of vibration.

A test was also conducted using a Model N524 Vibration Meter, with which the acceleration, velocity and displacement of a point could be determined by mounting a piezoelectric crystal at the point. Measurements were taken at the fan outlet and the contraction inlet before any changes were made. The decision was them made to mount the fan and motor on an integral base and put vibration isolators underneath.

The weight of the fan and motor was accurately determined and a frame was designed, on which the fan and motor were mounted integrally. A local Consultant was contacted, and the selection of the isolators was made on his recommendation. Figure 3.2, a detailed drawing of the isolators and the frame. A flexible canvas coupling was also installed between the fan outlet and the duct inlet, thus separating the test section as much as possible from the motor and fan.

The Model N524 Vibration Meter was again used and it was found that the maximum displacement at the duct outlet was reduced from .09 inches to .03 inches. The frequency of vibration, however, still coincided with the fan speed. The results of the test are shown in Table 3.1.

Although the vibration problem was not eliminated entirely, it appeared to be greatly reduced by the flexible-coupling and vibration isolators.

3.3 Flow Straighteners and Windtunnel

The wind tunnel arrangement, shown in Figure 3.1(b) was used by Van der Spiegel and Slusar and was re-arranged as shown in Figure 3.1(a). A section of duct was removed at the fan outlet and placed between the flow straightener, of which a detailed drawing is given in Fugure 3.3, and the contraction cone. Another flow straightener however, was installed at the fan outlet. The impeller of the fan was positioned on one side of the duct,and by placing the flow straightener at the fan discharge it was felt that a more uniform velocity profile would be obtained in the large duct. The windtunnel supports were also braced more fully to prevent movement of the duct since it was previously supported only by canvas straps.

3.4 Contraction Cone

Figure 3.4 shows a detailed drawing of the contraction cone. In order to determine the cause of instability and asymmetry of the flow, careful measurements of the roundness of the contraction cone were made. Figure 3.3.2 shows the set-up that was used to measure the profile at 13 different stations along the contraction cone and at each station measurements were taken at 16 points on the circumference. Table 3.4 shows the results of the test and Figure 3.4.1 shows the profile of the contraction cone.

It was found that the inlet and outlet flanges of the contraction cone were not parallel to each other and that the axis of the flanges did not coincide with the axis of the profile of the contraction cone. At the contraction inlet spacers were placed where needed between the duct and contraction cone flanges. The inside of the duct was then smoothed out by means of putty at the contraction inlet.

At the contraction outlet material was removed from the flange in order to make it perpendicular to the axis of the contraction profile.

Static pressure tops were also made at two new stations on the contraction cone, as shown in Figure 3.3.1

3.5 Straight pipes for Boundary Layer Growth

Figure 3.5 shows a detailed drawing of the ducts used in the test section for boundary layer growth from the contraction outlet to the diffuser inlet. Length to diameter ratios of 0.6, 1.6, 4.6, 10.6 and 16.6 can be obtained by using different combinations of the various duct sections. The duct sections were made with threaded couplings, which made the task of assembling the test section much easier.

3.6 Diffuser

Figure 3.6 is a detailed drawing of the diffuser which was attached to the boundary layer growth pipes. It was of cast aluminum construction and had 12 stations, equally spaced along its longitudinal axis, for measurements of the static pressure. The diffuser traversing

mechanism which was used by H. Krueger (1970) is described fully in his thesis.

3.7 Traversing Mechanisms

The traversing mechanism used for the initial calibration of the wind tunnel was the pitot-tube traversing apparatus used by R. Lipka and is described in his thesis (1968). A modification, however, had to be made to the flanges of the apparatus so that it could be used with the new boundary layer growth pipes (see Figure 3.7.1 for a detailed drawing of the apparatus.)

Another device was also required to hold a miniature hot wire X-probe rigidly in the test section and allow it to be moved to any position in the flow field at a given cross-section. Another requirement of the traversing mechanism was that a single hot wire probe, in the same plane as the X-probe, could be brought close to the X-probe and that the distance could be varied between them. The device shown in Figure 3.7.2 was used to fulfil the above requirements. It consisted of a split aerofoil in which the X-probe was fastened. The internal arrangement of the aerofoil was such that the lead wires from the probe could be brought out of the test section through the slots machined inside the aerofoil.

Provision was also made in the traversing mechanism to allow an angle probe (see section 3.9.10) to be brought through the wall of the pipe. The angle probe could be brought near the X-probe and by

means of the caliper scales the distance between the probes could be varied. Due to its size, the X-probe could not be brought closer to the wall than .200". The angle probe was used to determine the mean velocities, and some turbulence characteristics near the wall (.01" to .20").

For low velocity measurements at the contraction inlet the traversing mechanism shown in Figure 3.7.3 was used. The probe, supported by a copper tube, which passed diametrically through the duct could be positioned at any point on the diameter by sliding the tube in and out of the duct.

The low velocity anemometer, which is described in section 3.9.9 was also used to do measurements at the contraction inlet.

3.8 Platform

The platform shown in Figure 3.8 was built to allow easy access to the test section. A set of rails was positioned on the platform to support the diffuser and boundary layer growth pipes. Riding on these rails were two trolleys, one supporting the diffuser and the other supporting the boundary layer growth pipes.

3.9 Test Equipment

Items 3.9.1 - 3.9.6 are items of equipment used for the experimental work that were also used by Slusar and Van der Spiegel and are described in detail in their theses (1963).

3.9.1 - Two disa Type 55A01 constant temperature hot-wire anemometers, serial numbers 338 and 817.

3.9.2 - One Disa type 55A06 Random Signal Indicator and Correlator, serial number 320.

3.9.3 - One Disa type 55A30 Digital Voltmeter, serial number 321.

3.9.4 - Probe calibration equipment consisting of a Disa type 55D41 Calibration unit, serial number 240, together with a Disa type 55D42 motor control unit.

3.9.5 - Probe repair equipment consisting of a Disa type 55A11 micro-manipulator, used in conjunction with an Olympus V5-IV Zoom microscope, serial number 201316. A Unitek 1048B capacitor discharge power supply was used to supply power to the micro-manipulator.

3.9.6 - Miscellaneous manometers shown in Figure 3.9.6

In addition to the above mentioned equipment the following was also used:

3.9.7 - Disa Type 55D01 Anemometer

A Disa type 55D01 constant temperature hot-wire anemometer, serial number 515 was used to make turbulence measurements close to the wall with an angle probe. Figure 3.9.7 is a photograph of this instrument with an external D.C. Voltmeter.

The frequency response of this instrument was 0-350KHz, it had a probe operating resistance range of 0-200 ohms and a maximum available probe current of 2 amperes.

The D.C. Voltmeter with the instrument had operating ranges

of 30, 10, 3 and 1 mv. full scale. This meter, indicating bridge D.C. voltage, was accurate to ±2% of full scale deflection.

A Disa type 55D35 RMS voltmeter, serial number 171 was used in conjunction with the 55D01 anemometer. It had ranges of .001, .003, .01, .03, .1, .3, 1, 3, 10, 30, 100, 300 mt RMS full scale. The RMS value of the bridge voltage fluctuation of the anemometer could be read to an accuracy of 2%.

The Disa type 55D25 auxiliary unit was also connected to the 55D01 anemometer. This unit had a built in square-wave generator which was used for adjustment of the anemometer bridge balance and also to find the time response of the angle probe. It also had high-pass and low-pass filters, which were used to remove undesired components (such as noise and vibration) from the anemometer signal. This unit also permitted compensation for the DC component of the signals if they were fed to a recorder or a DC coupled oscilloscope, and the gain and phase relationships could also be altered.

3.9.8 - Disa Type 55D10 Linearizer

Two Disa-Type 55D10 linearizers, serial numbers 133 and 190 shown in Figure 3.9.8 were used in conjunction with the 55A01 anemometers. The output voltage of a constant temperature anemometer is a nonlinear function of the flow velocity U

under measurement. In small degrees of turbulence, this nonlinearity is not very important, since a small section of the calibration curve may be considered sufficiently linear. The distortion caused by the curvature of the calibration curve becomes noticable, however, at higher degrees of turbulence. The sensitivity of the wire also varies with different mean flow velocities.

The anemometer output voltage V and the flow velocity U are related by:

$$V^2 = A+BU^{\gamma} \quad \text{.....(3.8.8.1)}$$

where A,B, and n are constants whose values depend on the probe and anemometer.

The linearizer is an electronic analog computer whose basic transfer function at constant settings of the operating controls can be written as:

$$V_{out} = \chi(V_{in}^2 - V_{ino}^2)^m \quad \text{.....(3.8.8.2)}$$

where χ, V_{ino}, and m are constants.

Taking the anemometer output voltage V and putting it equal to the linearizer input voltage V_{in}, and then substituting equation (3.8.8.1) into equation (3.8.8.2) gives

$$V_{out} = \chi(A+BU^n-V_{ino}^2)^m \text{.....(3.8.8.3)}$$

Therefore, for $V_{ino}^2 = A$ and $m = \frac{1}{\gamma}$ the linearizer output

voltage will be proportional to the velocity U.

The exponent m of the linearizer could be adjusted from .9 to 5.1 with an accuracy of ± 2%.

3.9.9 - Disa Type 55D80 Low Velocity Anemometer

Figure 3.9.9 is a photograph of the low velocity anemometer, serial number 133, which was used in conjunction with the 55D81 low velocity transducer. The meter on the anemometer indicated flow direction and velocity in cm/sec in the range from 1-30 cm/sec with an accuraty of ± 1cm/sec. The anemometer could also be operated in the constant current mode which required calibration in a known air stream (1-2m/sec).

Calibration facilities within the anemometer permitted correction for various parameters such as air temperature, and sensitivity. The selectable filters on the anemometer could also be set to suppress unwanted signals such as those resulting from erratic air movements.

3.9.10 - Hot-Wire Probes

A Disa type 55A36 miniature hot-wire probe, shown in Figure 3.8.10 was used in conjunction with the 55D01 anemometer, serial number 515. The probe was mounted on a miniature probe holder and placed in the pipe traversing mechanism. It was particularly suited to making measurements very close to the wall of the pipe.

The 55A38 miniature hot-wire X-probe, Figure 3.9.10, was mounted directly in the aerofoil of the pipe traversing mechanism as shown in Figure 3.7.2. The two 55D01 anemometers, serial numbers 338 and 817, described in section 3.7.1 were used in conjunction with the 55A38 probe.

The 55D81 low velocity transducer shown in Figure 3.9.10 was used in conjunction with the 55D80 low velocity anemometer. The transducer contained a hot-wire probe which was vibrated at a fixed amplitude and frequency. The transducer was mounted in the test section as shown in Figure 3.9.10.

IV. EXPERIMENTAL TESTING PROCEDURE

4.1 PRELIMINARY CONSIDERATIONS

In order to determine the effect of the Reynolds number on the flow field in the contraction cone, pipe, and diffuser it was decided that tests should be conducted for diffuser mean inlet velocities of 50,100,150,200 and 250 ft/s. Since tests were to be conducted at five different speeds, a decision was also made to do tests using only the maximum length of boundary layer growth pipe, which corresponded to a length to diameter ratio of 16.6.

It was decided that the pitot-tube traversing apparatus would be used to calibrate the wind tunnel and also to obtain the velocity profiles at the contraction outlet and diffuser inlet. Taking the pitot tube measurements first provided a convenient check for the subsequent hot-wire measurements.

It was also decided that measurements would be taken at the contraction outlet and diffuser inlet at different points on the 2-6 and 4-8 traverses defined on Figure 4.1.

4.2 PITOT TUBE MEASUREMENTS

The test apparatus was assembled as shown in Figure 3.1 with the pitot tube traversing mechanism installed at the contraction cone outlet. A U-tube monometer was connected to the static pressure rings at the contraction outlet and inlet and a Betz micro-monometer was connected to the pitot tube. For calibration of the wind tunnel the following steps were taken:

1. The fan was set at an artibrary speed.
2. Pitot tube measurements were then taken on traverses 2-6 and 4-8.
3. Steps 1 and 2 were then repeated for different fan speeds until the entire velocity range of the fan had been covered.
4. For each of the different fan speeds the mean velocities were calculated and plotted against $\sqrt{\Delta P/\rho}$ which gave a straight line calibration curve. ΔP = the static pressure drop across the contraction cone (in merian red)

ρ = density of the air (lbm/ft^3)

Figure 4.2 shows the calibration curve obtained for the experimental set-up.

The formula -

$$\overline{U} = \frac{1}{2R^2} \int_{-R^2}^{R^2} u \, d(r^2)$$

was used to calculate the average velocities for a given fan speed where

$\overline{U}$ = average pipe inlet velocity (ft/sec.)

R = pipe radius (5cm)

r = any radial distance from the center line (cm)

u = velocity at any r (ft/sec)

To obtain $\overline{U}$, u was plotted vs r^2 for a given traverse and a

planimeter used to determine the area under the curve. The area was then divided by $2R^2$ to obtain the average velocity for a traverse. The average velocities for traverse 2-6 and 4-8 were again averaged to obtain the final average velocity.

For a specified average velocity the magnitude of the static pressure drop across the contraction cone was affected by the daily changes in barometric pressure and temperature and the density of the air had to be determined prior to each test. The relative humidity was also taken for each test, however, this remained very constant and the density of the air was not affected by it.

After the wind tunnel had been calibrated, it was noted that the velocity profiles on traverses 2-6 and 4-8 were very similar. Therefore it was decided to do tests on traverse 4-8 only. With the pitot tube traversing mechanism still at the contraction cone outlet, velocity measurements were made at average inlet velocities of 50, 100, 150, 200 and 250 ft/s. The pitot tube was then installed at the diffuser inlet and velocity measurements were again obtained at the five different speeds.

4.3 CALIBRATION OF HOT-WIRE PROBES

Calibration of the Disa type 55A36 miniature hot-wire angle probe and the Disa type 55A38 miniature X-probe with respect to a known air stream velocity was required. Before any hot-wire measurements were made, however, it was decided to check out the linearizers and the accuracy of the velocity measurements of the probes.

The stability of the linearizers with respect to a change in temperature was checked. With both linearizers at room temperature, a constant input voltage was applied and the output voltages were measured at regular time intervals of approximately 5 minutes. The linearizers were then placed in an oven in which the temperature could be controlled very accurately. The temperature was raised above room temperature and the output voltage was again read at regular intervals with the input voltage being kept constant. This was repeated at several higher temperatures, with the highest at 112°F.

The variation of the linearizer output voltage with respect to a variation in line voltage was checked by means of a Variac, with which the line voltage was varied ± 20% of the average value.

The results of the linearizer stability tests are shown in Table 4.3. The maximum change in output voltage that was detected was 1.5%, which occurred when the linearizers were allowed to cool down to room temperature.

The Disa type 55D41/42 calibration unit was used for the initial calibration of the 55A36 and 55A38 probes. To check on the reliability of the hot-wire measurements, the calibration was repeated several times. The velocity measurements were found to be accurate to within ±3% above 100 ft/s, the error being slightly higher for velocities below 100 ft/s.

For measurements in the experimental wind tunnel, the rise in ambient temperature in the test section affected the hot-wire measure-

ments. It was not known how to correct for the change in ambient temperature. Therefore it was decided to calibrate the probes in the experimental tunnel itself, since the pitot tube measurements had determined that the velocity profiles at the contraction outlet were very flat and the mean velocity could be determined accurately from the wind tunnel calibration curve. The following procedure was then followed to calibrate the probes.

1. The Disa type 55A36 and 55A38 probes were placed in the pipe traversing mechanism described in Section 3.6 with the X-probe positioned at the pipe center and angle probe ¼" away from the wall. The pipe traversing mechanism was then installed at the contraction outlet.
2. The 55A38 X-probe was connected to the Disa Type 55A01 anemometers, serial numbers 338 and 817, complete with Disa Type 55D10 linearizers and the 55A36 angle probe was connected to the Disa Type 55D01 anemometer, serial No. 515.
3. The probes were brought into operation as per the Disa instruction manuals.
4. The wind tunnel fan was set at an arbitrary speed and the Bridge D.C. Voltages of the anemometers were read as well as the pressure drop across the contraction cone, which was measured by the Betz micro-monometer.

5. The fan speed was changed and step four was repeated. This was done until the entire velocity range of the wind tunnel had been covered.

The voltages were then plotted versus velocity which was determined from the wind tunnel calibration curve. Figures 4.3.1 and 4.3.2 are examples of the probe calibration curves.

4.4 TURBULENCE MEASUREMENTS USING THE HOT-WIRE ANEMOMETER

At the pipe inlet and outlet, measurements were taken on the 4-8 traverse at the same mean inlet velocities mentioned previously. The procedure that was used at each mean inlet velocity is given below:

1. With the 55A38 X-probe at the pipe center, the 55A36 angle probe was used to take measurements from .01" to .2" away from the wall. At each point the Bridge D.C. voltage was read on the Digital Voltmeter and the root mean square of the fluctuation of the Bridge D.C. voltage was read on the RMS indicator of the Disa type 55D35 voltmeter.

2a. The 55A36 angle probe was then positioned .035" from the wall and measurements were taken with the 55A38 X-probe in the range .2" to 1.97" from the wall. At each point five measurements were taken with the wires of the probe in the position they are shown in Figure 4.4. These measurements were called

A_r, B_r, $(A+B)_r$, $(A-B)_r$ and the Bridge D.C. voltage. The A signal was from side 1 of the probe and the B signal from side 2. The Bridge D.C. Voltage measurement was read from the Digital Voltmeter and the other readings were taken from the RMS Indicator on the Random Signal Indicator and Correlator.

2b. The probe was rotated 90° about the longitudinal axis of the probe and five more measurements called A_ϕ, B_ϕ, $(A+B)_\phi$, $(A-B)_\phi$, and the Bridge D.C. Voltage were taken. These measurements were read from the same indicators as in 2a.

3. The pipe traversing mechanism was rotated 180° since the traversing mechanism did not allow the probe to travel over the entire traverse. Steps 1 and 2 were then repeated to obtain the remainder of the traverse.

The static pressure at the contraction inlet and outlet, and two intermediate stations on the contraction cone were measured for each of the mean inlet velocities as well as the pressure drop in the boundary layer growth pipes.

When the first series of tests were run using the above procedure the guide vanes at the fan inlet were in the fully open position. At a mean inlet velocity of 150 ft/s, however, considerable fluctuation

in the Δ P readings across the contraction cone was noted. For this mean inlet velocity the fan was operating at approximately 760 rpm, which is equivalent to a frequency of 12.66 Hz.

The natural frequency of vibration of the air in the large duct was found by means of the formula -

$$N = a/4\ell \quad \text{.....4.4.1}$$

where N = natural frequency of gas vibrations for a closed pipe,

a = the acoustic velocity of the air in the pipe,

ℓ = pipe length.

The length of the large duct of the experimental apparatus was approximately 23 feet.

The acoustic velocity was determined by means of the formula -

$$a = \sqrt{kg_cRT} \quad \text{.....4.4.2}$$

where k = ratio of constant pressure specific heat to the constant-volume specific heat at zero pressure (1.4 for air),

g_c = 32.17 lbm-ft/lbf-sec^2,

R = gas constant (53.34 ft-lbf/lbm-^oR,)

T = absolute temperature of the air, ^oR.

At a temperature of 539^oR

$$a = 1138 \text{ ft/s}$$

Therefore N = 12.35 Hz , which corresponds fairly closely with the fan frequency.

The resistance to the air flow was increased by nearly closing the inlet vanes. The airspeed of 150 ft/s was restored by increasing the fan speed. The fan no longer ran at the resonant frequency of the duct and the fluctuation of the ΔP reading was reduced considerably. Therefore, whenever tests were conducted at a mean inlet velocity of 150 ft/s the fan inlet vanes were always set at the nearly closed position.

4.5 LOW VELOCITY HOT-WIRE MEASUREMENTS

For low velocity hot-wire measurements in the large duct, the 55A38 hot-wire X-probe was calibrated in the Disa Type 55D41/42 calibration unit. The Hero alcohol manometer shown in Figure 3.8.6 was used to measure the pressure differential for low velocity calibration. For velocities in the range of 2-5ft/s it was found that higher accuracy was obtained by setting the gain of the linearizers at the maximum possible value in order to increase the sensitivity.

After calibration, the 55A36 probe was placed in the traversing mechanism described in section 3.6 and the measurements described in section 4.4 were taken at points on the 2-6 and 4-8 traverses at the contraction cone inlet for mean inlet speeds of 200 and 250 ft/s.

The Disa Type 55A80 low velocity anemometer (section 3.8.3) was also used to measure velocities in the large duct of the experimental apparatus. The Disa Type 55D81 low velocity transducer used in conjunction with the 55A80 anemometer was first calibrated in the 55D41/42 calibration unit and then placed in the probe holder as shown in Figure

3.8.10. The holder, together with the transducer was mounted in position 4 on the 4-8 traverse at the contraction inlet. Velocity measurements were made at mean inlet speeds of 50, 100, 150, 200 and 250 ft/s.

4.6 INTERPRETATION OF READINGS

The procedure followed for obtaining meaningful results from the turbulence is given in Hinze (1959) and is described in detail by Slusar (1969) and outlined below.

The Bridge D.C. Voltages from the anemometers were used to determine the mean velocities directly from the respective calibration curves of the 55A36 and 55A38 probes.

The turbulence intensities were calculated by means of the following formulas:

$$u'_x = \frac{(A+B)_r + (A+B)_\phi}{4m}$$

$$u'_r = \frac{(A-B)_r}{2m}$$

$$u'_\phi = \frac{(A-B)_\phi}{2m}$$

where

u'_x = intensity of the axial turbulence velocity component.

u'_r = intensity of the radial turbulence velocity component.

u'_ϕ = intensity of the turbulence velocity component perpendicular to the radial direction.

The r subscripted readings are those taken with the plane of the wires parallel to the radial direction and for the ϕ subscripted readings the plane of the probe was perpendicular to the radial direction.

The correlation coefficients $R_{\overline{u_x u_r}}$ and $R_{\overline{u_x u_\phi}}$ were obtained by means of the following formulas.

$$R_{\overline{u_x u_r}} = \frac{A_r^2 - B_r^2}{(A+B)_r (A-B)_r}$$

$$R_{\overline{u_x u_\phi}} = \frac{A_\phi^2 - B_\phi^2}{(A+B)_\phi (A-B)_\phi}$$

All of the above mentioned calculations were carried out by means of an IBM 360/65 computer.

V. ANALYSIS AND DISCUSSION OF RESULTS

5.1 INTRODUCTION

In this chapter the basic results of the experimental work, which are presented in Figures 5.1 to 5.17 will be discussed. The data was calculated by means of an IBM 360/65 computer and the program is given in the Appendix.

5.2 VELOCITY MEASUREMENTS

One of the main objectives at the start of the experimental testing was to obtain symmetric velocity profiles in the entire length of the test section. Figure 5.1 and 5.2 show the velocity profiles measured by means of the pitot tube. Figure No. 5.1 shows that the velocity profiles at the entrance to the boundary layer growth pipes are symmetric and that a flat velocity profile was produced by the contraction cone.

Figure 5.2 shows the diffuser inlet velocity profiles as measured by means of the pitot tube. This graph shows that the velocity profiles are symmetric and that the boundary layer growth pipes do not produce any undesirable effects on the profiles. In his thesis, H. Krueger (1970) shows the velocity profiles in the diffuser, which demonstrate that the flow in the diffuser is symmetric as well.

Starting at the contraction inlet, Figure No. 5.3 shows the static pressure at different points along the test section, up to the diffuser inlet. It can be seen that no adverse pressure gradients were detected in the contraction. It was not determined that the flow at the

exit was parallel, however, other than that, it may be concluded that the two basic requirements of a contraction cone are fulfilled, which are:

1. "The exit velocity must be uniform and parallel."

2. "There must be no regions of separation caused by adverse pressure gradients at the wall which may appear at the start of contraction and at the outlet." (Bossel 1969)

Figure No.5.4 and 5.5 show the velocity profiles on the 0-8 traverse as measured by means of the Hot-wire anemometers. The agreement between the 55A36 and 55A38 probes was found to be within ±2% at a mean inlet velocity of 250'/s, with the error decreasing as the mean inlet velocity was decreased.

The hot-wire velocity measurements were found to be within approximately 3% of the pitot tube measurements. The Bridge D.C. Voltage reading may have contributed a considerable amount to this error since it is accurate to ±1% at full scale deflection. There may also be an error of approximately ±1% in ΔP across the contraction cone for determining the mean inlet velocity. Change in the ambient temperature (±1°F) of the air in the test section affects the heat transfer from the wire and thus the Bridge D.C. Voltage is also affected.

Table 5.1 shows the results of the low velocity measurements at the contraction inlet made by means of the Disa 55D80/81 Low Velocity Anemometer. The second column shows the velocities obtained by the anemometer and the third column shows the theoretical value obtained

from the continuity equation, with the assumption that the flow is incompressible. For a mean inlet velocity of 50 ft/s the anemometer could be operated on the low velocity anemometer mode and no calibration was required. For the mean pipe inlet velocities of 100, 150, 200 and 250 ft/s the constant current mode of the anemometer was used. The error in these measurements were as high as 9% with the maximum error occurring at the mean pipe inlet velocity of 150 ft/s.

The main source of error in the low velocity measurements was in the method of calibration. The only facility available for probe calibration was the Disa Type 55A41/42 calibration unit. At 3.5 ft/s the error in the pressure measurement across the contraction of the calibration unit was approximately 5%. The error in the pressure measurements, however, increased to approximately 50% at 1 ft/s. From 0-1 ft/s the constant current mode of the anemometer was calibrated quite accurately by the LVA mode of operation.

The 55D80/81 anemometer was calibrated at room temperature. An increase of approximately 10°F. above room temperature was experienced in ambient temperature in the test section at a mean inlet speed of 250 ft/s. This introduced an error, since the increase in ambient temperature decreased the heat transfer from the wire, causing the anemometer to read low.

5.3 TURBULENCE MEASUREMENTS

Distributions of relative turbulence intensities $u'_x/\overline{U}_{x,max}$ $u'_r/\overline{U}_{x,max}$, and $u'_\phi/\overline{U}_{x,max}$ at the contraction inlet and outlet and the

diffuser inlet are shown in Figures 5.6 and 5.7 for mean inlet velocities of 200 and 250'/s. The turbulence intensities are constant across the entire cross-section at the inlet and outlet of contraction. The longitudinal turbulence intensity was reduced from approximately 2% to approximately .4% across the contraction cone, whereas the $u'_r/\overline{U}_{x,max}$, and $u'_\phi/\overline{U}_{x,max}$, remained relatively constant.

The turbulence intensities at the diffuser inlet vary considerably from a high at the wall of the pipe to almost zero at the centre. The level of turbulence in the central portion of the pipe at the diffuser inlet is the same as the turbulence level throughout the entire cross-section at the contraction outlet, which was almost zero. This indicates that the flow was not fully developed entering the diffuser as was previously mentioned by Slusar (1969) and van der Spiegel (1969). The velocity profiles shown in Figure 5.2 also bear out this fact.

Figure 5.8 shows the intensities of the three turbulence velocity components relative to the maximum velocity in the pipe at each of the five mean inlet velocities. According to Hinze (1959) -

> "The turbulence is called isotropic of its statistical features have no preference for any direction, so that perfect disorder reigns".

As can be seen in Figure 5.8, the degree of anisotropy increases towards the wall of the pipe. The longitudinal turbulence velocity component has the highest value and the radial component has the smallest value. These results show the same general trend as those obtained by J. Laufer (1954) for fully developed turbulent pipe flow and Klebanoff (1954) in

a boundary layer along a smooth wall with zero pressure gradient. The relative turbulence intensities are lower than those obtained by Laufer, however, this is to be expected since the flow in the pipe has not become fully developed turbulent flow. The intensities for the mean inlet velocities of 150, 200 and 250 ft/s were relatively equal, whereas the values for 50 and 100 ft/s were somewhat lower.

Plotting the turbulence intensities relative to the wall-friction velocity, as is done in Figures 5.9, 5.10 and 5.11 - shows that close to the wall u'_x is approximately 1.75 times the wall friction velocity and u'_r is about .75 of the wall friction velocity for mean inlet velocities of 150, 200, and 250 ft/s: Laufer (1954) obtained approximately 2.6 and 1 respectively for these values. From Figure 5.9 it can be seen that u'_x reaches a maximum value at about a/R =.05, whereas Laufer (1954) showed that this occurred at a/R = .0017.

Figure 5.12 shows the distribution of turbulent kinetic energy per unit mass $(\frac{1}{2}\overline{q^2})$at the diffuser inlet for the five mean inlet velocities. Since the turbulence intensities were at a maximum near the wall, the turbulence energy is also at a maximum near the wall. If, however, $\overline{q^2}/U_*^2$ is plotted as shown in Figure 5.13, it is seen that the data for the mean inlet velocities of 150, 200 and 250 ft/s form a single line. Figure 5.5 shows that the boundary layer for mean inlet velocities of 150, 200 and 250 ft/s was nearly the same, whereas the velocity profiles for the 50 and 100 ft/s mean inlet velocities were not as fully developed.

The Reynolds numbers, based on the mean velocity and pipe

diameter, for the five different speeds are 27,500, 195,000, 292,000, 390,000, and 476,000. From Figures 5.9, 5.10 and 5.11 it can be seen that the Reynolds number does not have an effect on the turbulence intensities with respect to the friction velocity provided that the boundary layer is of the same thickness. A similar conclusion may be drawn from Figure 5.13 for the turbulence energy divided by the square of the friction velocity. The turbulence intensities indicate the thickness of the boundary layer, since the turbulent region fills approximately the same region of the pipe as the boundary layer does.

The correlation coefficients $R_{\overline{u_x u_r}}$ and $R_{\overline{u_x u_\phi}}$ were plotted versus a/R in Figures 5.14 and 5.15. $R_{\overline{u_x u_r}}$ remained fairly constant at -.5 in the region of the pipe from a/R = .1 to .3 and then approached zero as the potential core was reached. This occurred for the mean inlet velocities of 150, 200 and 250 ft/s. $R_{\overline{u_x u_r}}$ for 100 ft/s mean inlet velocity showed the same general trend as the higher velocities, however, the maximum value was only -.4 and remained so only from a/R = 1. to .15. For the mean inlet velocity of 50'/s the measurements with the X-probe were mainly in the potential core, where the turbulence level remained constant at nearly zero, and therefore $R_{\overline{u_x u_r}}$ remained constant as well for this speed.

Laufer obtained values of $R_{\overline{u_x u_r}}$ for fully developed pipe flow from -.3 near the wall, to approximately -.5 within the boundary layer, with the value becoming zero at the centre of this pipe. Therefore the values of $R_{\overline{u_x u_r}}$ obtained for mean inlet velocities of 100, 150, 200, and

250 ft/s compare quite well with those of Laufer.

The correlation coefficient $R_{\overline{u_x u_\phi}}$ shows the same general trend as $R_{\overline{u_x u_r}}$, however, the magnitude is smaller and the points appear to be more erratic.

Figure 5.16 shows the turbulent shear stress divided by the friction velocity. The same general trend was indicated by the shear stress as was exhibited by the turbulent energy. Plotting the shear stress over the turbulent energy versus a/R as in Figure 5.17 shows that a fairly constant value of 0.15 for $\overline{u_x u_r}/\overline{q}^2$ is obtained in the turbulent region of the pipe. This trend was also shown by Laufer and also by Klebanoff in boundary layer flow.

The errors involved in obtaining the mean velocities have been discussed previously in this chapter. The probable errors in the turbulence parameters which have just been discussed, are considerably higher, however, than the error in the velocity measurements. The accuracy of the meter readings was approximately 3%. Therefore the error in the determination of the correlation coefficients could be as high as 10% due to the method in which it was determined. (Section 4.6)

For the low velocity measurements, however, the error in the turbulence parameters was considerably higher, due to the large fluctuations in the meter readings. A 30% error in the turbulence parameters at the contraction inlet was estimated.

5.4 CONTRACTION CONE DESIGNS

The results of the designs for the 16/1 and 89:1 contraction cones are shown in Figures 5.18 to 5.50. 5.18 shows the wall contours of the contractions for which solutions were obtained. The 16/1 contraction was designed by Bossel, and the 89:1 is the contraction that was used in the experimental test apparatus. The dotted contour shows the proposed change to the existing contraction cone.

The theoretical velocities at the centre line and the wall of the different contraction cones are shown in Figure 5.19. This Figure shows that theoretically no adverse pressure gradients were produced by the 89:1 contraction cone. This was verified by experimental evidence, since Figure 5.3 shows that no adverse pressure gradients were detected. The pressure gradient, however, changes very abruptly at the exit, x=2.26, and for this reason it was felt that a new contraction should be built. Figure 5.13 also shows the centreline and wall velocities for the design on an 89:1 contraction which had been increased in length by approximately 1 foot over the existing contraction cone.

The theoretical and experimental velocity profiles at the exit are shown in Figure 5.20 and the agreement is very good. The theoretical entrance velocity profile is also shown in Figure 5.20. The solution is periodic axially and, hence, does not in practice satisfy the near-uniform stream conditions obtained at inlet and outlet of a contraction, at any point either up-stream or down-stream. The fact that the entrance and exit velocity distributions in a contraction cannot be both uniform and

parallel if entrance and exit are a finite distance apart as a basic result of potential theory and not of the particular solution used.

The design method by Bossel, which was described in Chapter 2, was found to be quick and relatively simple once the computer program for it had been determined. With this method, existing contraction cones can be analysed and the case tested gave experimental evidence to support the method.

The method by Bossel produces a contraction cone of finite length, whereas in the methods used by Tsien, Szczeniowski and Cohen and Ritchie, the shortness of contraction could not be predetermined. Also, in the method used by Cohen and Ritchie, it appeared to be difficult to obtain the proper contraction ratio. The computation for these methods is also considerably more than for the method used by Bossel.

The method used by Thwaites also produced a contraction of finite length. If, however, a large number of terms (more than 6) in the Fourier Series were to be determined, the computation increased considerably.

Bossel also investigated the possibility of interchangeable exit sections. The contour of the first half of the contraction cone was kept the same and only the latter portion of it was altered for different contraction ratios. Therefore, if it was desirable to use different contraction ratios in an experimental set-up, only the latter portion of the contraction need be changed. This could produce a considerable saving in manufacturing. This feature is not possible with the other design

methods mentioned above, since the contraction contour would not necessarily be the same for any portion of the contraction cone for different contraction ratios.

VI. CONCLUSIONS AND RECOMMENDATIONS FOR FUTURE WORK

From the measurements that were taken the following conclusions may be made:

1. The flow in the test section is symmetric.
2. Contraction reduces the longitudinal turbulence intensity.
3. The turbulence intensities at the diffuser inlet are non-isotropic.
4. The flow entering the diffuser is not fully developed turbulent flor.
5. Using the friction velocity U_* as a similarity parameter, it was found that the turbulence parameters were independent of the Reynolds number in the range 97,500. to 476,000., provided the turbulent boundary layer was of the same thickness.
6. The turbulent region of the pipe fills approximately the same portion of the pipe as the boundary layer does.
7. The ratio of the turbulent shear stress to the turbulent kinetic energy has a constant value in the turbulent boundary layer.
8. The trends in the turbulence parameters mentioned above are similar to those found by previous investigators in fully developed pipe flow.

For a better understanding of the effect of contraction on turbulence, more accurate methods of determining turbulence parameters upstream of the contraction should be devised. A more accurate method of probe calibration should also be determined for hot-wire measurements in the velocity range from 0-5 ft/s than was used in the experimental work of this thesis. A method of measuring the velocity adjacent to the wall in the contraction cone should be devised, and the possibility of using an angle probe for this should be looked into.

In order to obtain a complete picture of the flow in contraction cones, several different contraction ratios should be built and tested.

REFERENCES

BOSSEL, H.H., (1969) "Computation of Axisymmetric Contractions," AIAA Journal, Vol. 7, No. 10, pp. 2017-2020.

COCKRELL, D.J. & MARKLAND, E. (1963) "A Review of Incompressible Diffuser Flow," Aircraft Engineering, Vol.35, pp.286-292.

COHEN, M.J. & RITCHIE, N.J.B.(1962) "Low Speed Three-Dimensional Contraction Design," Journal of the Royal Aeronautical Society Vol. 66, pp. 231-236.

DISA, (1966) Instruction and Service Manual for Type 55D01 Anemometer Unit, Denmark: Disa Electronik.

DISA, (1966) Instruction and Service Manual for Type 55D10 Linearizer, Denmark: Disa Electronik.

DISA, (1969) Instruction and Service Manual for Type 55D80/81 Low Velocity Anemometer, Denmark: Disa Electronik.

HINZE, J. O. (1959) "Turbulence. An Introduction to its Mechanism and Theory. New York: McGraw-Hill Book Company Inc.

KRUEGER, H. (1970) Turbulent Flow in a Diffuser, M.Sc. Thesis, University of Manitoba.

LAMB, H. (1879) Hydrodynamics, 6th edition, Dover, New York, (1945 Reprint) pp. 134-139

LAUFER, J. (1954) The Structure of Turbulence in Fully Developed Pipe Flow, NACA Report 1174.

LIPKA, R. (1968) An Experimental Investigation of A Straight Conical Diffuser, M.Sc. Thesis, University of Manitoba.

con't.

LITCHY, L.C. (1967) Combustion Engine Processes. New York: McGraw-Hill Book Company Inc.

MCDONALD, A.T. & FOX, R.W. (1965) An Experimental Investigation of Incompressible Flow in Conical Diffusers, ASME Reprint 65-FE-25.

SLUSAR, G.G. (1969) Turbulence Measurements in a Straight Conical Diffuser, M.Sc. Thesis, University of Manitoba.

SPRENGER, H. (1959) Experimental Investigation of Straight and Conical Diffusers, Mitt. inst. Aerodyn, Zurich (27).

SZCENIOWSKI, B. (1943) "Contraction Cone for a Wind Tunnel," Journal of the Aeronautical Sciences, Vol. 10, No. 8, pp. 311,312

THWAITES, B. (1946) "On the Design of Contractions for Wind Tunnels," R&M 2278, British Aeronautical

VAN der SPIEGEL, P. (1969) An Experimental Investigation of the Turbulent Boundary Layer in a Straight Conical Diffuser, M.Sc. Thesis, University of Manitoba.

TABLE 3.1

VIBRATION MEASUREMENTS

CONTRACTION INLET

Reeds Vibrometer (CPS)	RPM	Displacement (inches)
600	602	.03
700	700	.022
800	800	.04
850	850	.05
875	875	.09
883	883	.08
900	900	.06
925	925	.05
950	950	.03
1000	1000	.03
Fan Outlet		
600	600	.025
700	700	.02
800	800	.02
850	850	.02
900	900	.02
950	950	.02
1000	1000	.01

After the corrective measures mentioned in section 3.1 had been made, the fan was run over the above range and the maximum displacement was found to be .03 inches.

TABLE 3.3

CONTRACTION ROUNDNESS MEASUREMENTS

Stations	A	B	C	D	E	F	G	H	I	J	K	L	M	N	O	P
1	0	-3	+7	0	-14	-26	-27	-10	-54	-58	-50	-33	-21	-24	-17	-14
2	0	-8	-20	-30	-86	-104	-79	-101	-119	-100	-99	-75	-39	-24	+2	+1
3	0	+37	+8	-31	-67	-79	-75	-98	-86	-71	-119	-124	-112	-55	-16	-13
4	0	+40	+18	-10	-25	-40	-54	-21	+20	-56	-122	-200	-140	-68	-40	-39
5	0	-20	-34	-24	-31	-36	-60	-17	+10	-16	-79	-173	-119	-73	-56	-40
6	0	-10	-23	+25	+14	+14	+17	+24	+32	+40	-57	-100	-56	-64	-29	-47
7	0	-16	-5	+43	+30	+39	+28	+29	+43	+45	-35	-85	-88	-61	-25	-72
8	0	-21	+12	+53	+59	+42	+24	+40	+18	+30	-51	-112	-95	-86	-14	-62
9	0	+39	+22	+94	+64	+62	+134	+92	+80	+75	+14	-23	-50	-46	+77	-12
10	0	-8	+41	+79	+78	+56	+106	+104	+99	+977	-8	-27	-45	-57	+29	-11
11	0	+19	+77	+82	+123	+87	+105	+141	+120	+97	+48	+5	-16	-50	+24	-34
12	0	+24	+50	+74	+47	+80	+98	+128	+100	+78	+57	+69	+32	-5	+4	-32
13	0	+148	+181	+113	+101	+183	+157	+100	+128	+131	+109	+111	+80	+86	+35	+10

All measurements in thousands of an inch.

TABLE 4.3

LINEARIZER STABILITY TESTS

55D10 LINEARIZER, SERIAL # 133

Time PM	Temp. °F	Input Voltage	Output Voltage
2:45	77	6.98	8.99
2:50	77	6.97	8.98
3:00	98	6.97	8.92
3:05	102	6.97	8.90
3:10	102	6.97	8.89
3:15	104	6.97	8.86
3:20	105	6.97	8.84
3:25	105	6.97	8.82
3:30	106	6.97	8.79
3:35	106	6.97	8.77
3:40	107	6.97	8.76
3:45	107	6.97	8.74
3:50	108	6.97	8.72
3:55	108	6.97	8.71
4:00	108	6.97	8.69
4:05	108	6.97	8.68
4:10	108	6.97	8.66
4:15	108	6.97	8.66
4:45	77	6.97	8.655
5:00	77	6.97	8.685
5:15	77	6.98	8.90

A ±20% change in line voltage caused .04 variation in output voltage.

55D10 LINEARIZER, SERIAL # 190

Time PM	Temp. °F	Input Voltage	Output Voltage
12:50	78	6.99	9.03
1:00	76	6.99	9.00
1:05	76	6.99	9.00
1:30	98	6.98	9.01
1:35	99	6.98	9.00
1:40	99	6.98	9.01
1:45	106	6.98	9.01
1:50	109	6.98	9.03
1:55	112	6.98	9.02
2:10	78	6.98	8.96
2:15	76	6.97	8.95
2:20	76	6.97	8.94
2:25	76	6.97	8.93
2:30	77	6.97	8.91
2:35	77	6.97	8.91

Varying the line voltage from +20% to -20% caused a voltage fluctuation of .03mv. The lower line voltage had the greatest effect.

TABLE 5.1

LOW VELOCITY MEASUREMENTS

Mean Pipe Inlet Velocity (ft/s)	Hot Wire Results (ft/s)	Theoretical Values From Equating of Continuity (ft/s)	% Error
50	.589	.562	-4.58
100	1.1	1.124	+2.2
150	1.85	1.685	+8.91
200	2.1	2.25	+7.14
250	2.65	2.81	+6.27

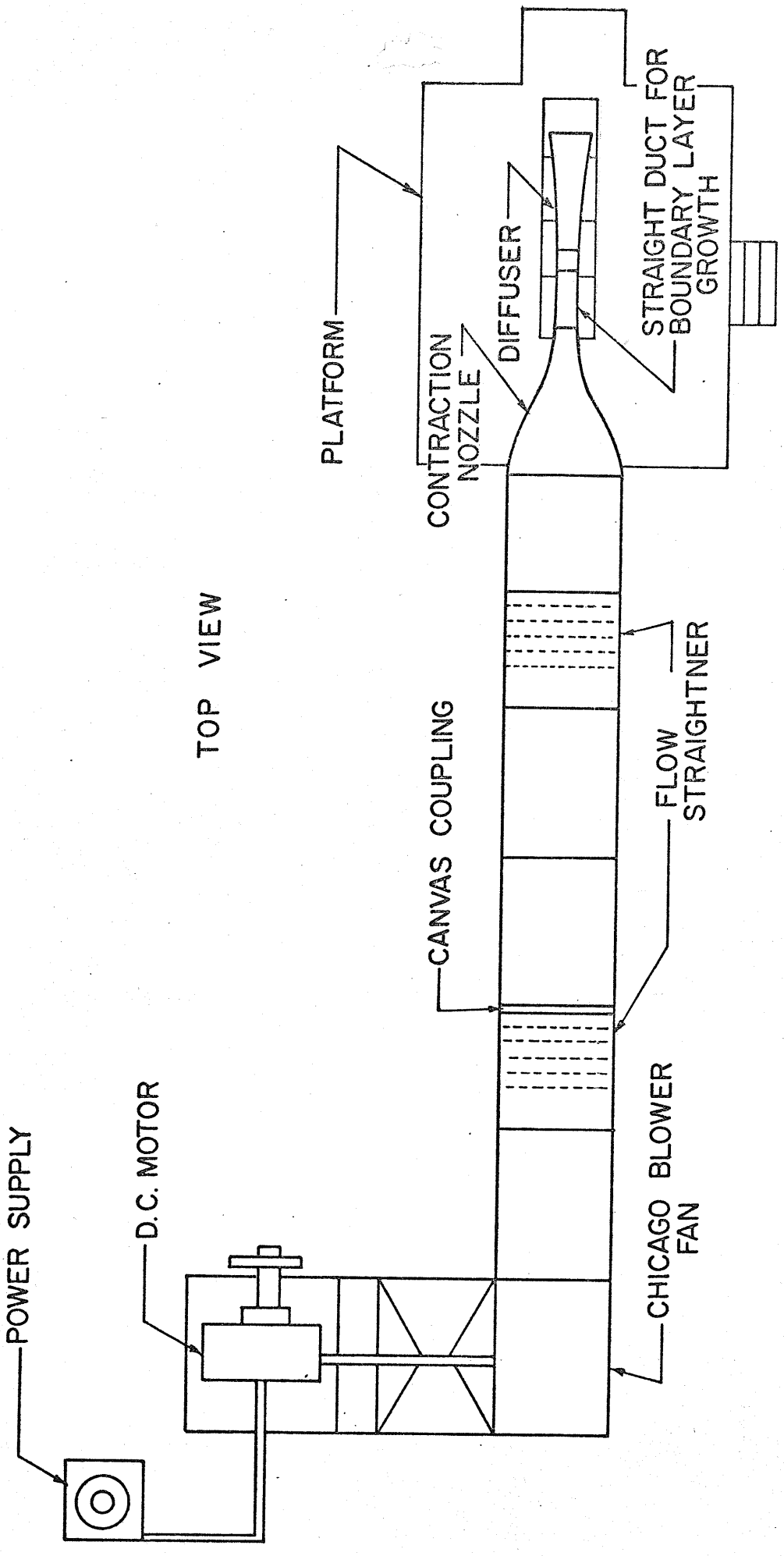

FIGURE 3.1 (a) EXPERIMENTAL APPARATUS

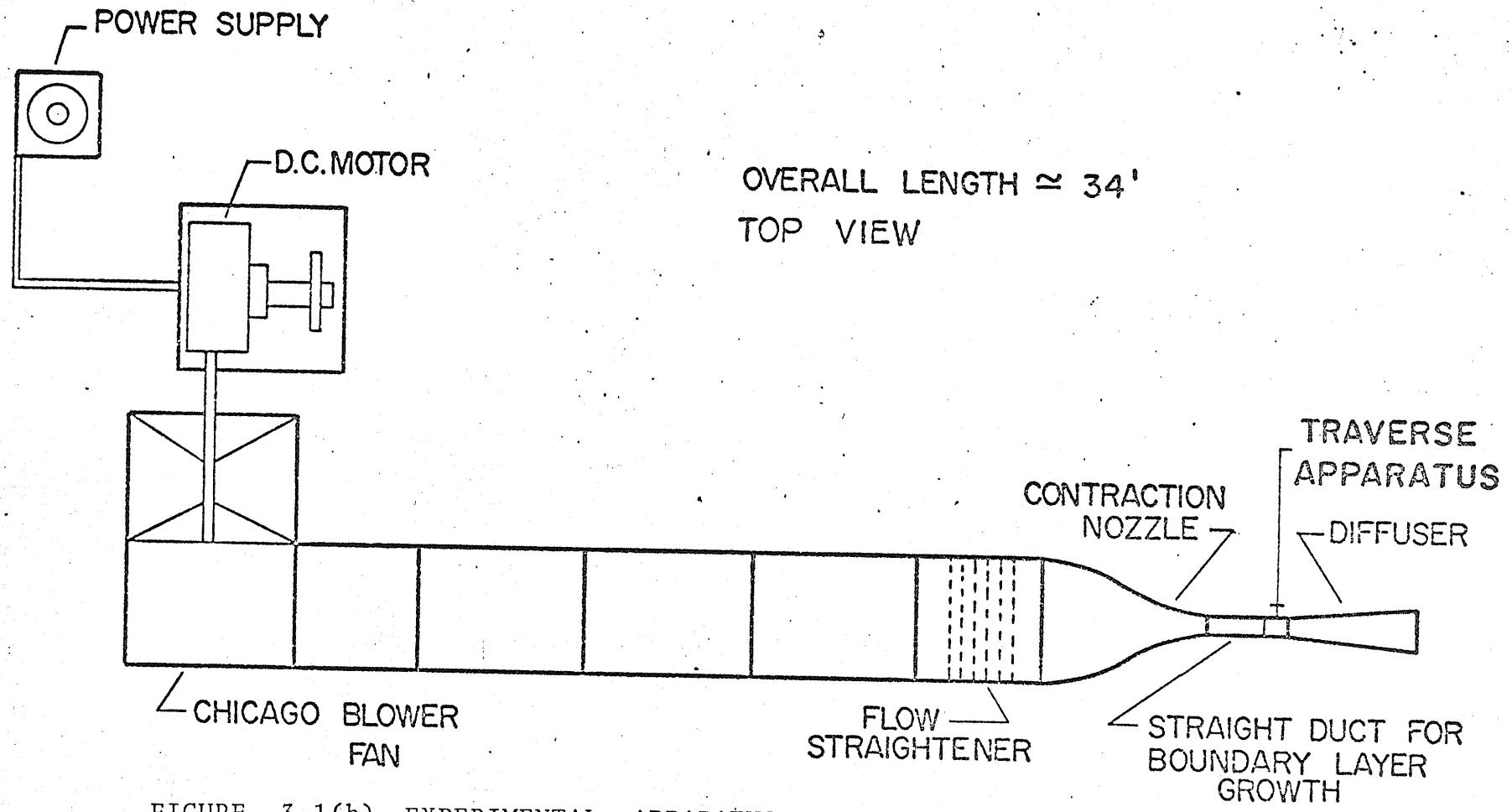

FIGURE 3.1(b) EXPERIMENTAL APPARATUS BEFORE MODIFICATIONS

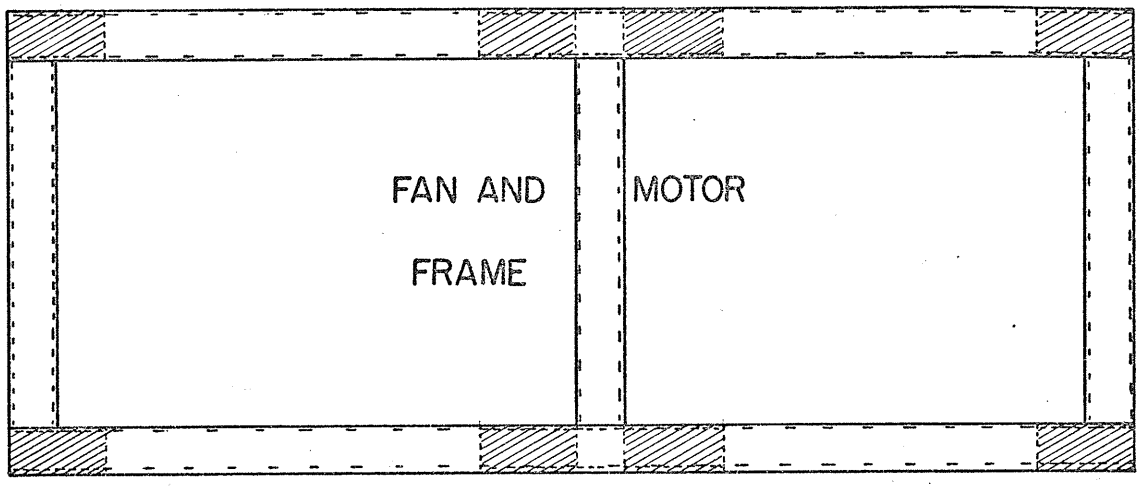

FAN OUTLET

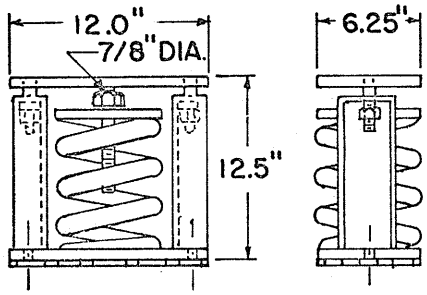

MSLCR-SINGLE SPRING

SIDE VIEW

LOCATION OF SPRING

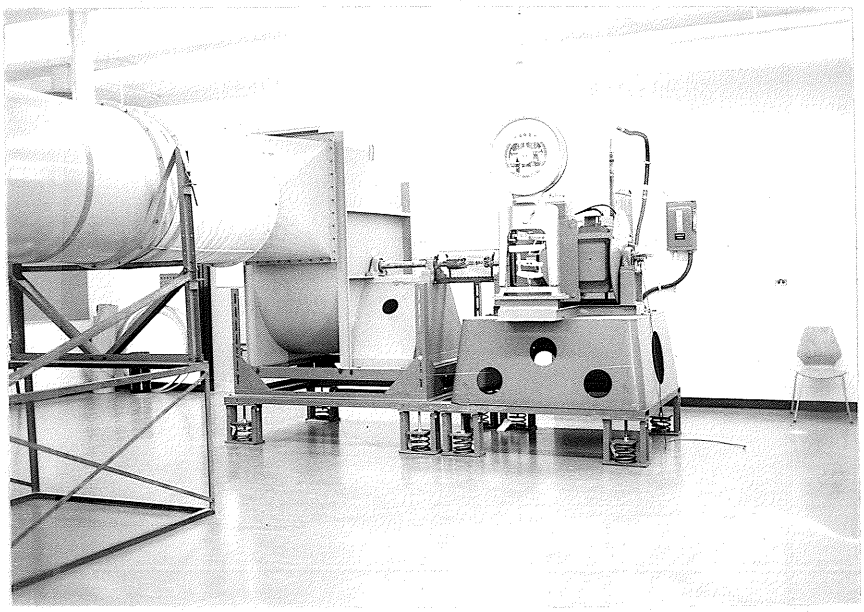

FIGURE 3.2

VIBRATION ISOLATORS AND FRAME

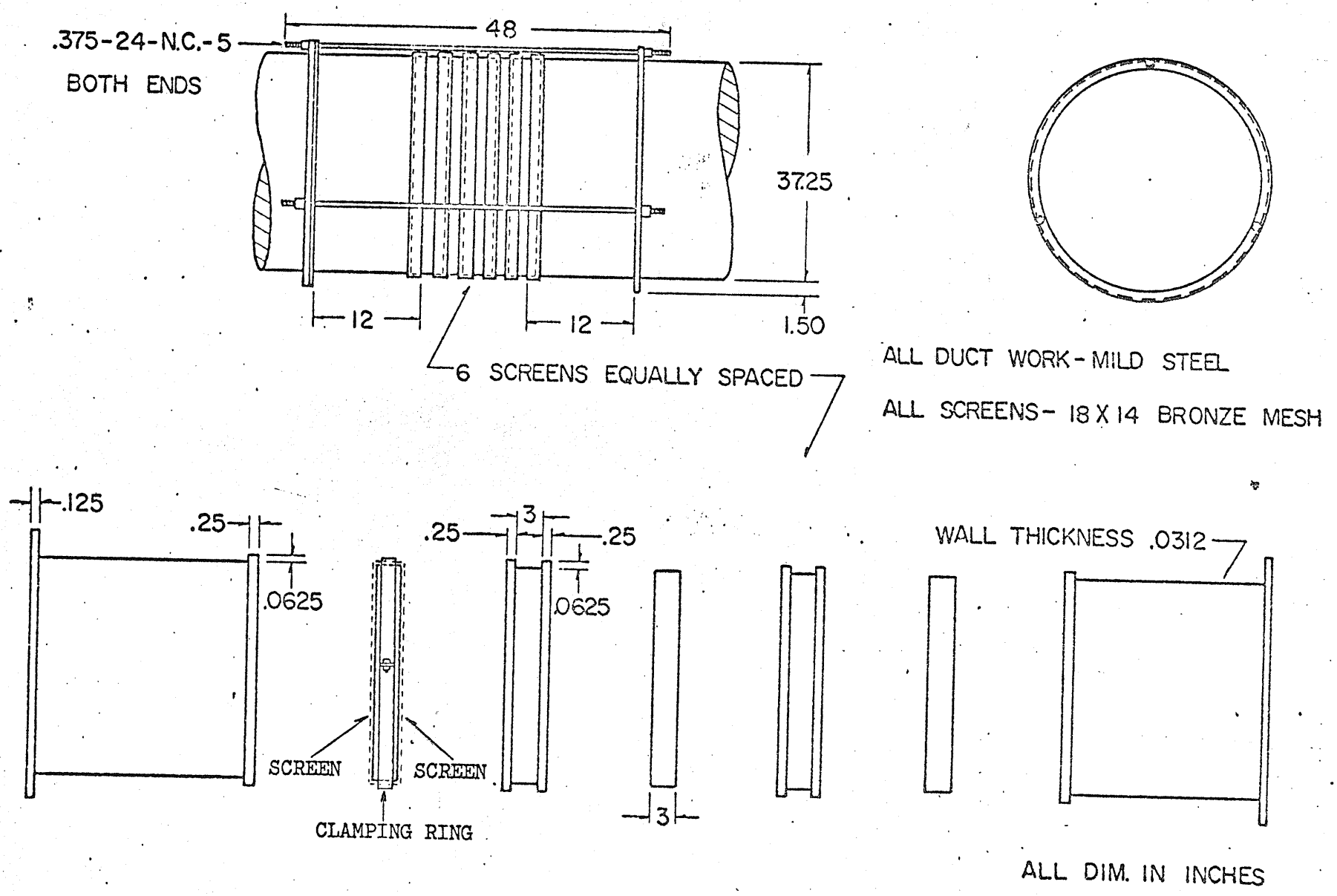

FIGURE 3.3 FLOW STRAIGHTENER

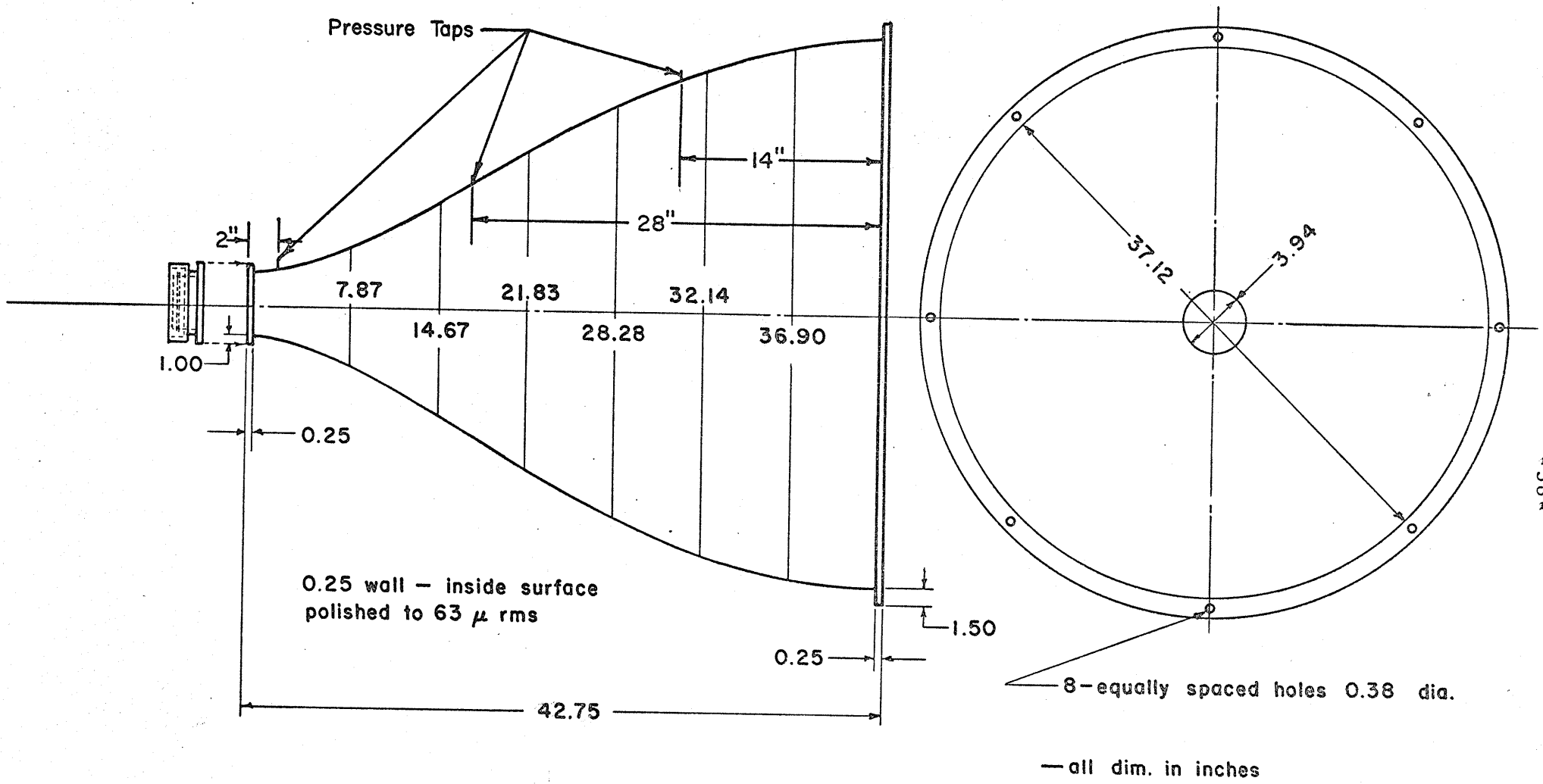

FIGURE 3.4.1 CONTRACTION NOZZLE

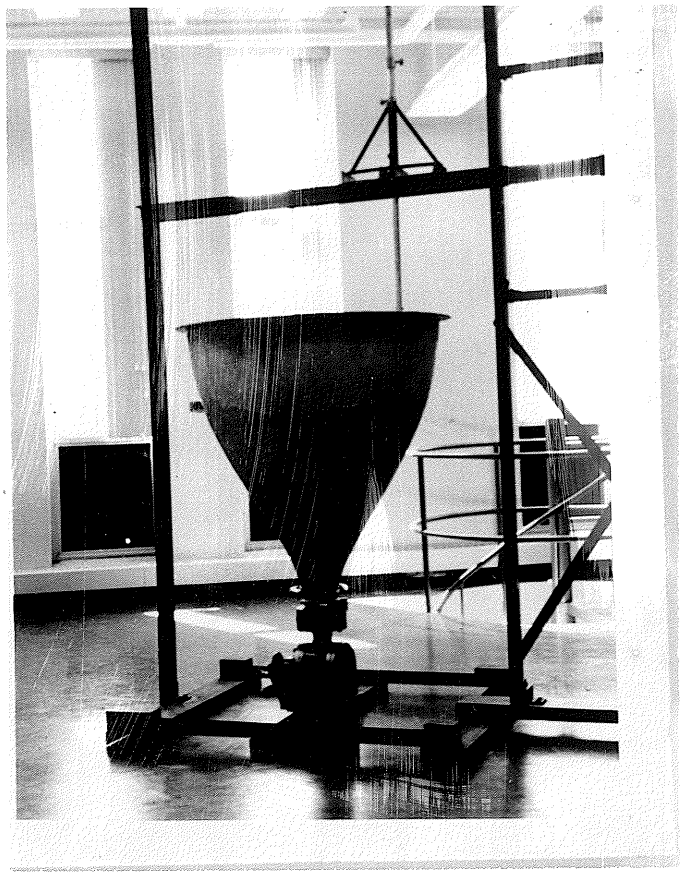

FIGURE 3.4.2

CONTRACTION ROUNDNESS MEASURING APPARATUS

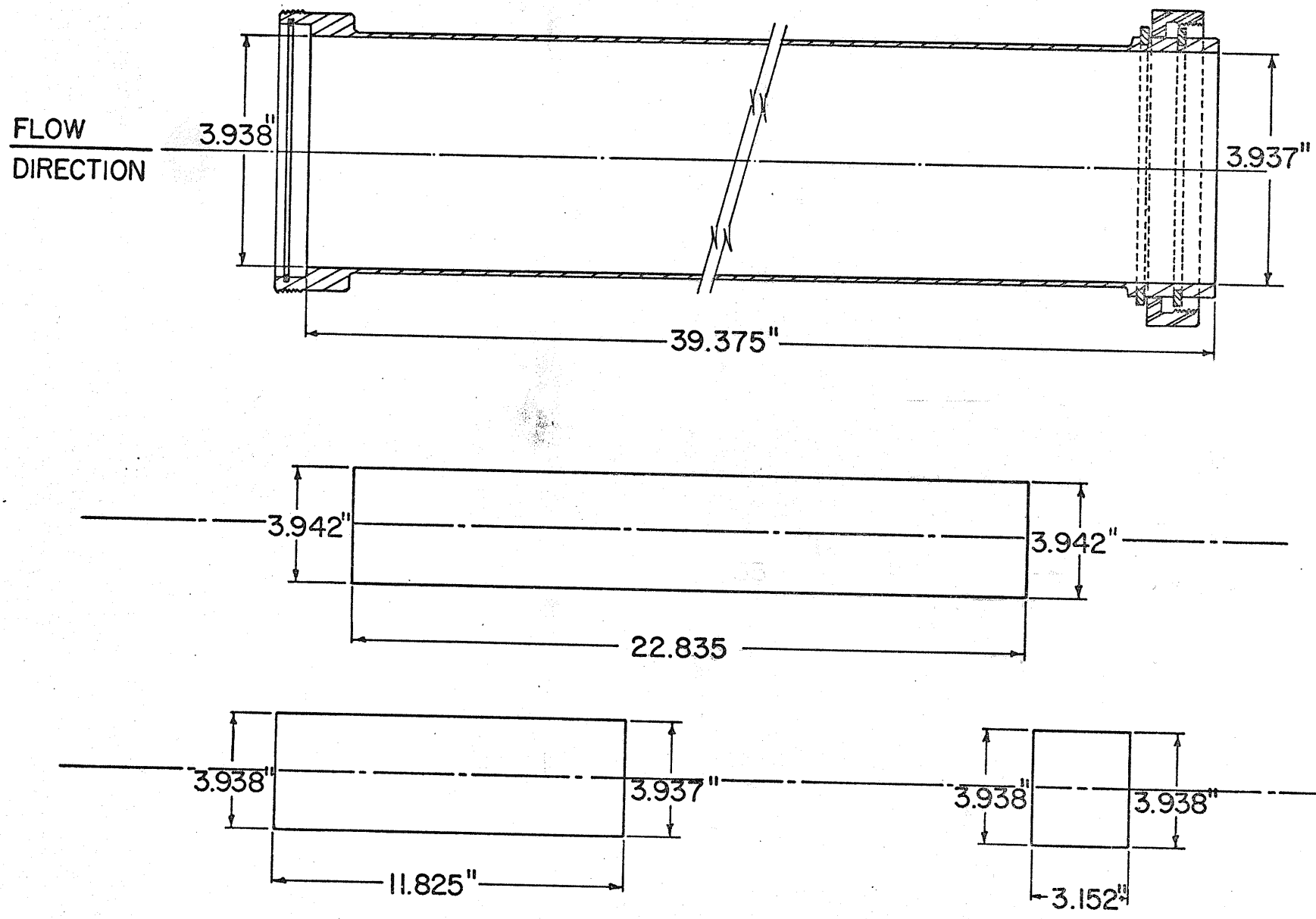

FIGURE 3.5 BOUNDARY LAYER GROWTH PIPES

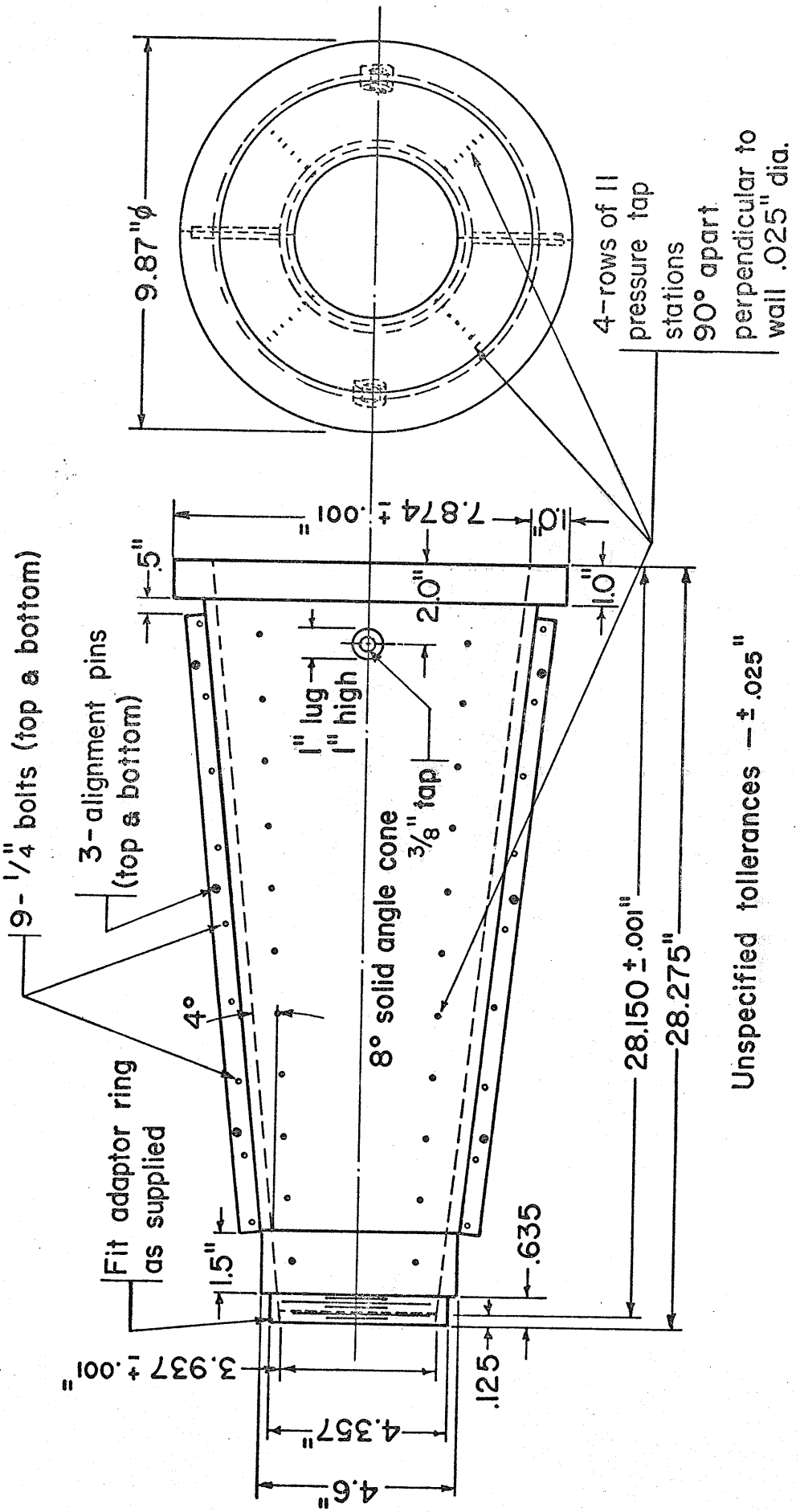

FIGURE 3.6 CONICAL DIFFUSER

Not To Scale

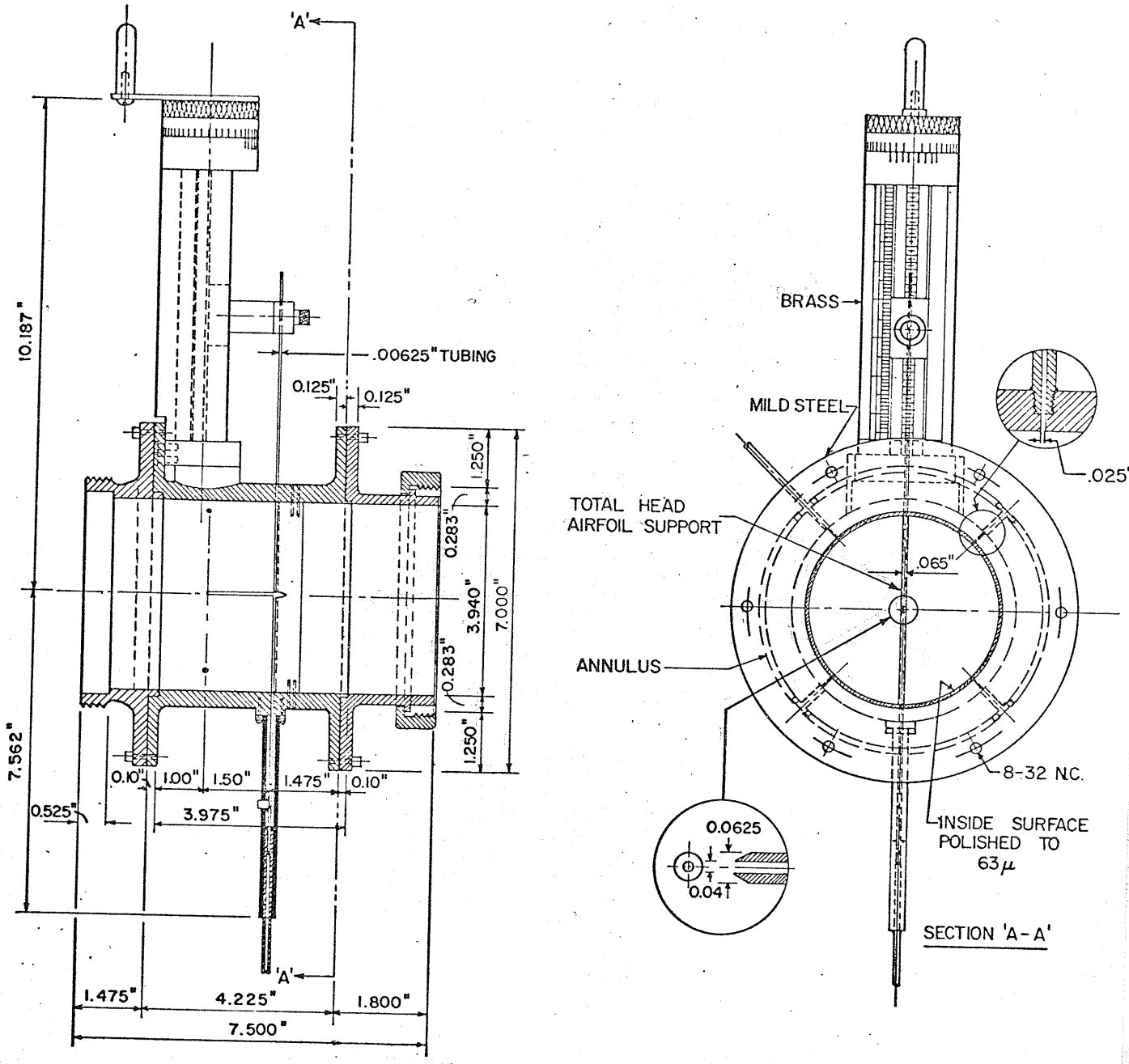

FIGURE 3.7.1

PITOT TUBE TRAVERSING MECHANISM

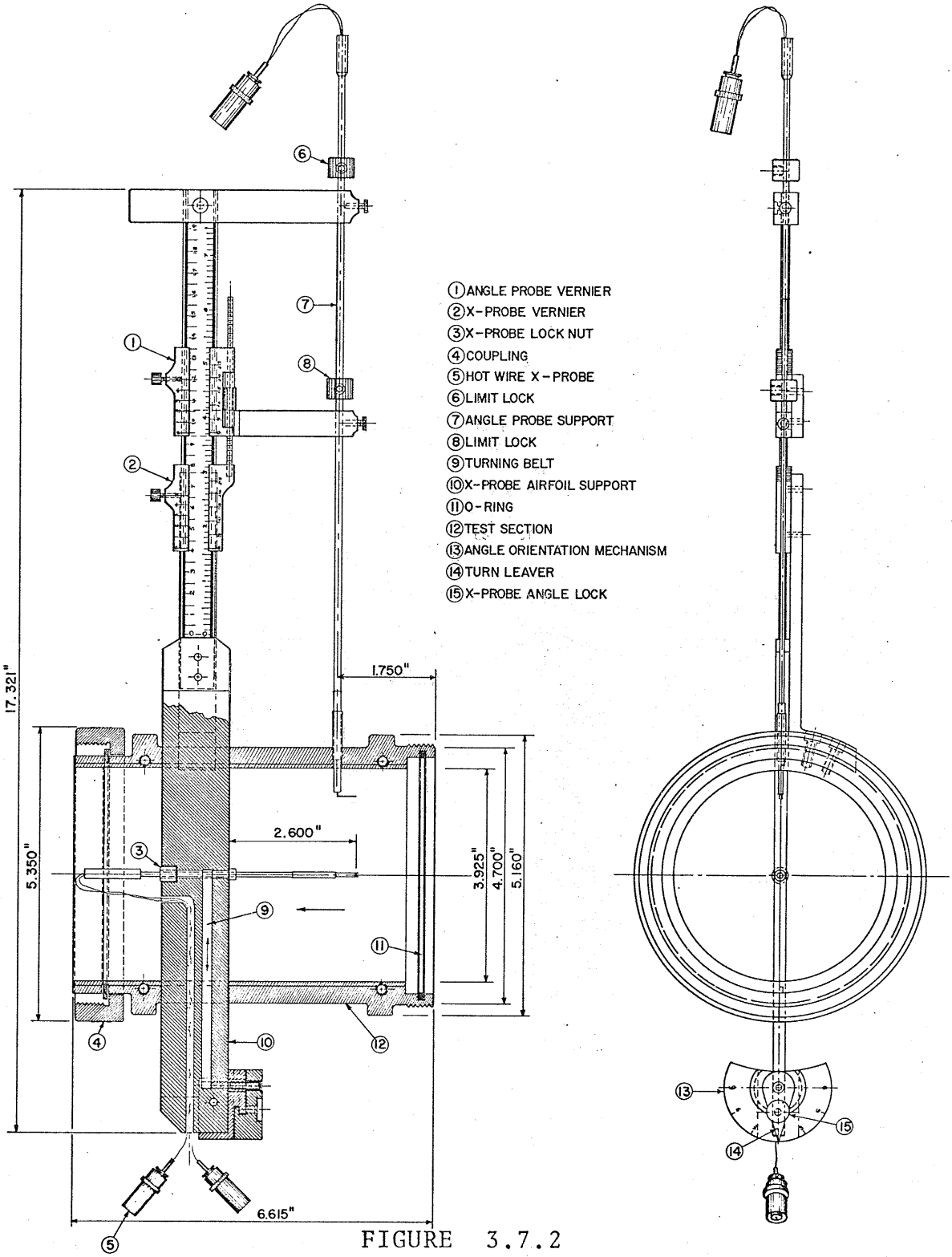

FIGURE 3.7.2

PIPE TRAVERSING MECHANISM

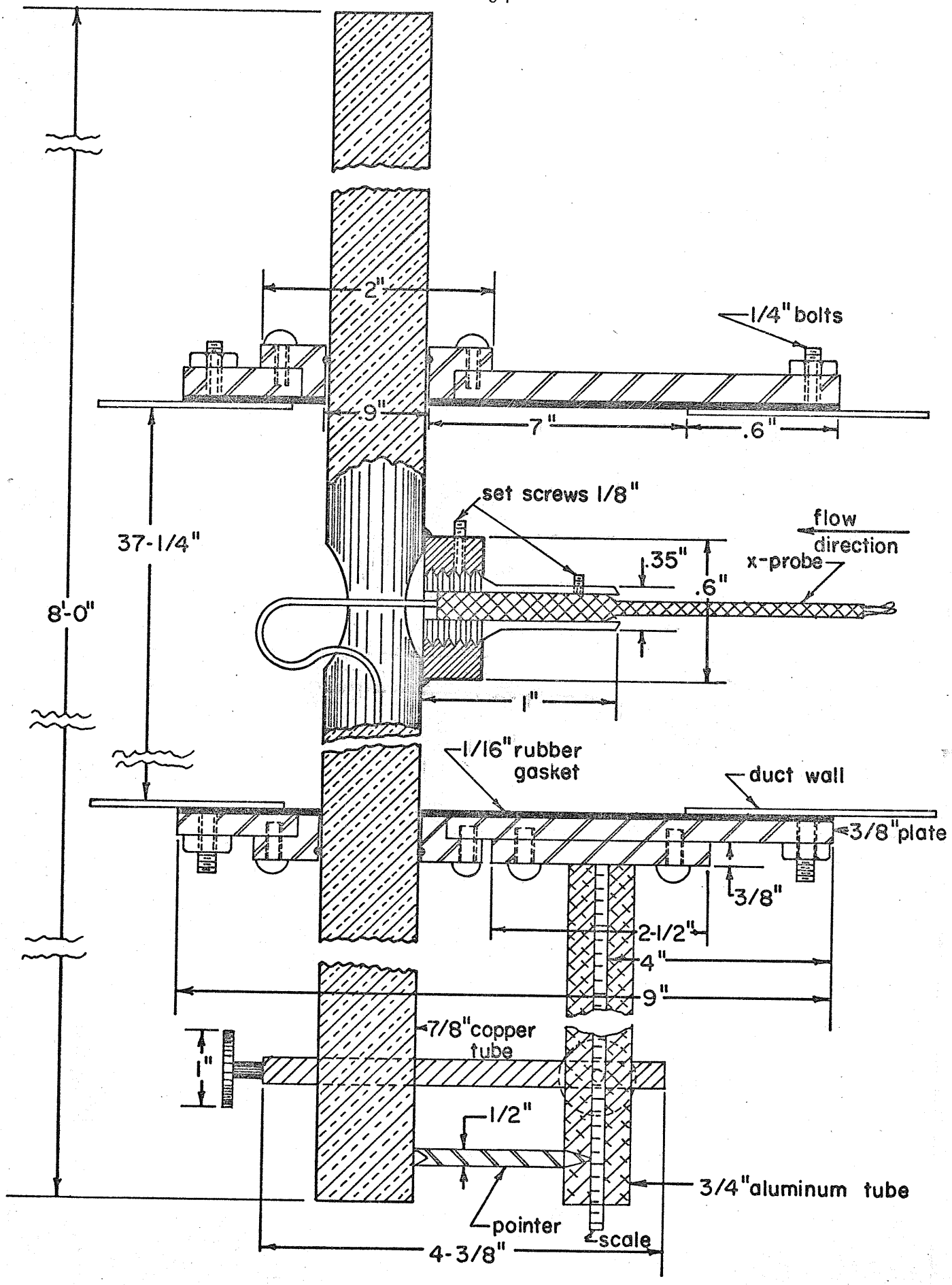

FIGURE 3.7.3

LOW VELOCITY TRAVERSING MECHANISM

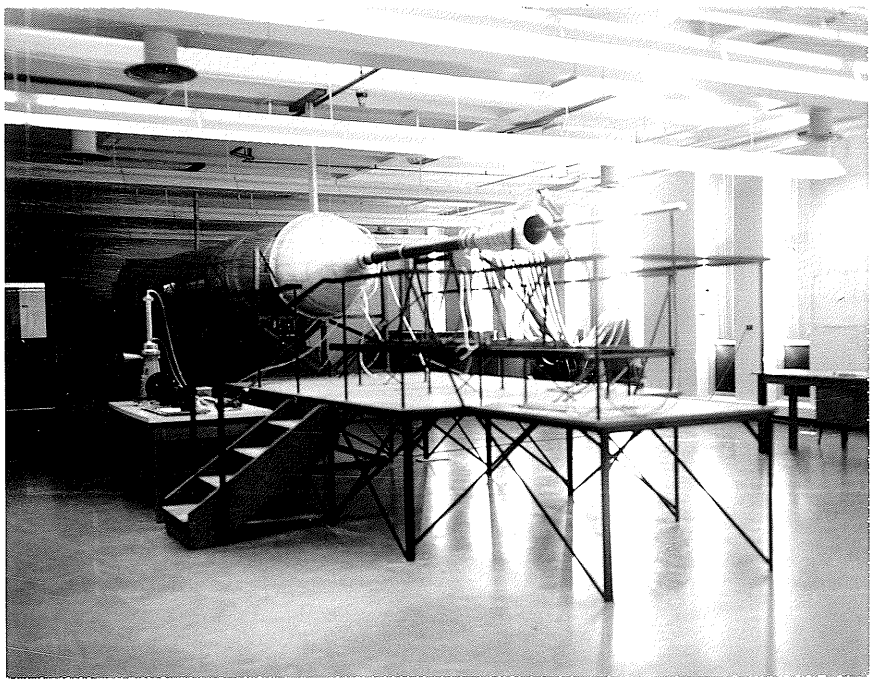

FIGURE 3.8 PLATFORM

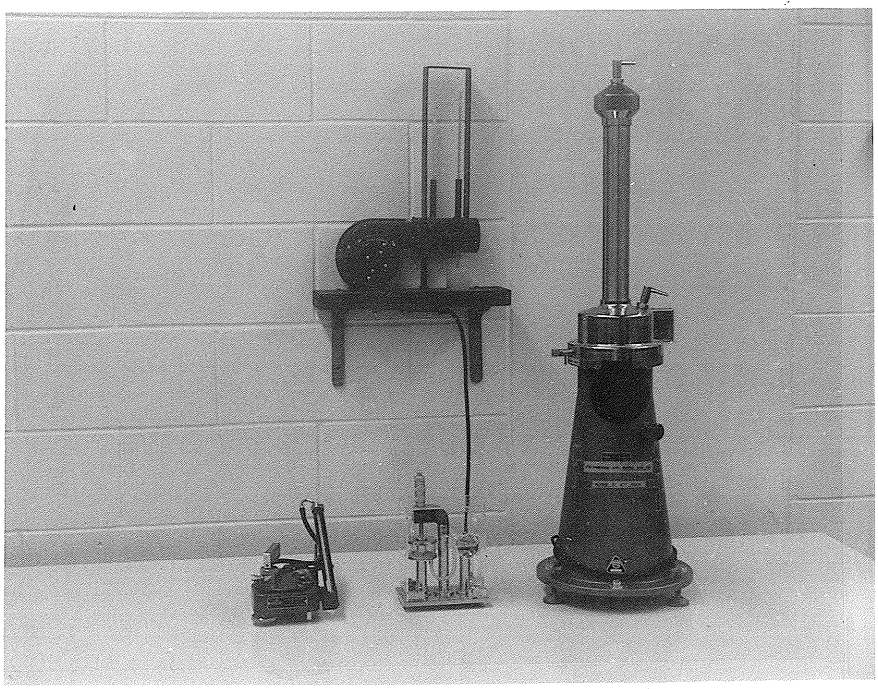

FIGURE 3.9.6 MANOMETERS

LEFT : DISA MICROMANOMETER

CENTER: HERO ALCOHOL MANOMETER

RIGHT: BETZ MICROMANOMETER

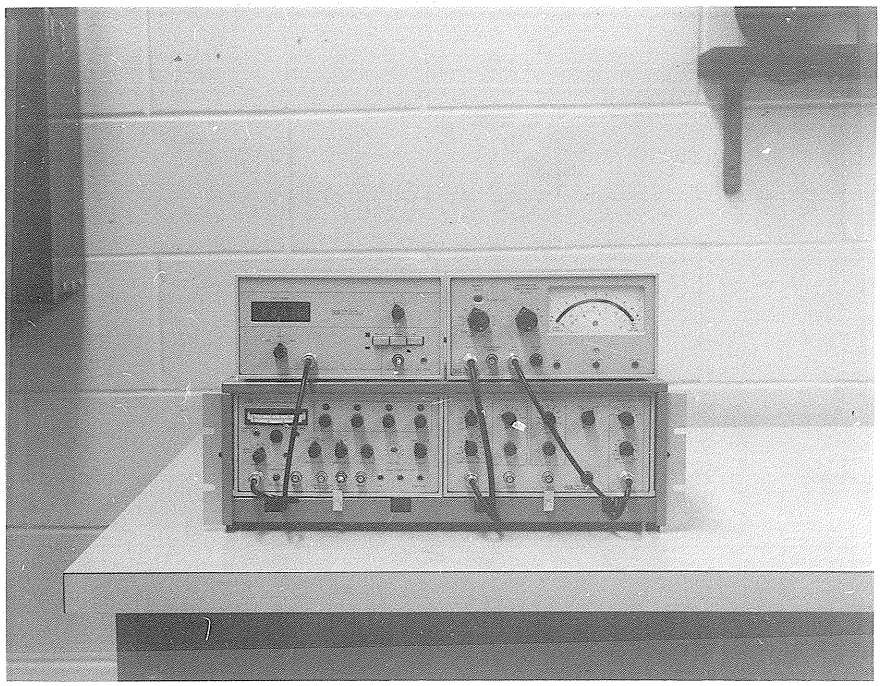

FIGURE 3.9.7

TOP LEFT: DIGITAL VOLTMETER

TOP RIGHT: DISA TYPE 55D35 RMS VOLTMETER

BOTTOM LEFT: DISA TYPE 55D01 ANEMOMETER

BOTTOM RIGHT: DISA TYPE 55D25 AUXILIARY UNIT

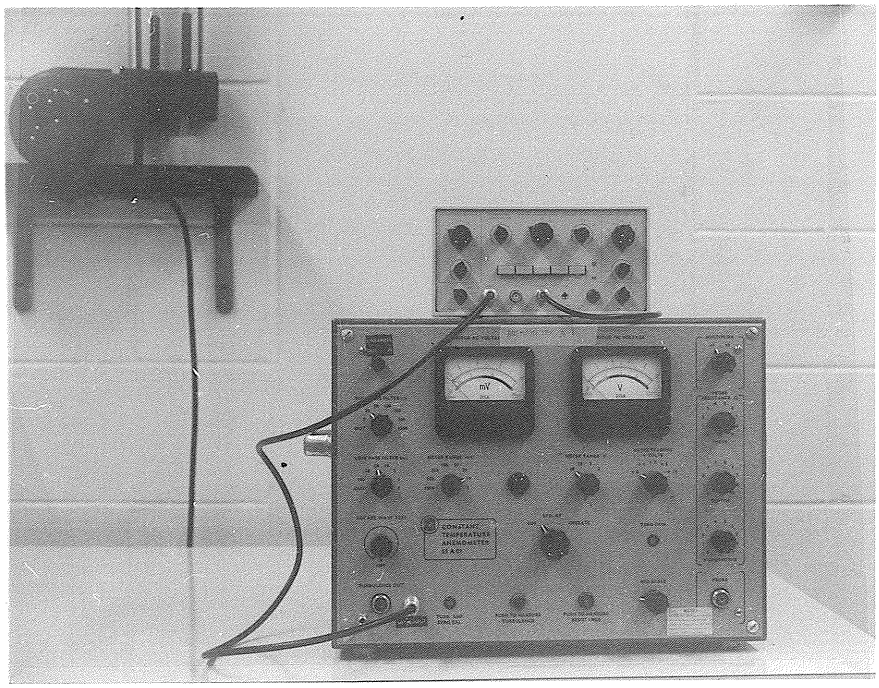

FIGURE 3.9.8

TOP: DISA TYPE 55D10 LINEARIZER

BOTTOM: DISA TYPE 55A01 ANEMOMETER

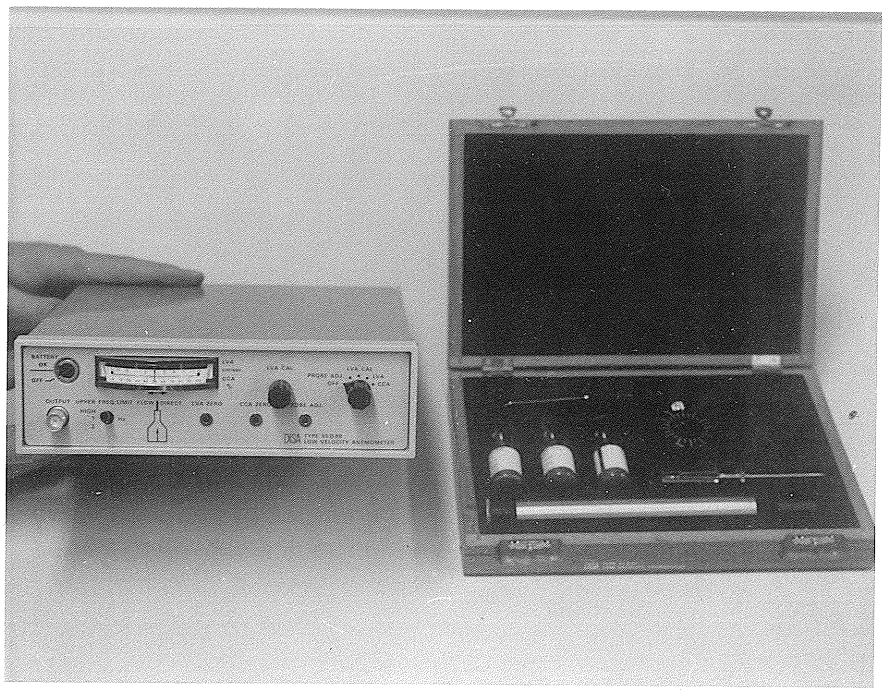

FIGURE 3.9.9

LOW VELOCITY ANEMOMETER

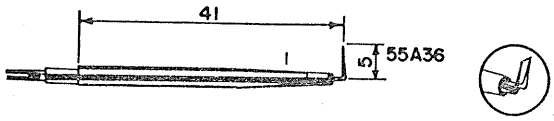

Type 55 A36 Miniature Hot-wire Probe

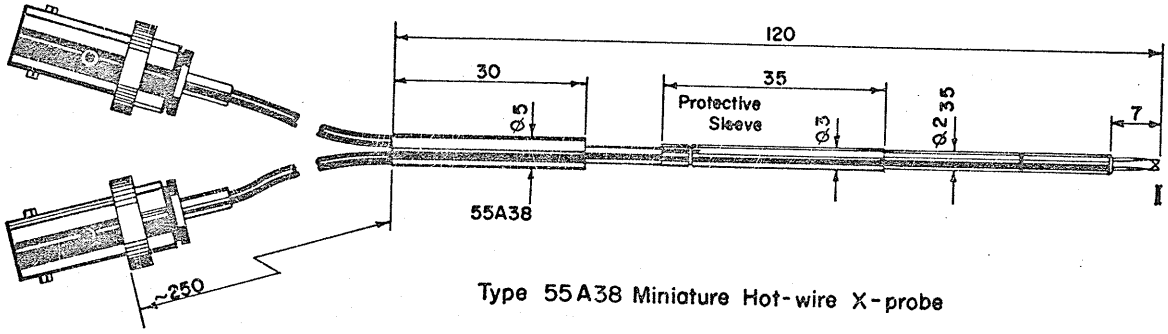

Type 55 A38 Miniature Hot-wire X-probe

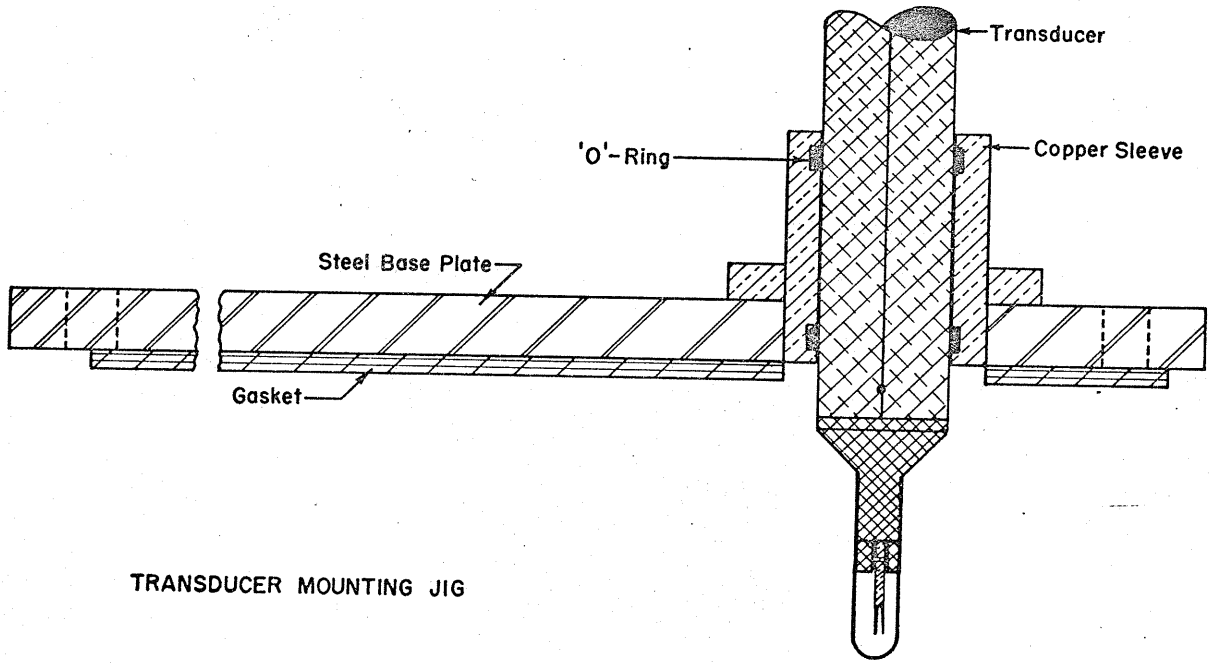

TRANSDUCER MOUNTING JIG

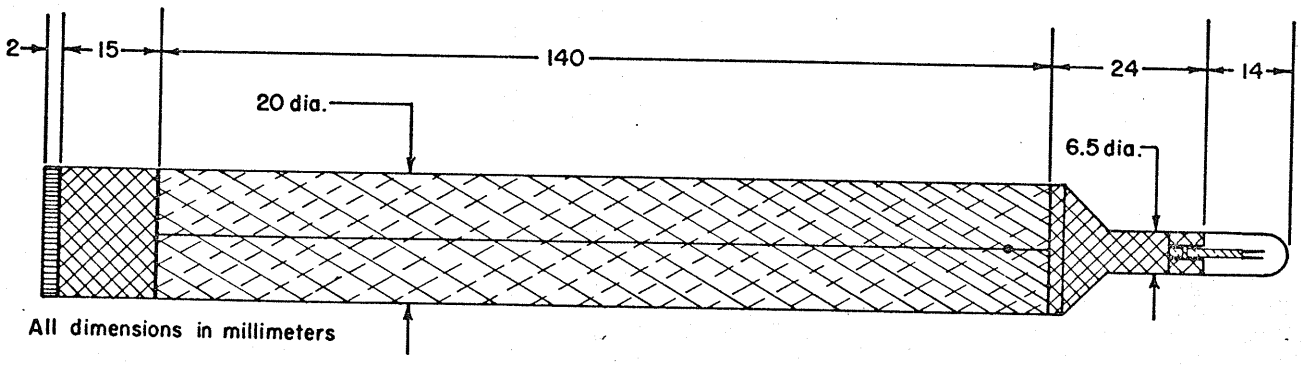

DIMENSIONAL OUTLINE OF TRANSDUCER

FIGURE 3,9,10 HOT WIRE PROBES

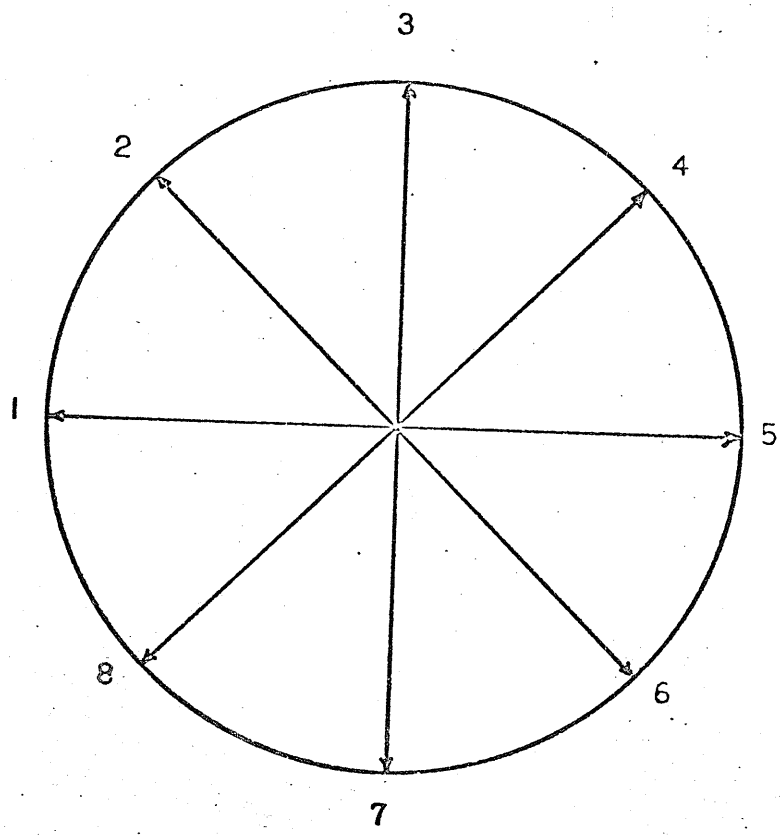

OUTLET OF DIFFUSER- LOOKING IN TOWARDS FAN

FIGURE 4.1

PIPE TRAVERSES

(1-5, 2-6, 3-7, 4-8)

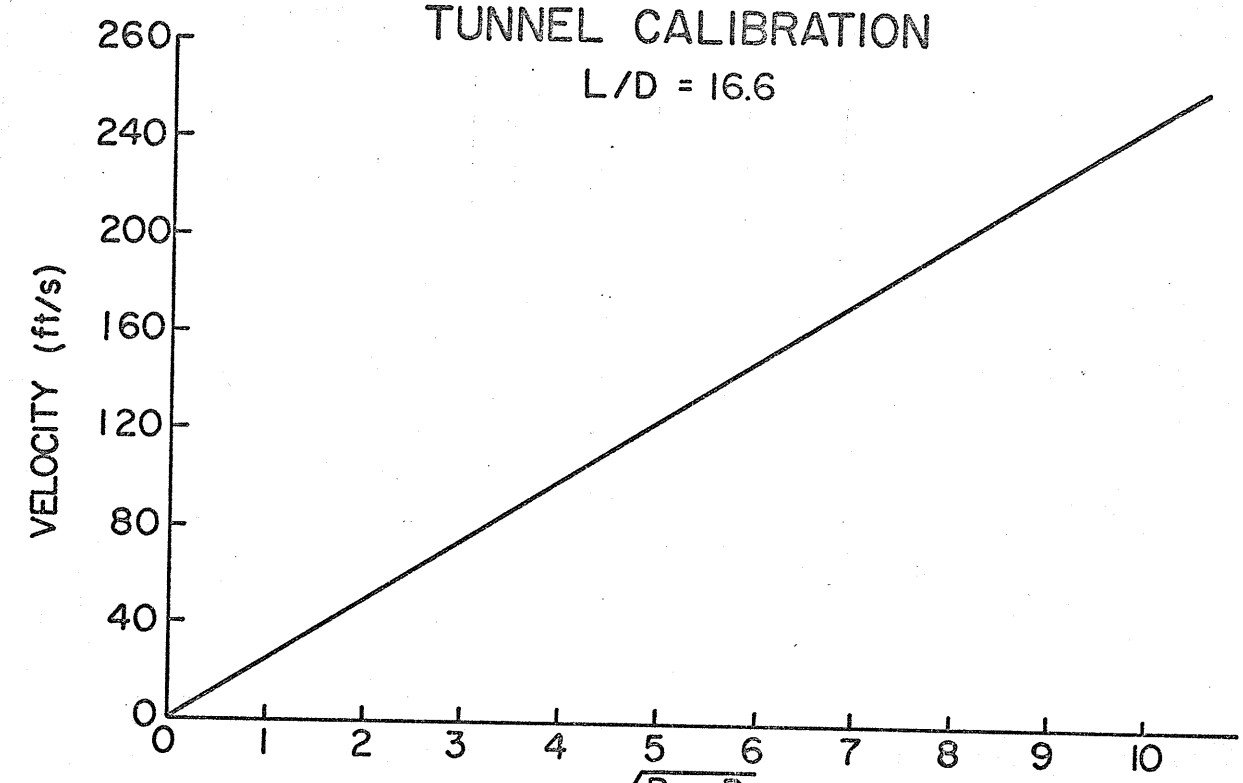

FIGURE 4.2 $\sqrt{\frac{P_1 - P_2}{\rho}}$

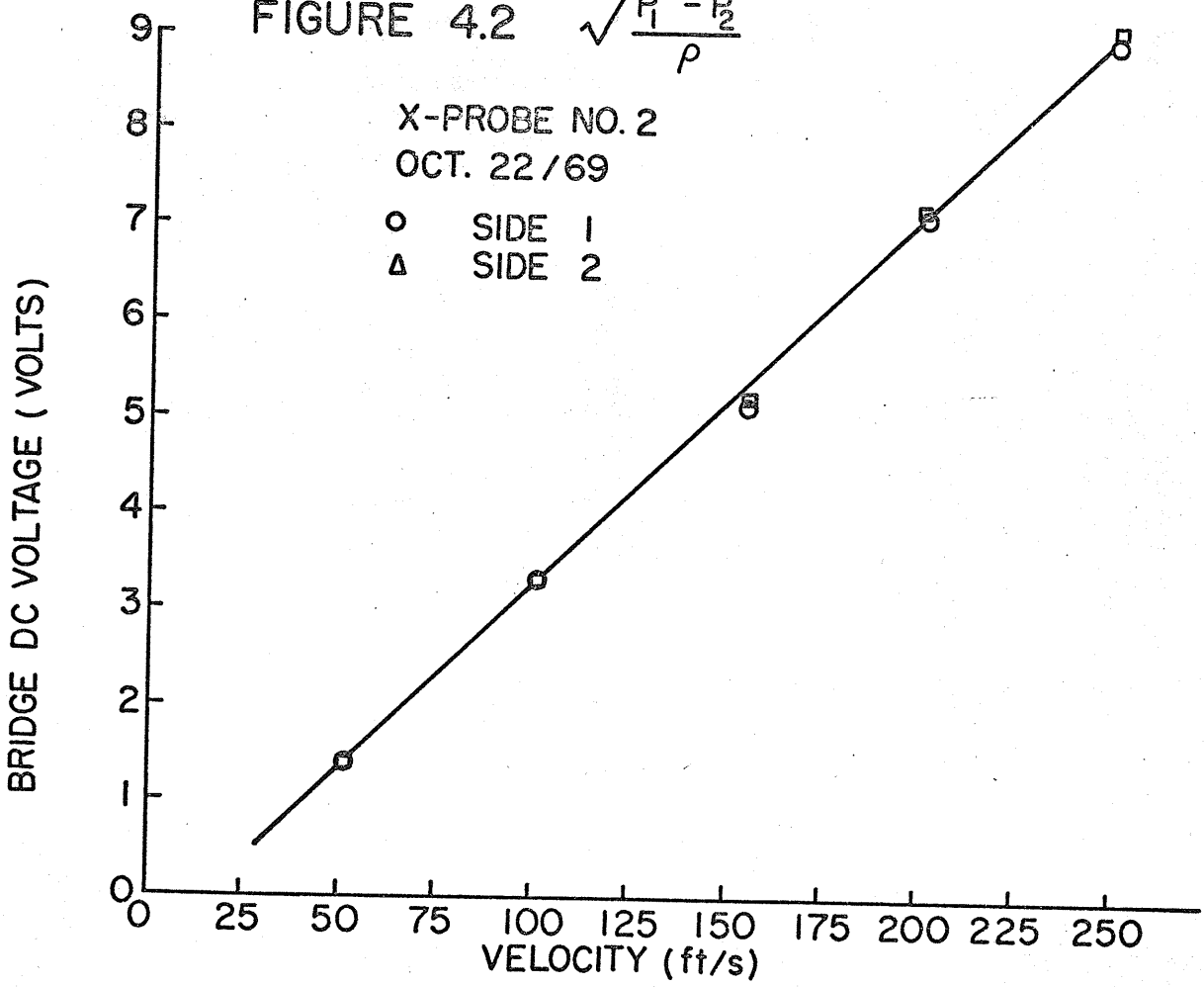

FIGURE 4.3.1 X PROBE CALIBRATION

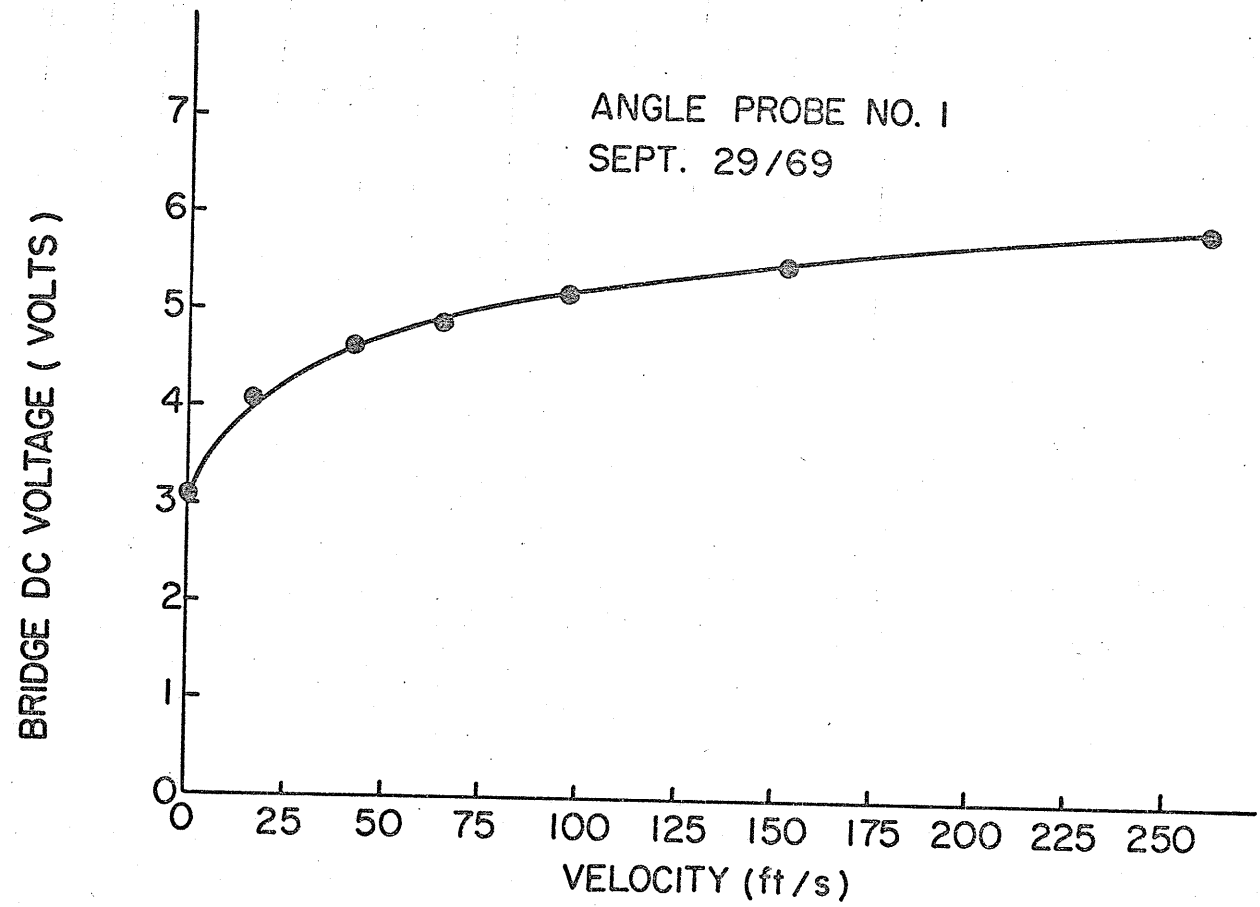

ANGLE PROBE CALIBRATION
FIGURE 4.3.2

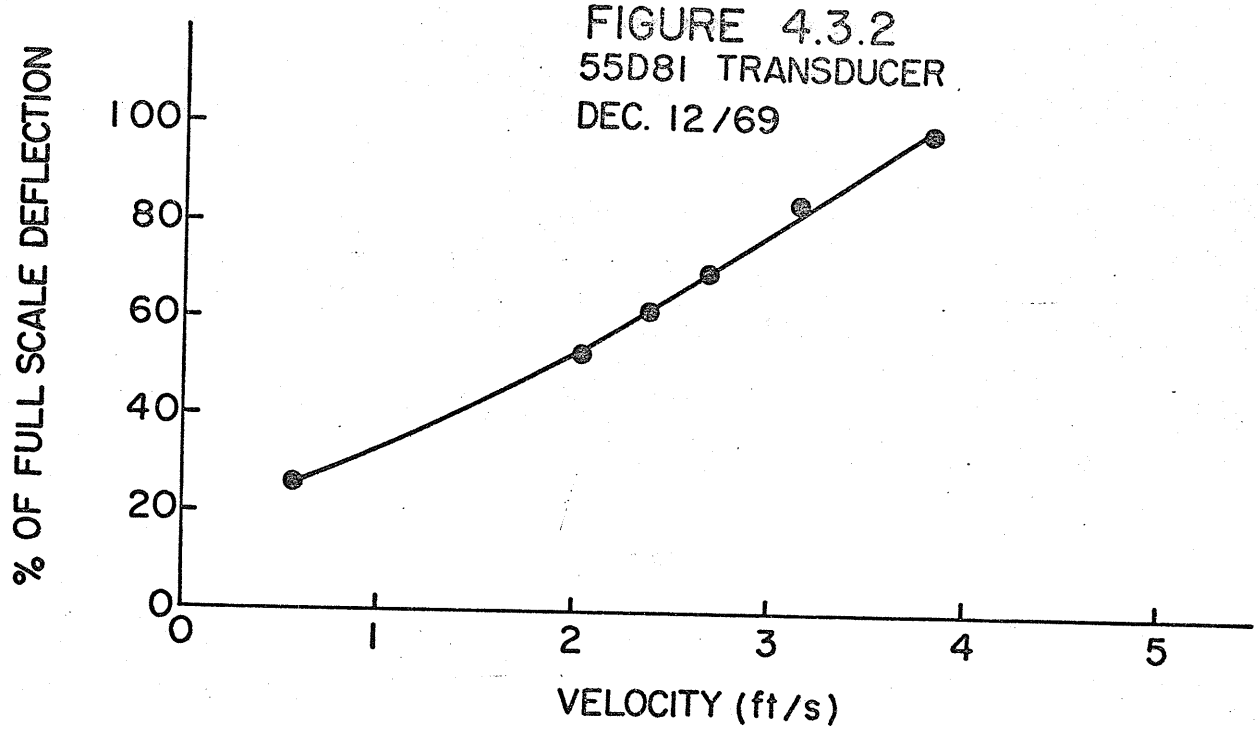

FIGURE 4.5 55D80/81 LOW VELOCITY CALIBRATION

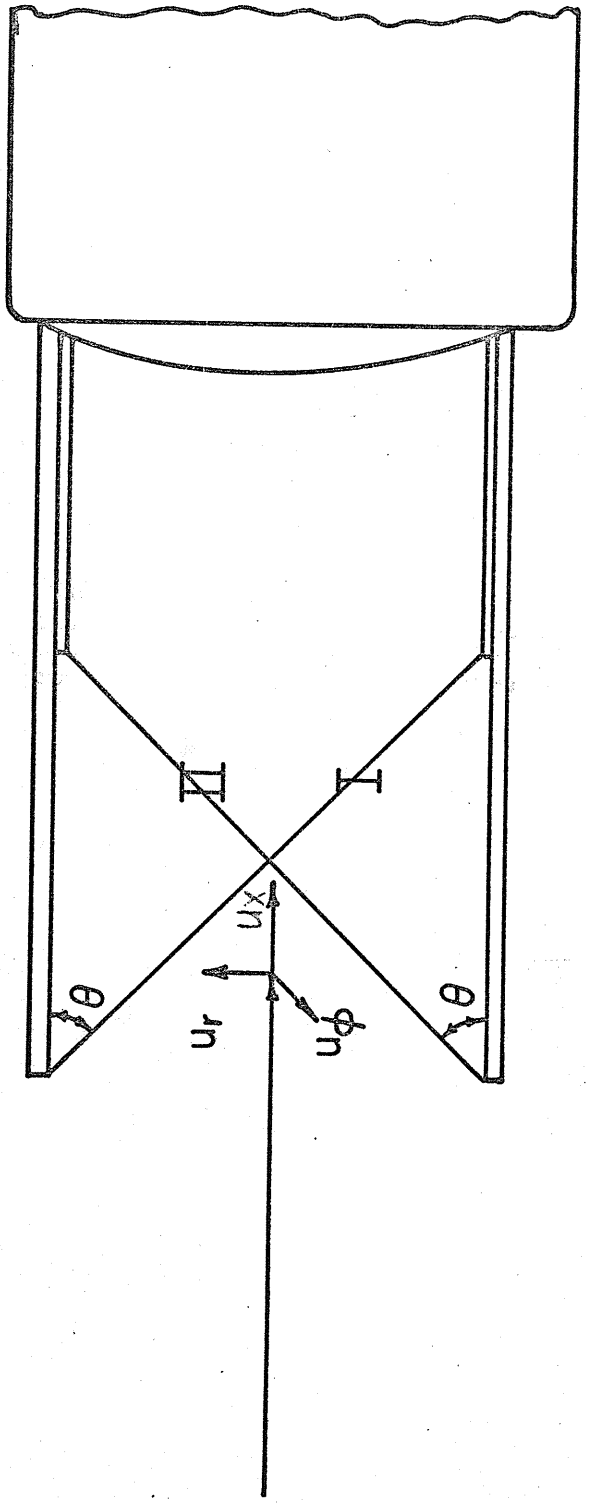

FIGURE 4.4 X-PROBE CONFIGURATION

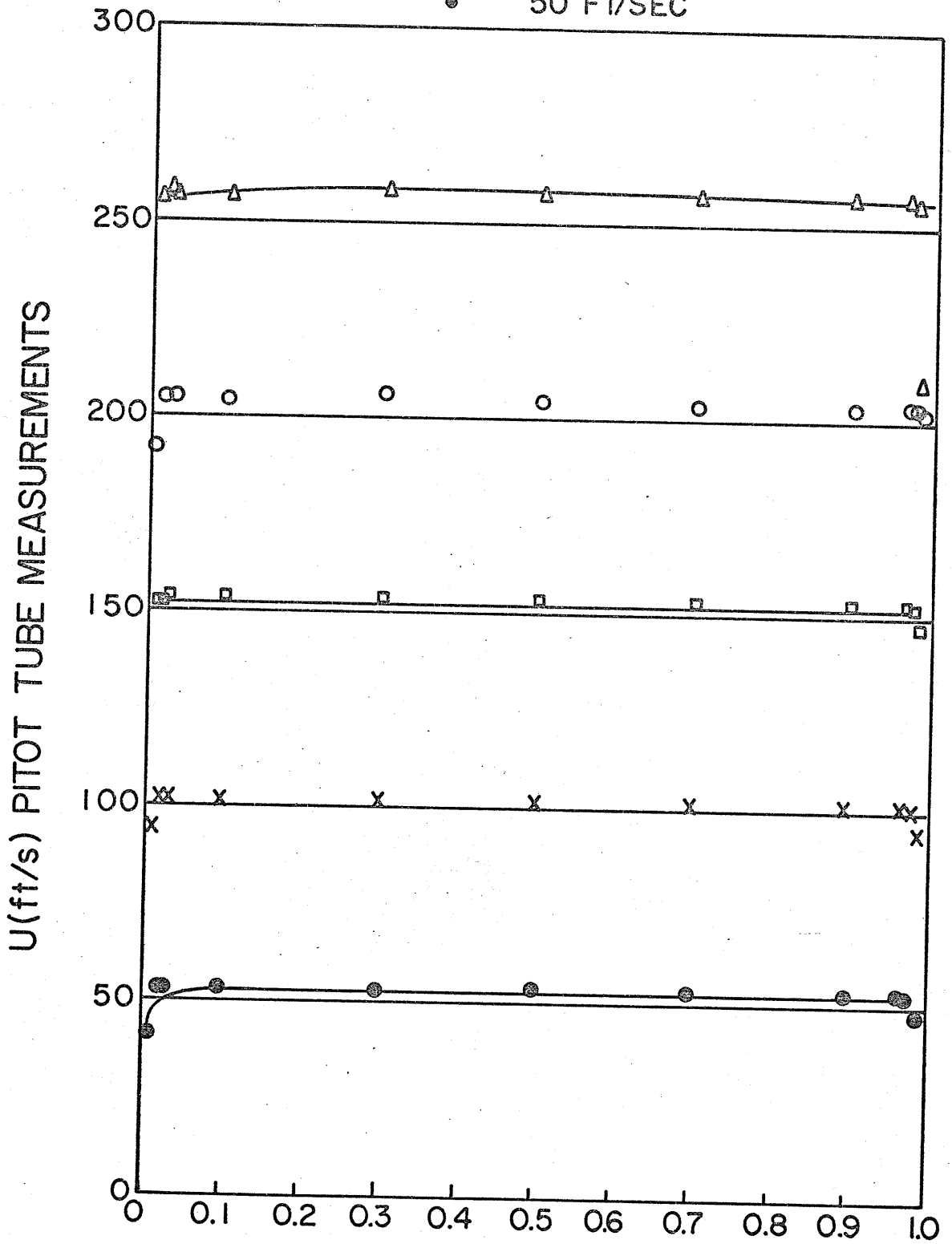

FIGURE 5.1
CONTRACTION OUTLET VELOCITY VERSUS a/D

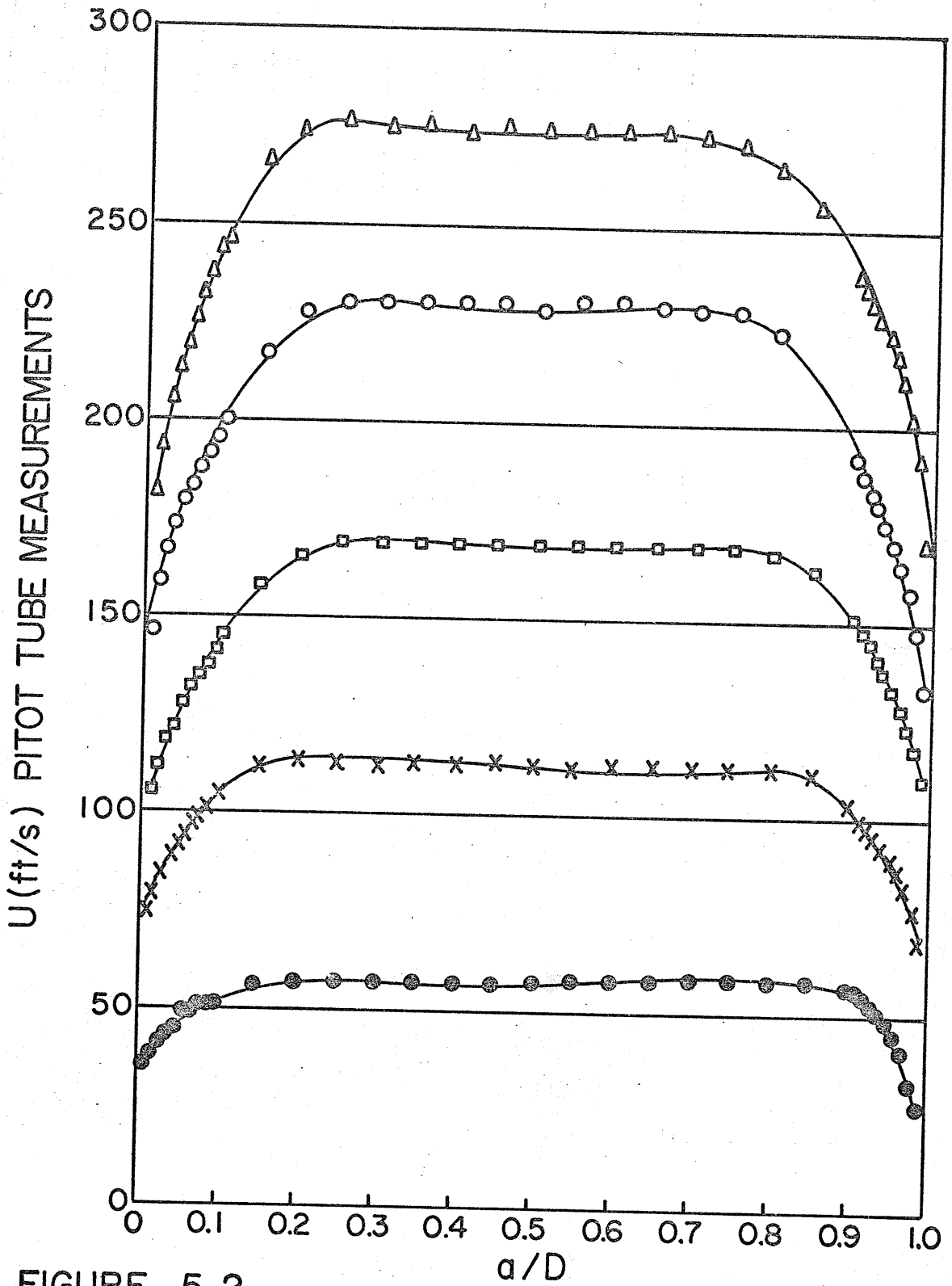

FIGURE 5.2
DIFFUSER INLET VELOCITY VERSUS a/D

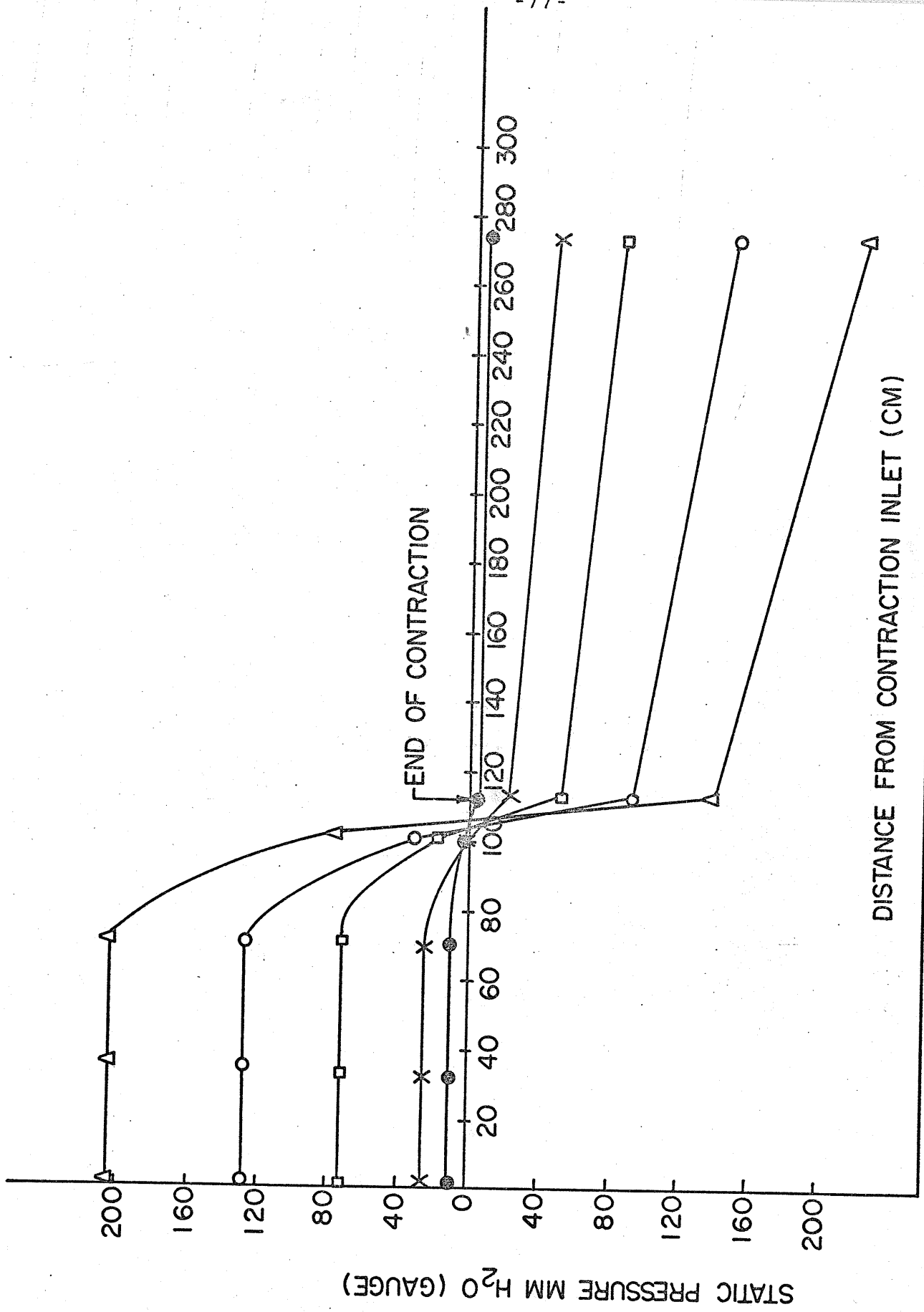

FIGURE 5.3 STATIC PRESSURE IN CONTRACTION AND BOUNDARY LAYER GROWTH PIPES

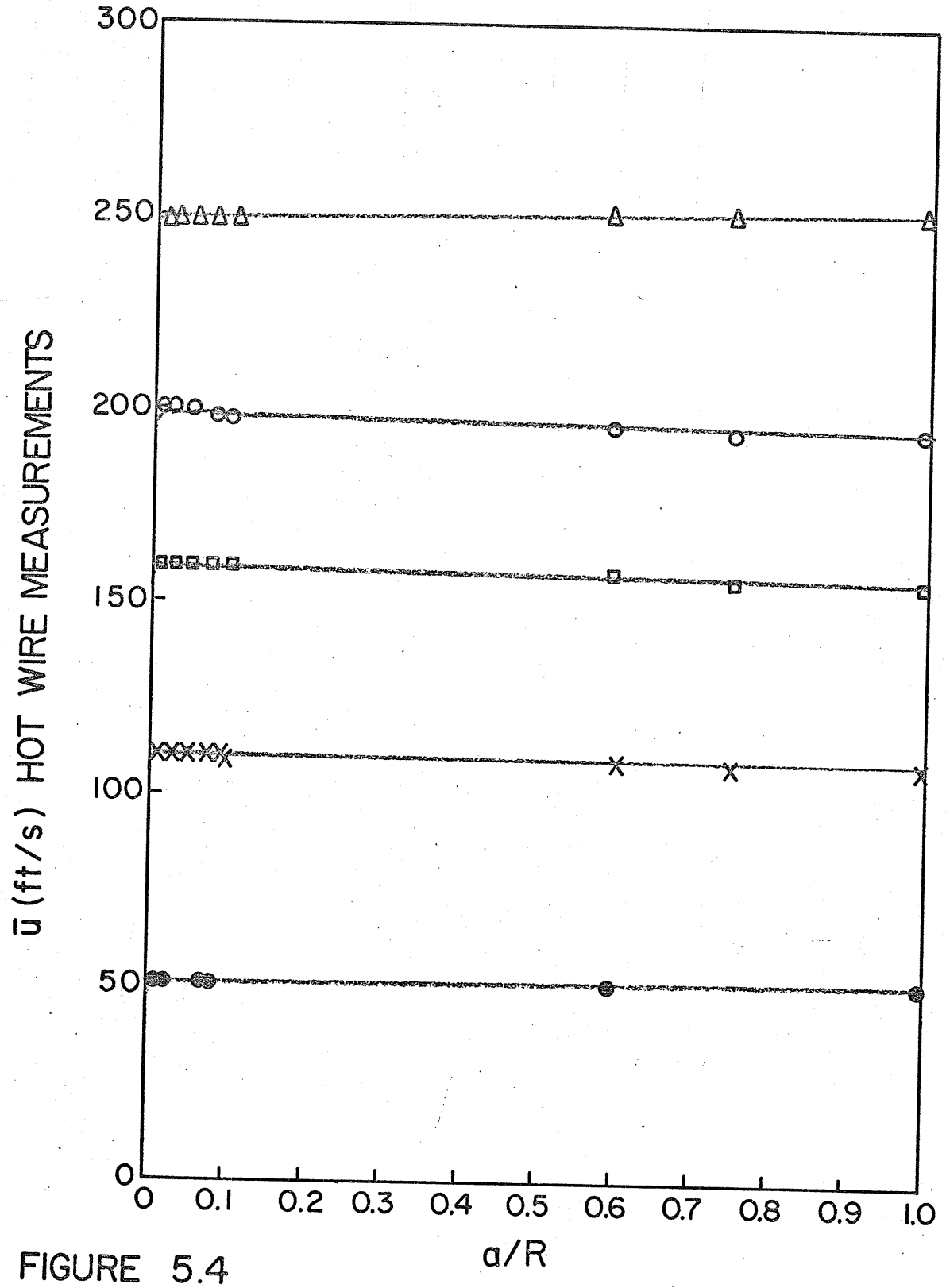

FIGURE 5.4
CONTRACTION OUTLET VELOCITY VERSUS a/R

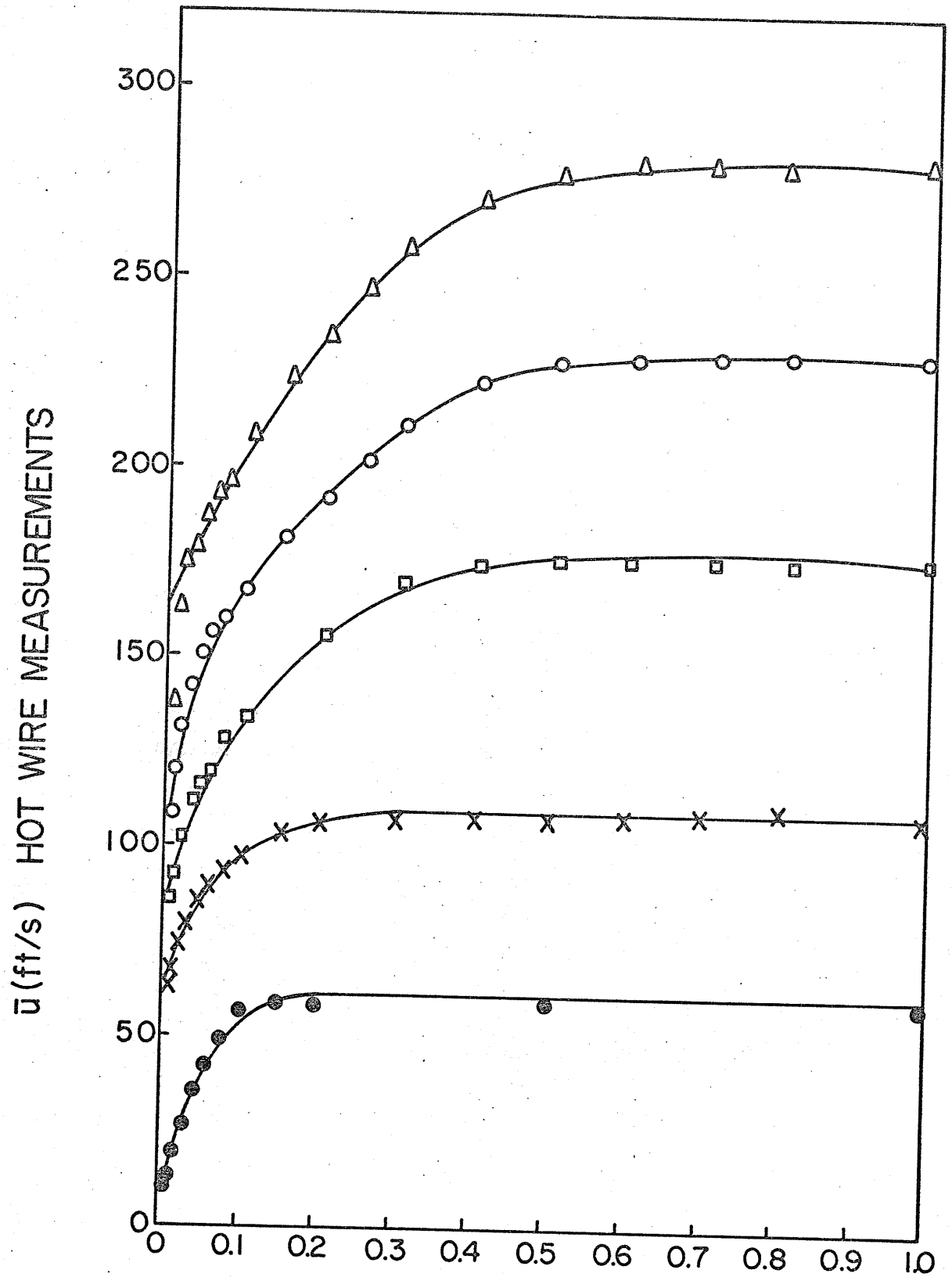

FIGURE 5.5
DIFFUSER INLET VELOCITY VERSUS a/R

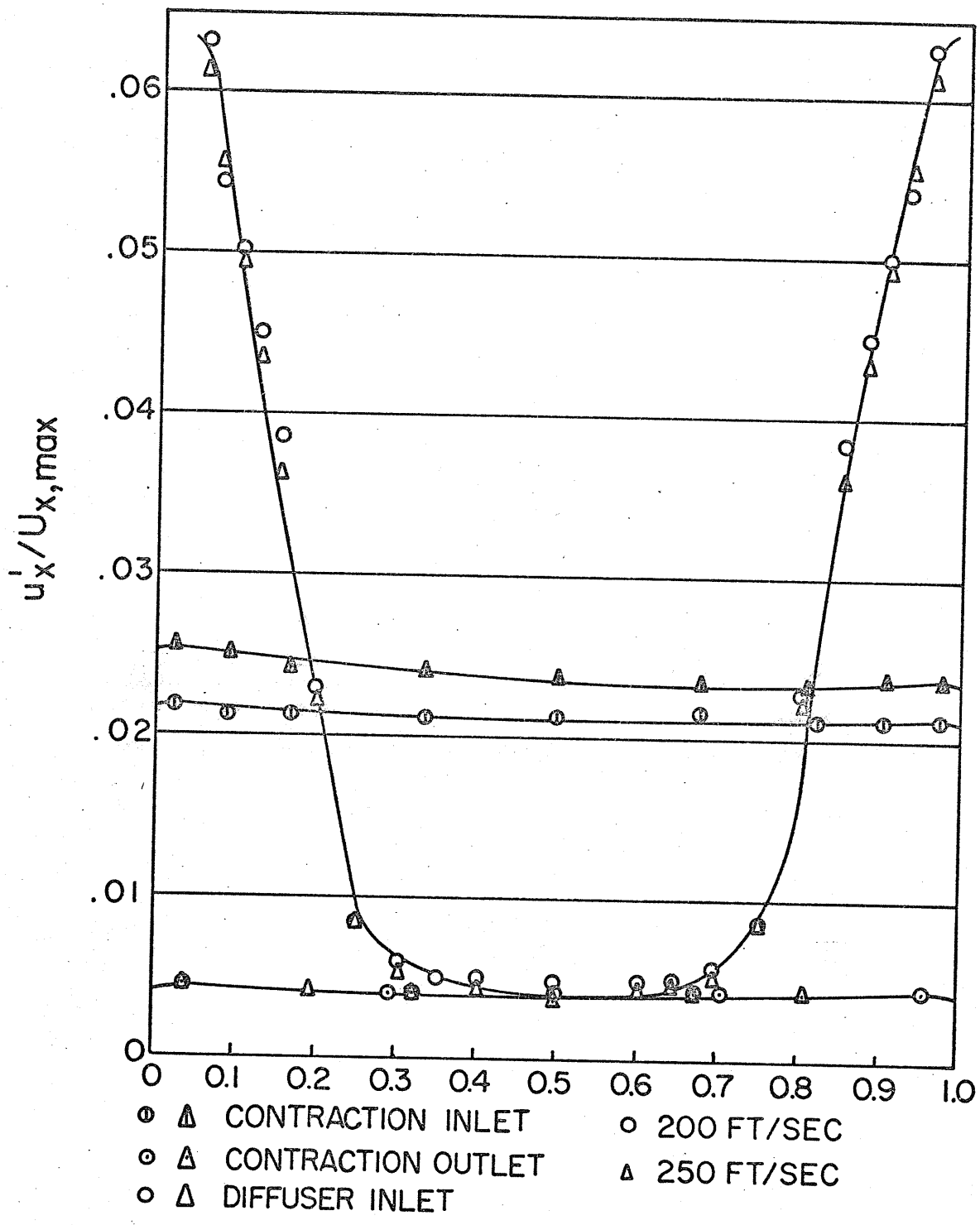

FIGURE 5.6 LONGITUDINAL TURBULENCE INTENSITY VERSUS a/D

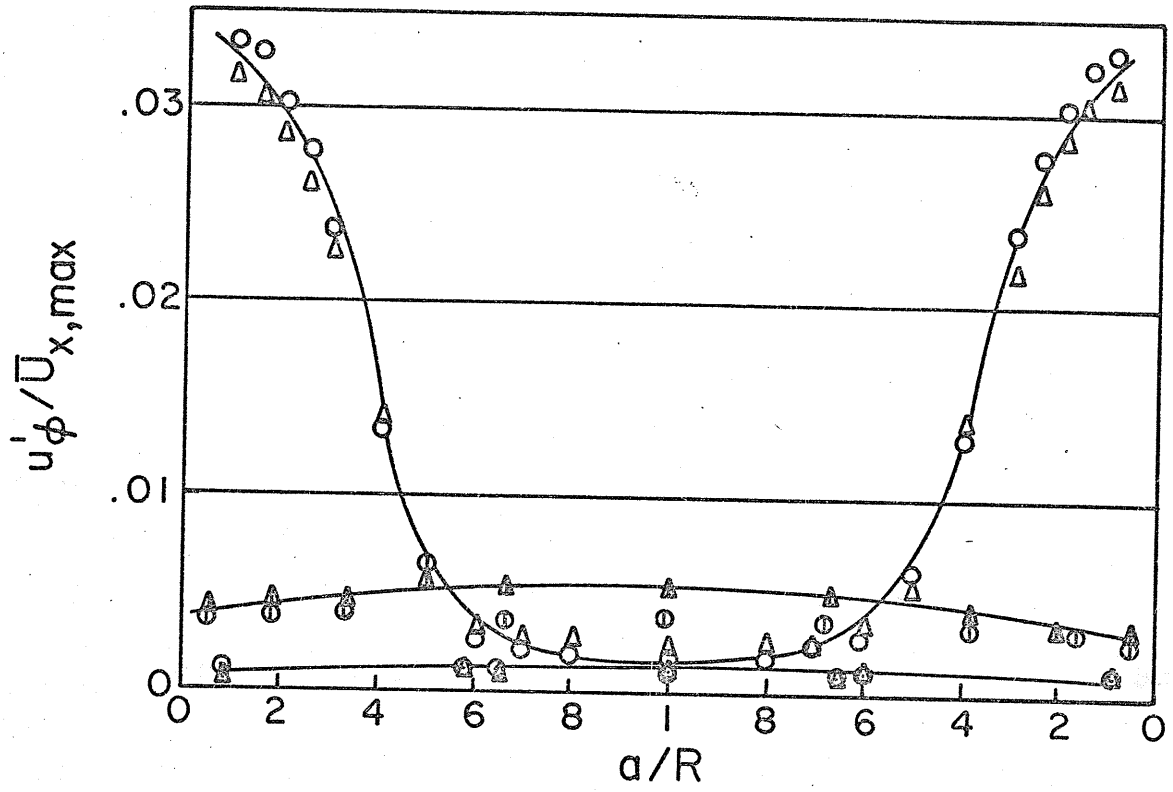

AZMUTHAL TURBULENCE INTENSITY VERSUS a/R

⊕ Δ CONTRACTION INLET ○ 200 FT/SEC
⊙ Δ CONTRACTION OUTLET Δ 250 FT/SEC
○ Δ DIFFUSER INLET

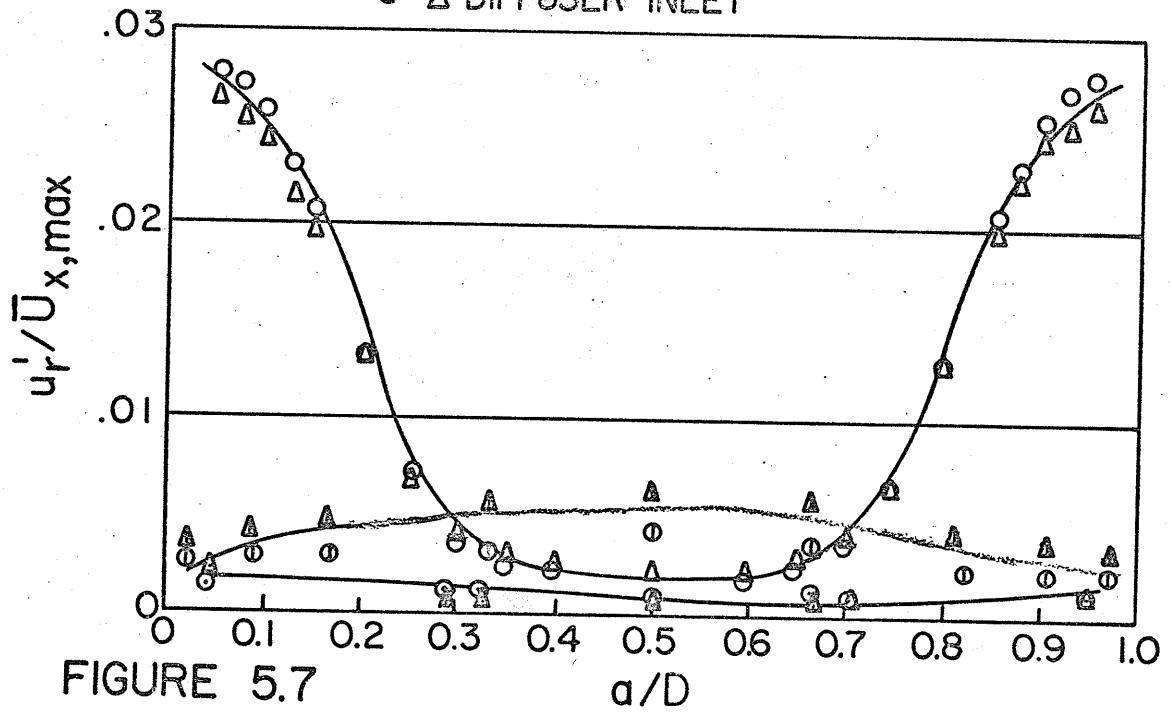

FIGURE 5.7
RADIAL TURBULENCE INTENSITY VERSUS a/D

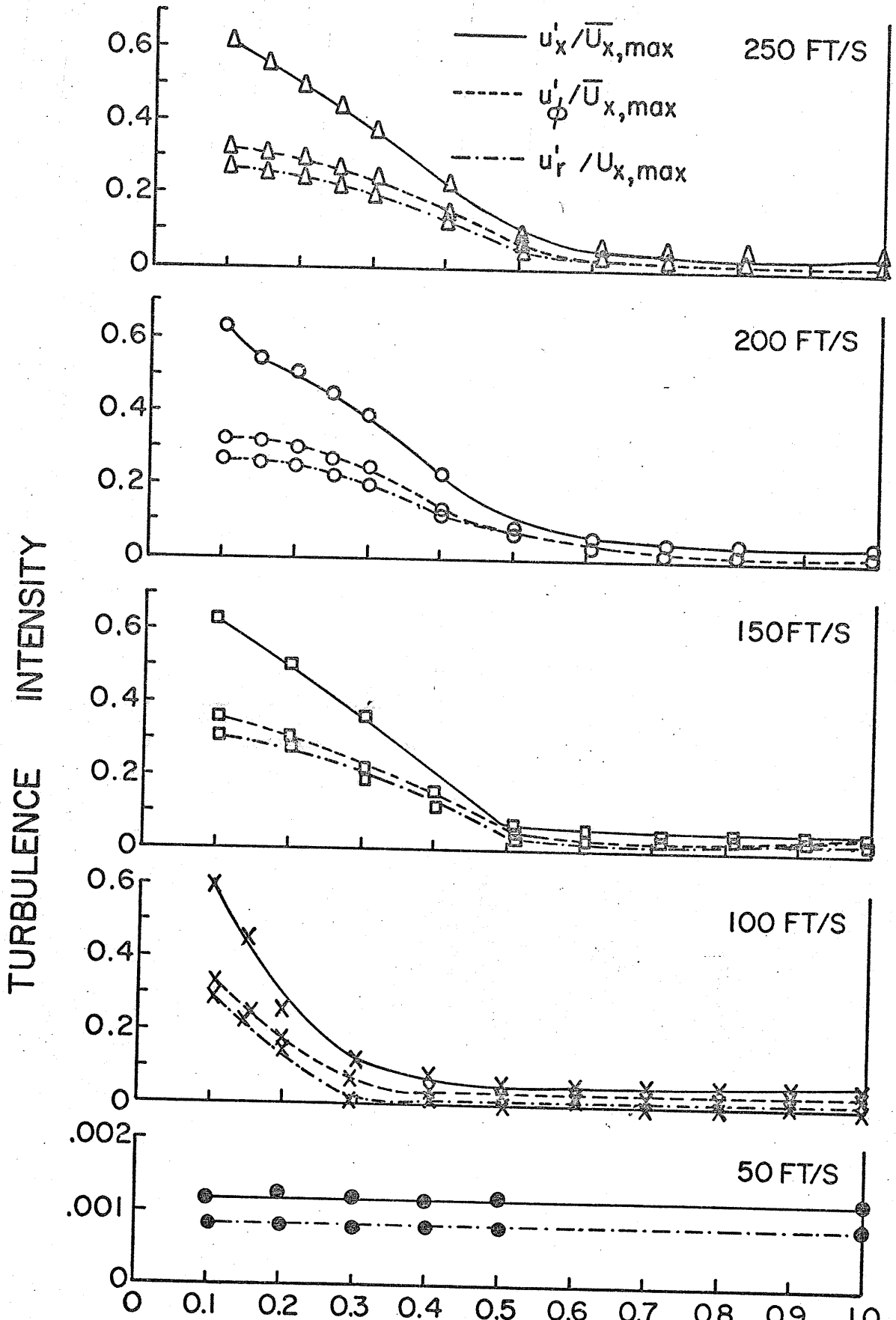

FIGURE 5.8
TURBULENCE INTENSITIES VERSUS a/R DIFFUSER INLET

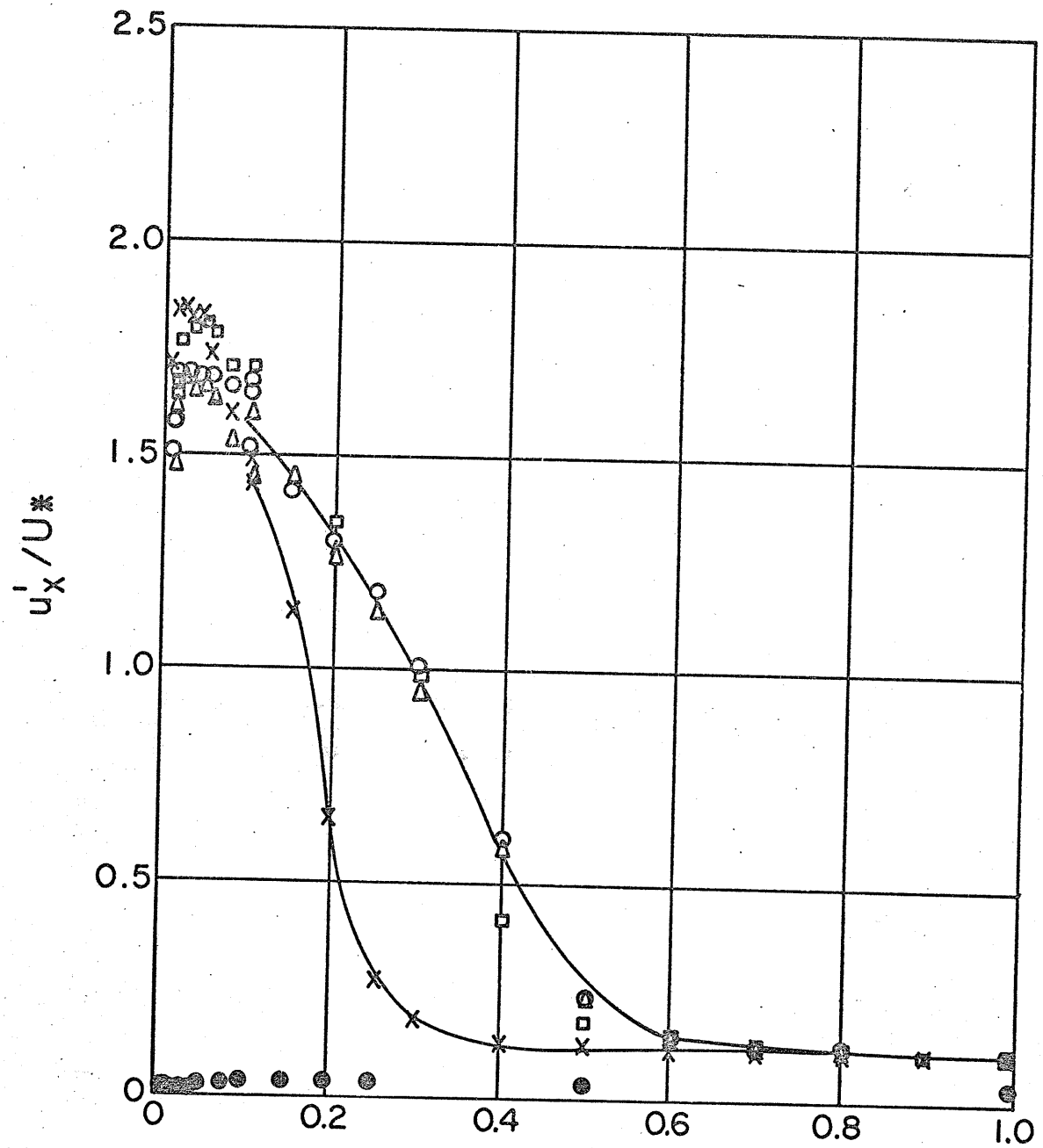

FIGURE 5.9
LONGITUDINAL TURBULENCE INTENSITY RELATIVE TO THE WALL FRICTION VELOCITY VERSUS a/R DIFFUSER INLET

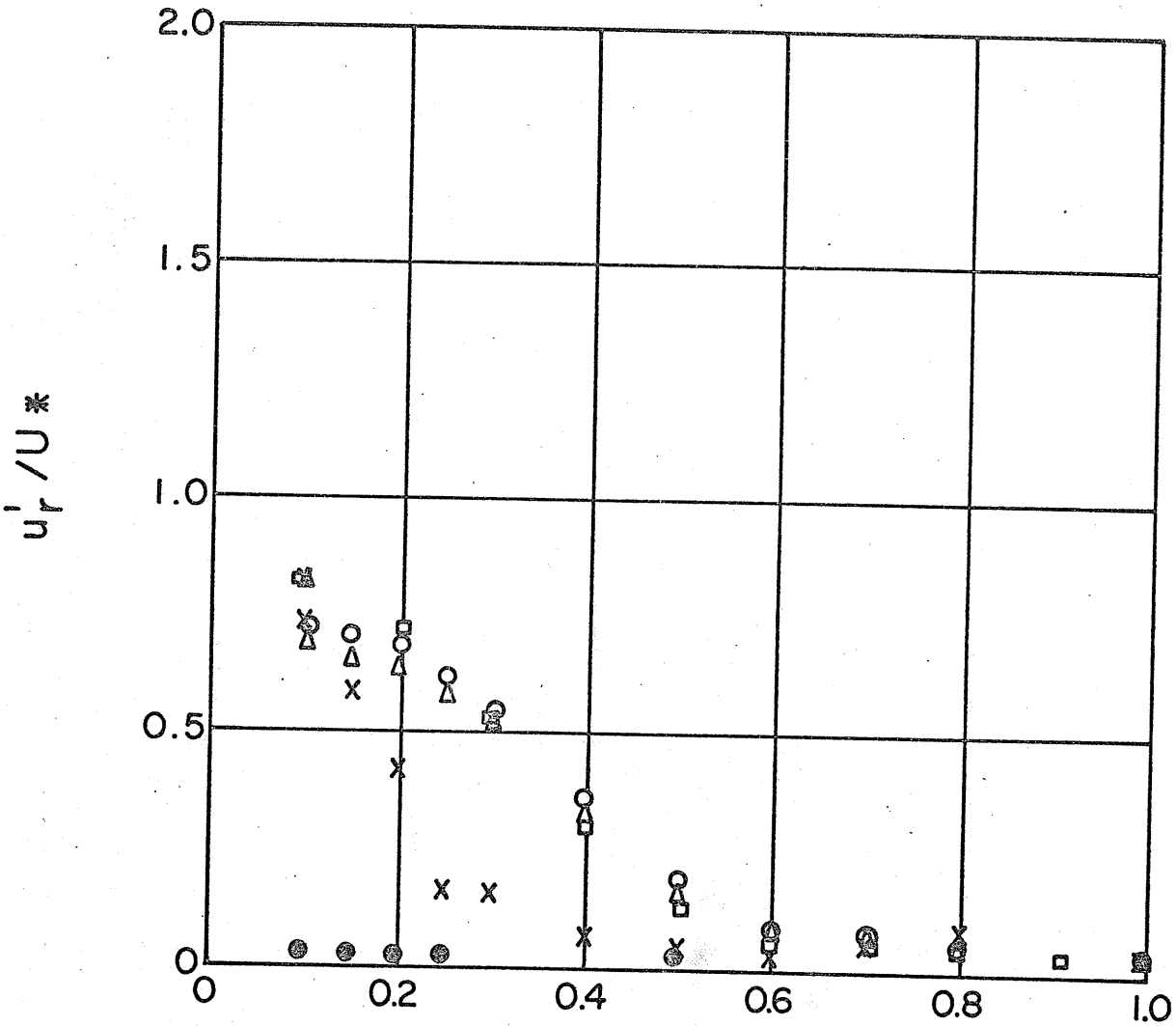

FIGURE 5.10
RADIAL TURBULENCE INTENSITY RELATIVE TO THE WALL FRICTION VELOCITY VERSUS a/R

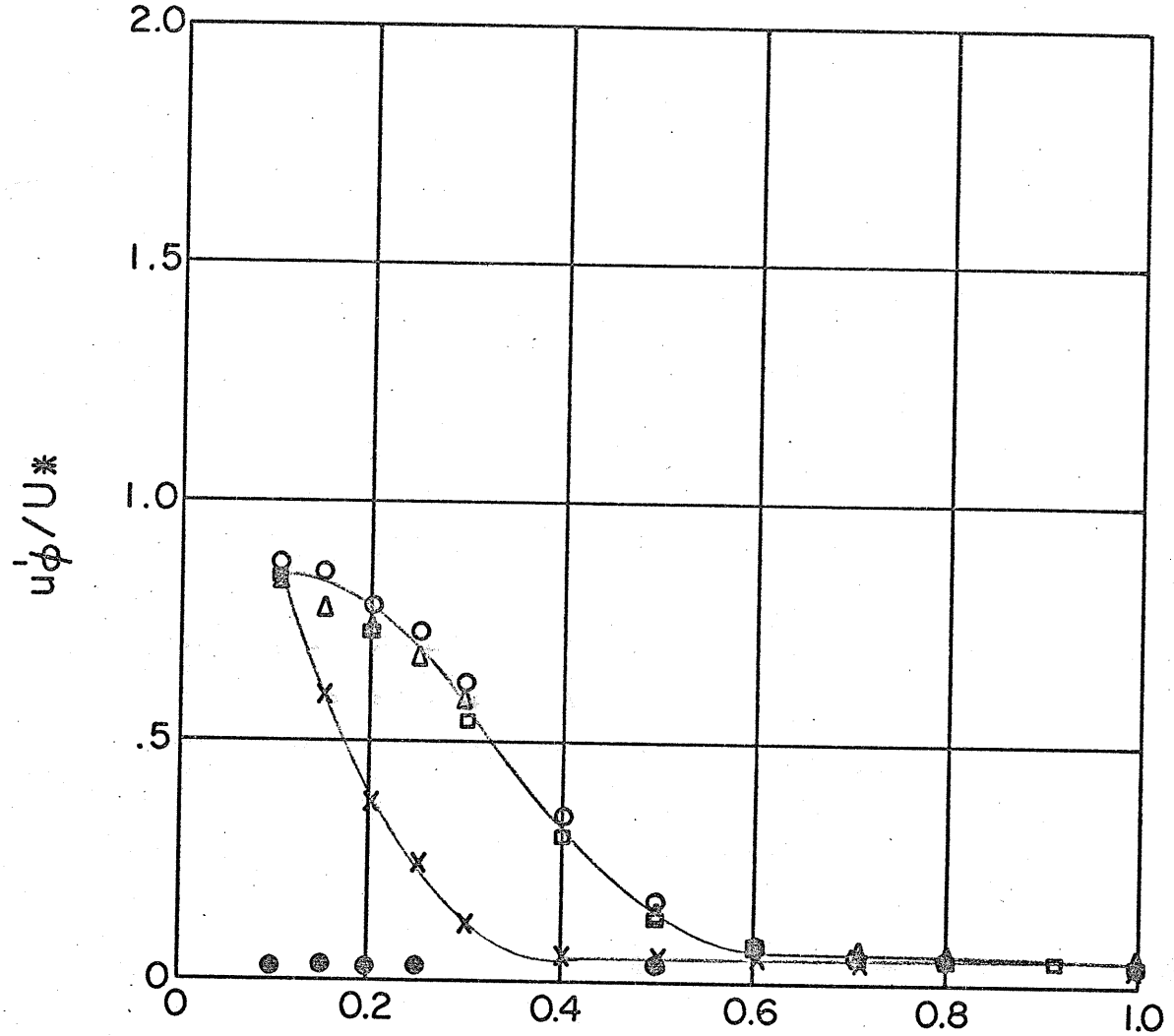

FIGURE 5.11
AZMUTHAL TURBULENCE INTENSITY RELATIVE TO THE WALL FRICTION VELOCITY VERSUS a/R

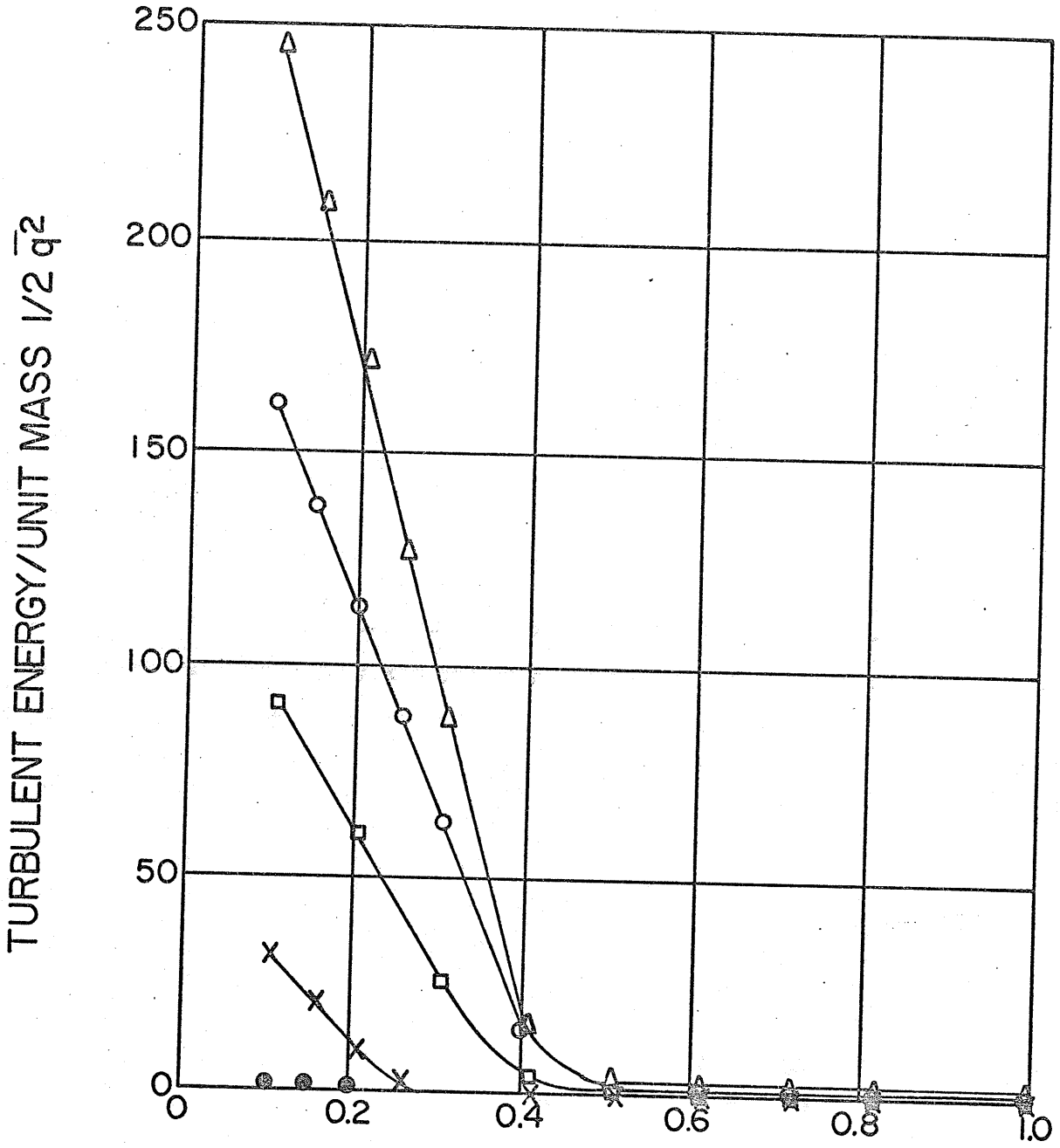

FIGURE 5.12
TURBULENT ENERGY VERSUS a/R DIFFUSER INLET

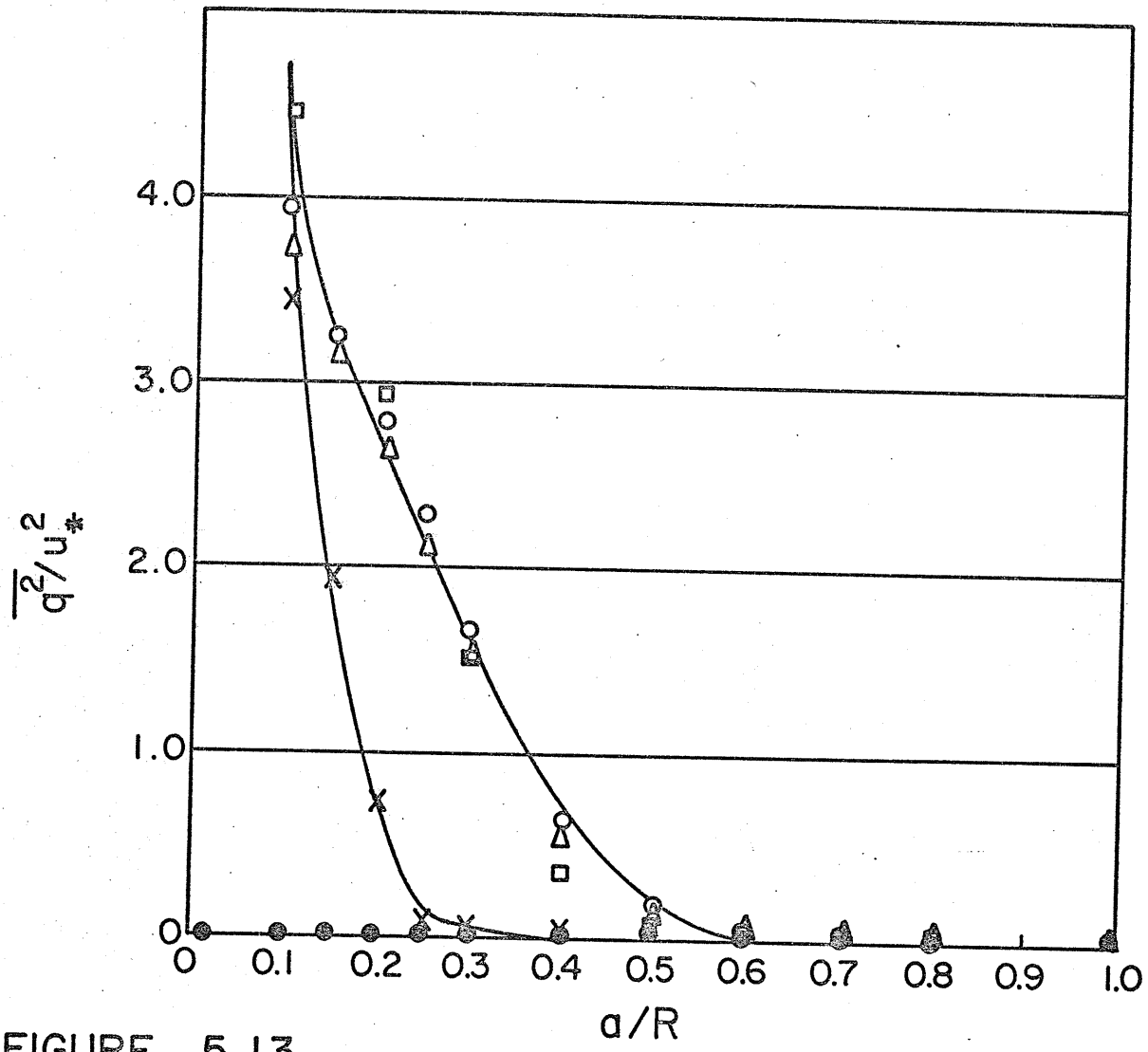

FIGURE 5.13
2 X TURBULENT ENERGY / FRICTION VELOCITY VERSUS a/R DIFFUSER INLET

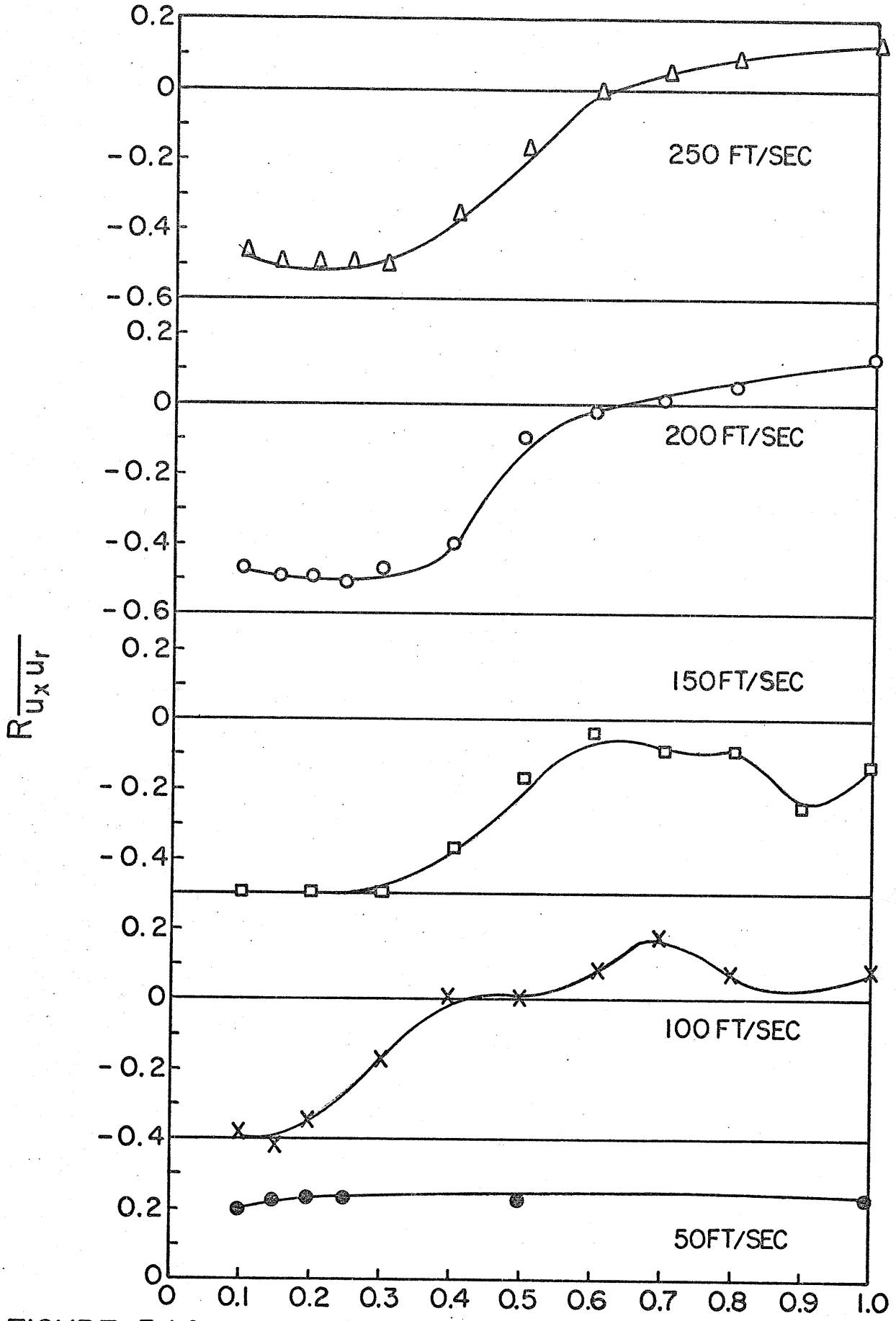

FIGURE 5.14
CORRELATION COEFFICIENT $R_{\overline{u_x u_y}}$ VERSUS a/R DIFFUSER INLET

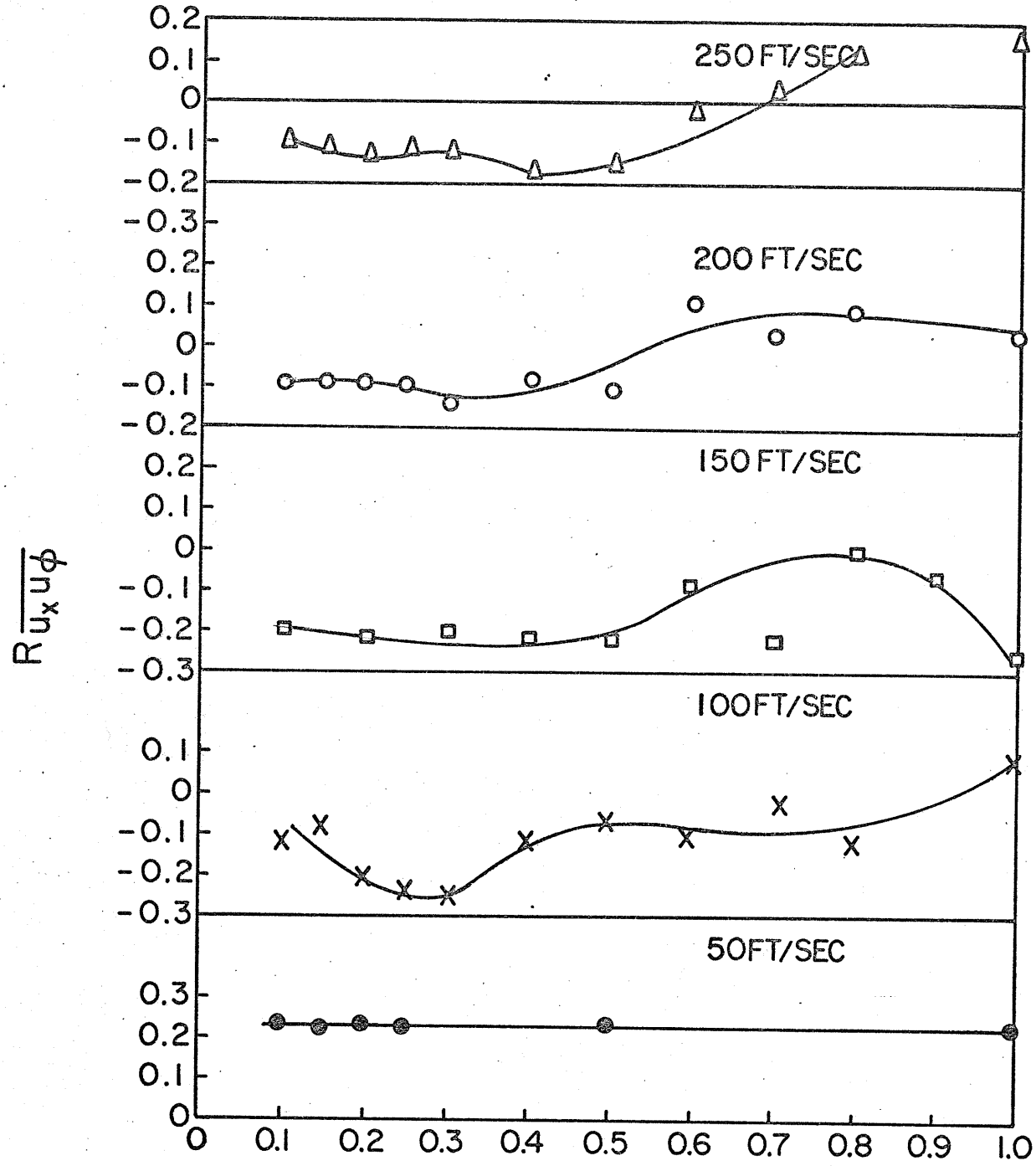

FIGURE 5.15
CORRELATION COEFFICIENT $R_{\overline{u_x u_\phi}}$ VERSUS a/R DIFFUSER INLET

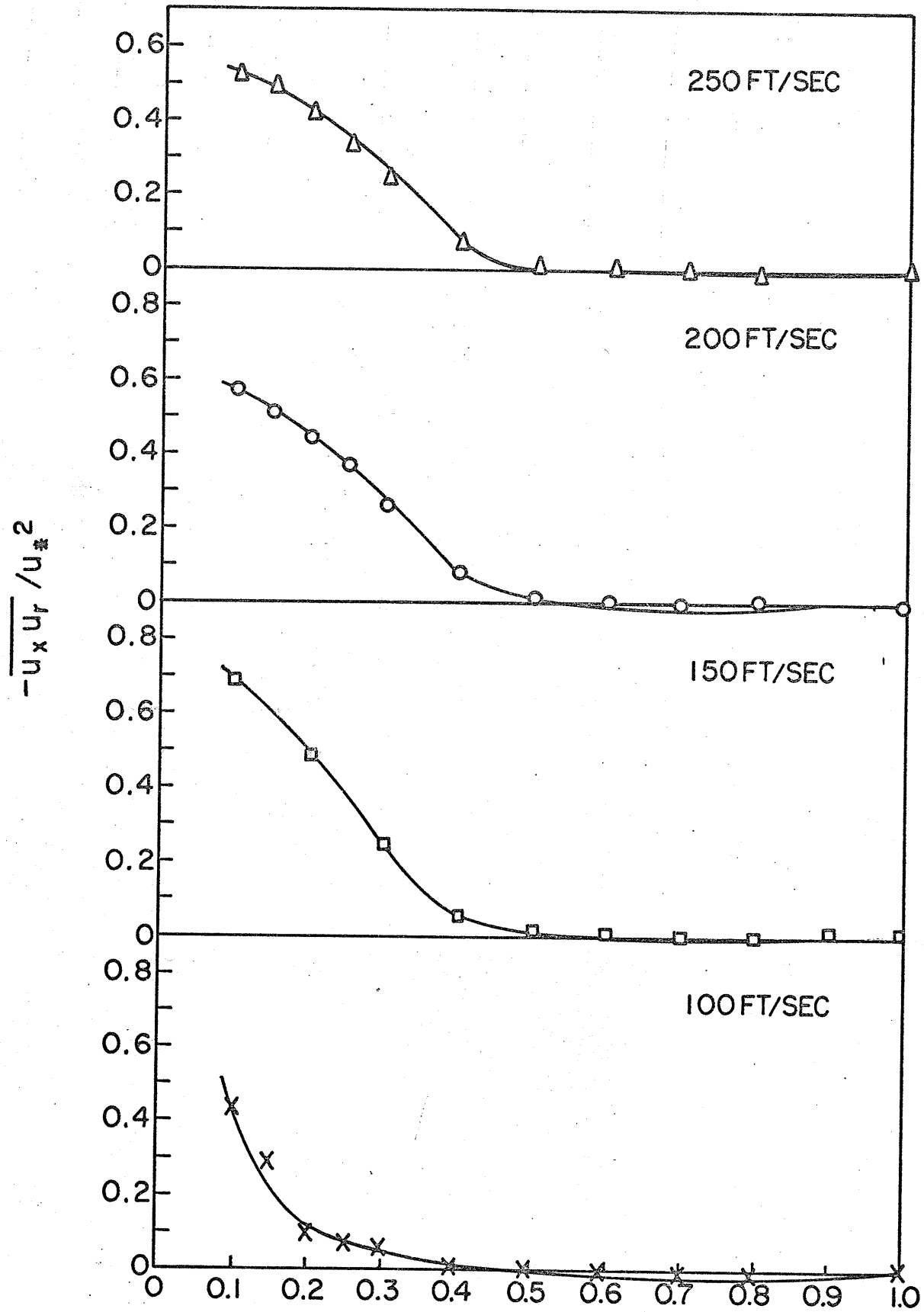

FIGURE 5.16

TURBULENT SHEAR STRESS/FRICTION VELOCITY VERSUS a/R DIFFUSER INLET

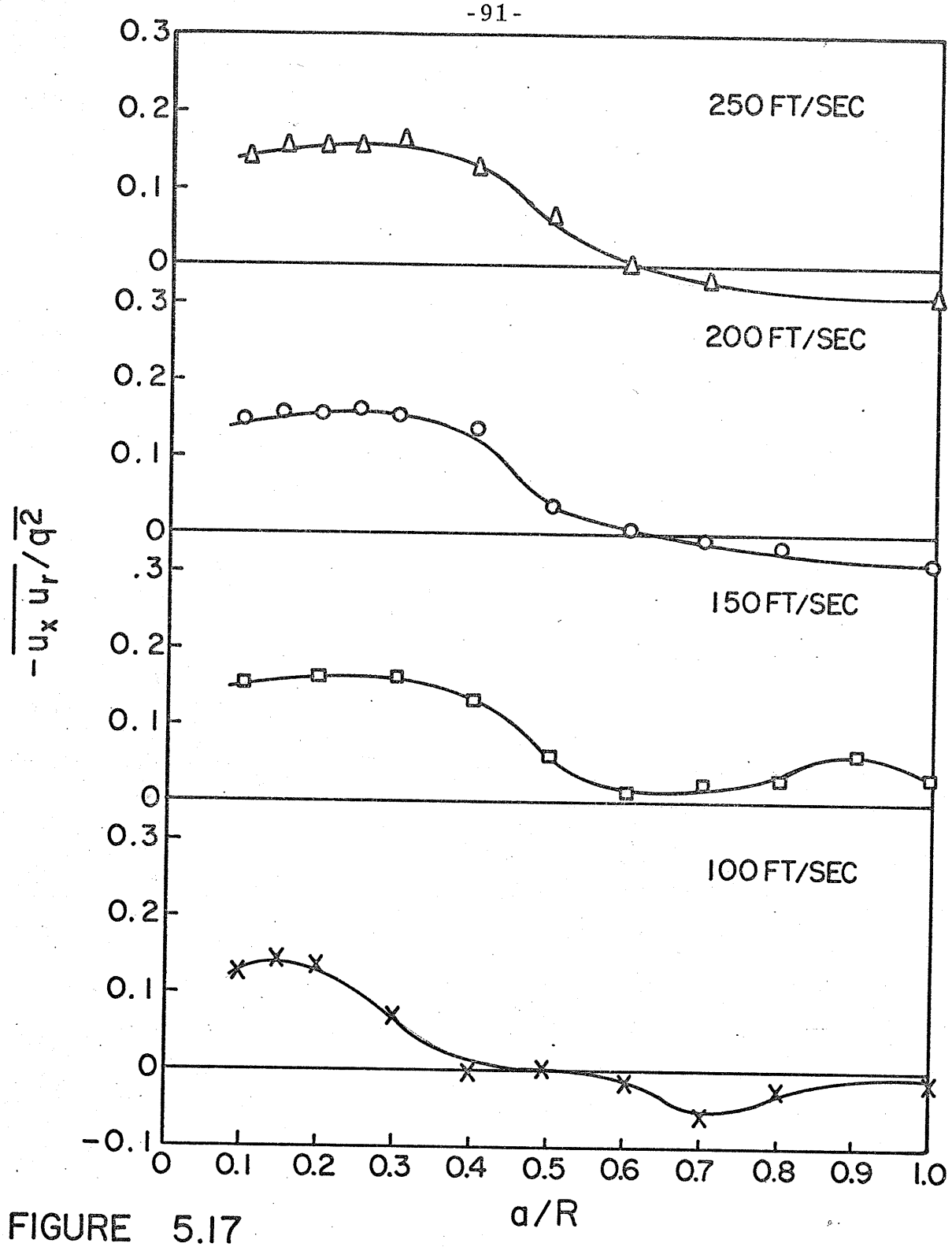

FIGURE 5.17
TURBULENT SHEAR STRESS/TURBULENT ENERGY VERSUS
a/R DIFFUSER INLET

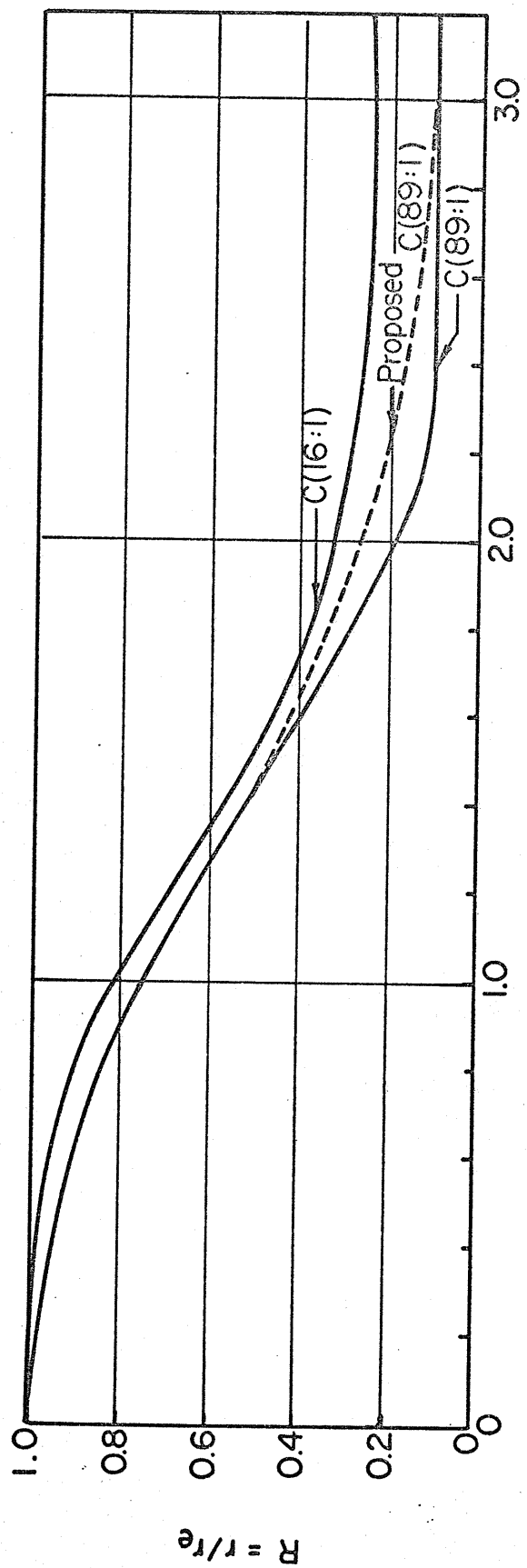

FIGURE 5.18 CONTRACTION CONTOURS

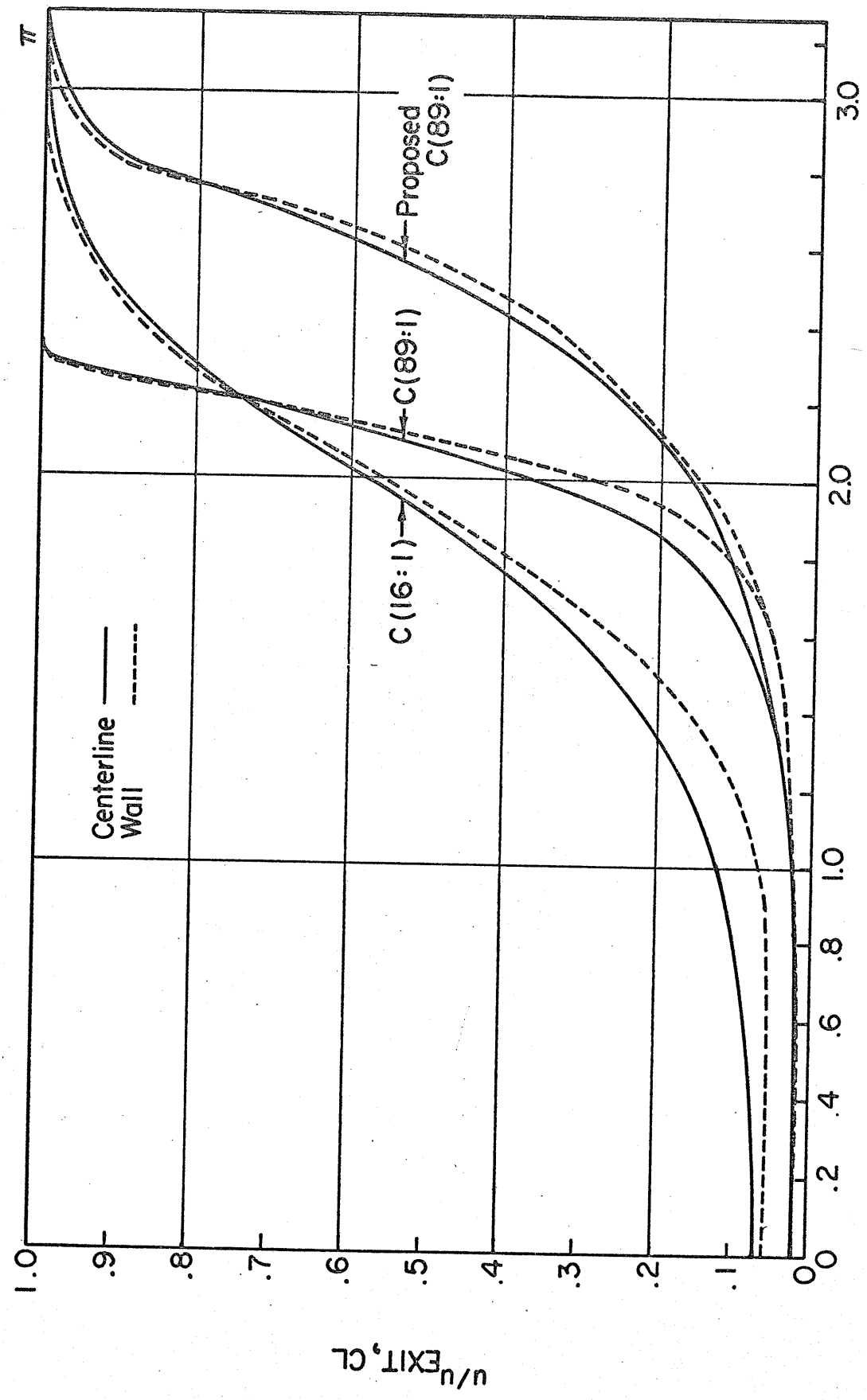

FIGURE 5.19
THEORETICAL VELOCITY DISTRIBUTION FOR 16/1 AND 89/1 CONTRACTIONS

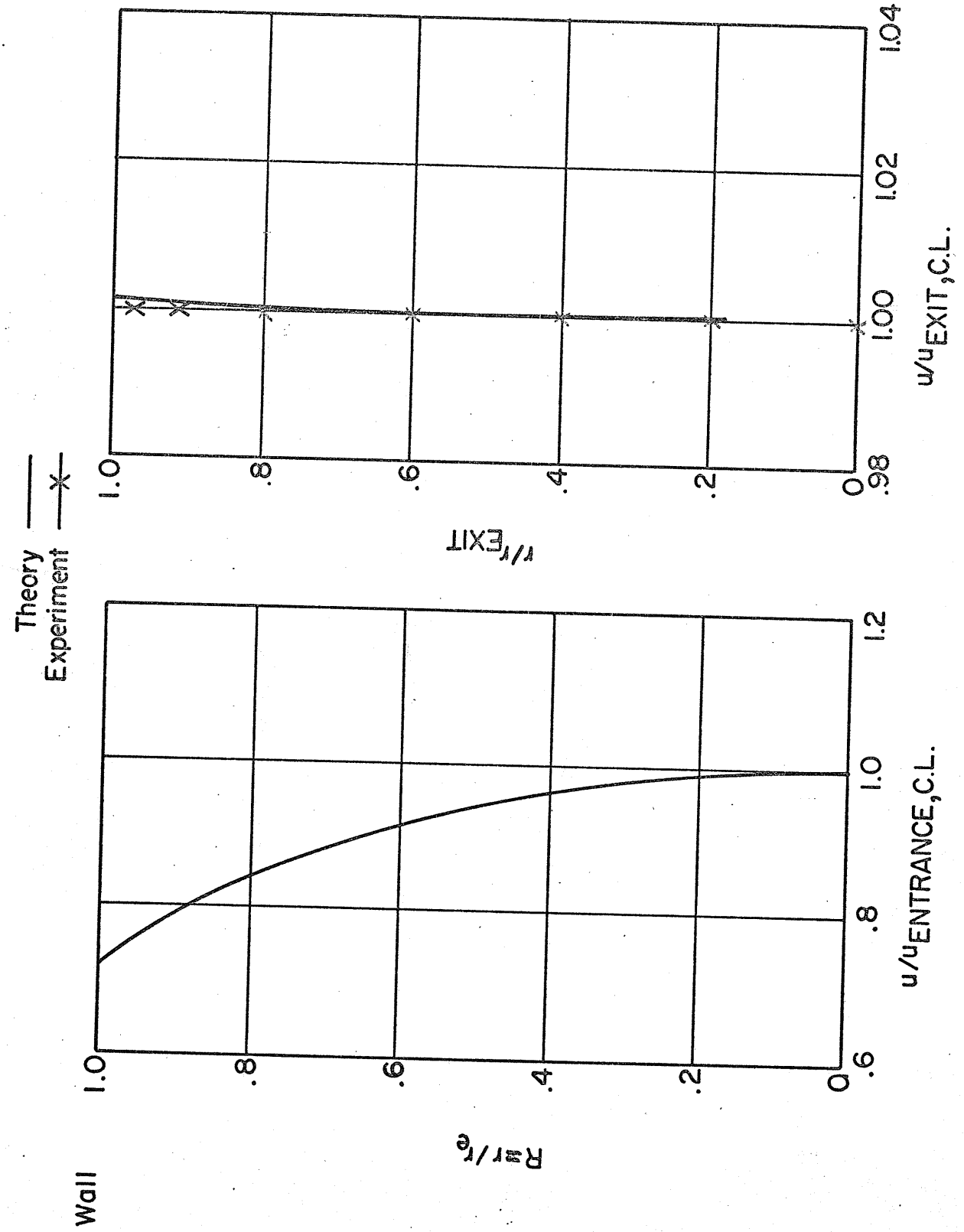
Theory
Experiment
Wall
r/r_EXIT
1.0
.8
.6
.4
.2
0
.98
1.00
1.02
1.04
u/u_EXIT, C.L.
R=r/r_e
1.0
.8
.6
.4
.2
0
.6
.8
1.0
1.2
u/u_ENTRANCE, C.L.

FIGURE 5.20

APPENDIX A

Computer Programs Used to Design Contraction Cones and to Calculate Turbulence Parameters

-Contents-

The Contration Cone Design Program solved a set of simultaneous equations for the Fourier coefficients in the series solution to the flow field in a contraction cone for which the contour was prescribed. The stream function and velocities were also calculated at several hundred points within the contraction.

The program for calculating the turbulence parameters calculated the following:

u_x' , u_r' , u_ϕ' , $\overline{q}^2 = (\overline{u}^2 + \overline{v}^2 + \overline{w}^2)$, $R_{\overline{u_x u_r}}$, $R_{\overline{u_x u_\phi}}$, $\overline{u_x u_r}$, $\overline{u_x u_\phi}$, U_*, and a/R.

```
      DIMENSION A(33),B(33),RA(50),BI(50),S(50),U(50),PSI(61,33),Z(33),
     X(33),V(50),AR(50),S1(50),AR1(50),V1(50)
      DOUBLE PRECISION CD(33,33),DD(33,1),CC(1089),D
      COMMON A1,B1,Z1,A2,B2,Z2
      PRINT 130
      PRINT 140
      READ 150,NN,PSIEX
      PRINT 150,NN,PSIEX
      NEND=NN+1
      PRINT 160
      DO 10 N=1,NEND
      READ 170,Z(N),R(N)
      PRINT 170,Z(N),R(N)
   10 CONTINUE
      DO 30 I=1,NEND
      C=R(I)**2/2.
      CD(I,1)=DBLE(C)
      DD(I,1)=DBLE(PSIEX)
      DO 20 N=1,NN
      J=N+1
      XN=FLOAT(N)
      RIN=XN*R(I)
      ZIN=XN*Z(1)
      X=RIN
      CALL I0(X,RI0)
      ZI=RI0
      CALL INUE(X,1,ZI,RI)
      BI1=RI
      C=(1./XN)*R(I)*BI1*COS(ZIN)
      CD(I,J)=DBLE(C)
   20 CONTINUE
   30 CONTINUE
      K=C
      DO 50 J=1,NEND
      DO 40 I=1,NEND
      K=K+1
      CC(K)=CD(I,J)
   40 CONTINUE
   50 CONTINUE
      CALL DGELG(DD,CC,NEND,1,1.0E-14,IERC)
      DO 60 I=1,NEND
      D=DD(I,1)
      A(I)=SNGL(D)
   60 CONTINUE
   70 PRINT 180
      DO 80 N=1,NEND
      NP=N-1
      PRINT 190,NP,A(N)
   80 CONTINUE
      PRINT 200
      DO 120 I=1,NEND
      WRITE (6,210) Z(I)
      RA(1)=0
      DO 90 J=2,10
      RA(J)=R(I)*.1*(J)
   90 CONTINUE
      WRITE (6,220) (RA(J),J=1,10)
      DO 110 K=1,10
```

```
      DO 100 L=2,NEND
      AR(1)=A(1)*RA(K)**2/2.
      V(1)=A(1)
      X=RA(K)*(L-1)
      CALL I0(X,RI0)
      ZI=RI0
      CALL INUE(X,1,ZI,RI)
      B(L)=RI
      BI(L)=RI0
      S(L)=COS(Z(I)*(L-1))
      U(L)=BI(L)*S(L)*A(L)
      V(L)=V(L-1)+U(L)
      S1(L)=S(L)*B(L)*A(L)/(L-1)*RA(K)
      AR(L)=AR(L-1)+S1(L)
  100 CONTINUE
      AR1(K)=AR(L)
      V1(K)=V(L)
  110 CONTINUE
      WRITE (6,230) (AR1(K),K=1,10)
      WRITE (6,240) (V1(K),K=1,10)
  120 CONTINUE
      RETURN
  130 FORMAT(1H ,    'FLOW FIELD IN A CONTRACTION CONE FOR A PRESCRIBED
     2STREAMLINE')
  140 FORMAT (1H ,34H FOURIER ORDER NN, PSI EXTERNAL:    )
  150 FORMAT (1I10,1F10.5)
  160 FORMAT (53H AXIAL COORDINATE (Z) AND CORRESPONDING RADIUS (R):
  170 FORMAT (2F10.5)
  180 FORMAT (32H  FOURIER COSINE COEFFICIENTS     )
  190 FORMAT (I10,F30.15)
  200 FORMAT('1' ,   'STREAM FUNCTIONS AND VELOCITIES INSIDE CONTRACTIO
     3')
  210 FORMAT (6H X(I)=,F10.5//)
  220 FORMAT (6H R      ,10F10.5)
  230 FORMAT (6H PSI    ,10F10.5)
  240 FORMAT (6H U      ,10F10.5///)
      END
```

```
C       S=SLOPE
C       S1=(A+B)r ,   S2=(A-B)r
C       D1=(A-B)ϕ ,   D2=(A-B)ϕ,
        WRITE(6,1)
      1 FORMAT('1',10X'DIFFUSSER INLET    '//02X'U(A)'5X'UP'6X'VP'6X'WP'5X
       1RUV'5X'RUW'6X'TE'6X'U*'5X'UP/U*'4X'VP/U*'4X'WP/U*'4X'UA/U*'4X'U+'
       1X'Y/D'//)
        DATA S,D,DELP,SW,DEW/.0374,3.94,14.0,.0721,.0001680/
      3 READ(5,4,END=100)V1,V2,A1,B1,S1,D1,A2,B2,S2,D2,Y
      4 FORMAT(F6.3,F6.3,F6.4,F6.4,F6.4,F6.4,F6.4,F6.4,F6.4,F6.4,F6.3)
        U1=50.0+26.715*(V1-1.30)
        U2=50.0+26.715*(V2-1.30)
        UA=(U1+U2)/2
        UP1=S1/(2*S)
        UP2=S2/(2*S)
        UP=(UP1+UP2)/(2)
        VP=D1/(2*S)
        WP=D2/(2*S)
        UE=UP**2
        VE=VP**2
        WE=WP**2
        TE=.5*(UE+VE+WE)
        TAUO= (3.14*D**2/(4.0*144.))*5.2*DELP/25.40/((3.94*3.14/144. )*69
       20625)
        RO=SW/32.17
        UTAU=(TAUO/RO)**.5
        RUV=(A1**2-B1**2)/(S1*D1)*UP*VP/(UTAU**2)
        RUW=(A2**2-B2**2)/(S2*D2)
        X=Y/(D/2.)
        U=UP/UTAU
        V=VP/UTAU
        W=WP/UTAU
        U3=UA/UTAU
        Z=(Y*UTAU/DEW)/12.
        WRITE(6,5)UA,UP,VP,WP,RUV,RUW,TE,UTAU,U,V,W,U3,Z,X
      5 FORMAT(1H0,12F8.4,F8.0,F8.3)
        GO TO 3
    100 CALL EXIT
        END

$ENTRY
```